AD-A087 859 NOTTINGHAM UNIV (ENGLAND) DEPT OF CIVIL ENGINEERING F/G 13/2
PERMANENT DEFORMATION OF FLEXIBLE PAVEMENTS.(U)
JUN 80 S F BROWN, B V BRODERICK, J W PAPPIN DA-ERO-78-G-114
UNCLASSIFIED NL

1 OF 2
AD A087859

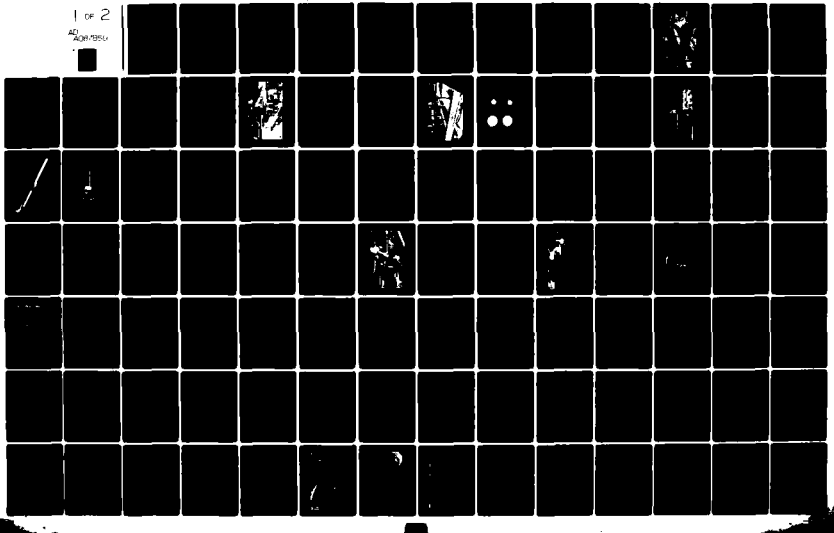

(3)

# PERMANENT DEFORMATION OF FLEXIBLE PAVEMENTS

Final Technical Report

by

S.F. Brown, B.V. Brodrick and J.W. Pappin

June 1980





EUROPEAN RESEARCH OFFICE

United States Army

London England

GRANT NUMBERS DAERO-77-G-061 & DAERO-78-G-114

University of Nottingham, England

UNCLASSIFIED

SECURITY CLASSIFICATION OF THIS PAGE (When Data Entered)

## REPORT DOCUMENTATION PAGE

READ INSTRUCTIONS BEFORE COMPLETING FORM

1. REPORT NUMBER

2. GOVT ACCESSION NO. AD-A087859

3. RECIPIENT'S CATALOG NUMBER

4. TITLE (and Subtitle)

Permanent Deformation of Flexible Pavements.

5. TYPE OF REPORT & PERIOD COVERED

Final Technical Report. Sept 78 — June 80

6. PERFORMING ORG. REPORT NUMBER

7. AUTHOR(s)

S. F. Brown, B.V. Broderick, J. W. Pappin

8. CONTRACT OR GRANT NUMBER(s)

DAERO-78-G-114

DA-ERO-791-G-061

9. PERFORMING ORGANIZATION NAME AND ADDRESS

Dept. of Civil Engineering
University of Nottingham
Nottingham NG7 2TD, England

10. PROGRAM ELEMENT, PROJECT, TASK AREA & WORK UNIT NUMBERS

611 02A
1T161102BH57-01

11. CONTROLLING OFFICE NAME AND ADDRESS

U. S. Army Research, Development & Standardization Group- UK - Box 65
FPO New York, NY 09510

12. REPORT DATE

June 1980

13. NUMBER OF PAGES

75

14. MONITORING AGENCY NAME & ADDRESS (if different from Controlling Office)

15. SECURITY CLASS. (of this report)

UNCLASSIFIED

15a. DECLASSIFICATION/DOWNGRADING SCHEDULE

16. DISTRIBUTION STATEMENT (of this Report)

Distribution unlimited. Approved for public release.

17. DISTRIBUTION STATEMENT (of the abstract entered in Block 20, if different from Report)

18. SUPPLEMENTARY NOTES

19. KEY WORDS (Continue on reverse side if necessary and identify by block number)

Flexible pavements, Deformation, Structural analysis, pavements, asphalt, resilient strain, pavement performance, fabric inclusions.

20. ABSTRACT (Continue on reverse side if necessary and identify by block number)

Seven pairs of pavement with granular bases were tested under controlled conditions. One pavement in each pair contained fabric inclusions. An improved testing facility was developed, including: (1) servo-hydraulic system for the loading carriage; (2) amplification and read-out system for pressure cells; 3) linearizing unit for strain coils; (4) transducers for measuring vertical and resilient deflection; (5) techniques for measuring in situ strain on fabric inclusions; (6) extensive use of nuclear density meter to monitor pavement and foundation materials.

(continued next page)

DD FORM 1 JAN 73 1473 EDITION OF 1 NOV 65 IS OBSOLETE

UNCLASSIFIED

SECURITY CLASSIFICATION OF THIS PAGE (When Data Entered)

The following conclusions are drawn:

1) No improvement in performance resulted from fabric inclusions.
2) No consistent reduction in in-situ stresses, resilient strains, or permanent strains was observed as a result of fabric inclusions.
3) No consistent improvement in densities resulted from fabric inclusions.
4) Some slip apparently occurred between fabric and soil on those pavements which involved large deformations. The slip occurred between fabric and crushed limestone base rather than between fabric and silty-clay subgrade.

A finite element program (SENOL) using a secant modulus, incrementally-interactive analysis has been developed to model problems involving materials with non-linear resilient stress-strain characteristics.

A two-stage approach was used to calculate permanent deformations. The first stage was an axisymmetric resilient analysis; the second stage was a plane strain analysis.

Transient stresses in base and subgrade were not well predicted in the tests; measured values were higher than predicted. However, resilient strains were well predicted in all layers.

Rut depths were not reliably predicted, predicted ruts were 20% deeper than measured ruts for single track tests, but measured ruts were 31% deeper than predicted for multitrack tests.

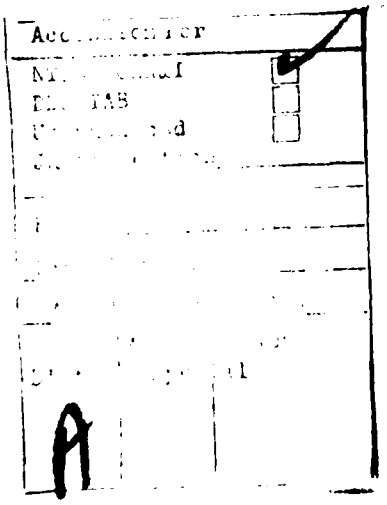

## CONTENTS

# CHAPTER ONE

## INTRODUCTION

The project described in this report was concerned with a continuing investigation into procedures for the prediction of permanent deformation in flexible pavements. An earlier project, also sponsored by the European Research Office of the US Army on the same general topic, resulted in a final report (1) with the major findings summarised by Brown and Bell (2,3). Whereas the earlier work was concerned with full depth asphalt construction, this present project has considered pavements with unbound granular bases and relatively thin asphalt surfacings. Furthermore, the potential of certain non-woven fabrics for improving performance of this type of permanent pavement structure has been assessed. This aspect of the work was made possible by sponsorship from ICI Fibres Ltd.

In designing flexible pavements using methods which rely on structural analysis and a knowledge of the mechanical properties of the constituent materials, the possibility of failure by excessive rutting is still dealt with by a semi-empirical approach (e.g. 4,5,6,7). This involves the calculation of the resilient vertical strain at formation level and its comparison with a maximum allowable value based on back analysis of pavements of known performance characteristics. In contrast, the possibility of fatigue cracking failure in the asphalt may be considered within a detailed, fundamentally based framework (e.g. 4,5,6,7).

Several projects have endeavoured to develop analytical procedures for the prediction of the rut depth developing in a pavement under given conditions and these were reviewed by Barksdale and Hicks (8).

Since the surface rut develops as a consequence of vertical permanent strains throughout the depth of the pavement, its accurate prediction requires that the pavement be adequately modelled in all layers. For fatigue cracking, only the maximum tensile strain in the asphalt layer needs to be predictable, which is a less demanding requirement.

The earlier project at Nottingham (1) showed that the basic approach, originally put forward by Barksdale (9) and Romain (10), could be followed but that a number of practical and analytical problems remained to be solved. Permanent deformation in asphalt pavements only develops seriously at temperatures above about 20°C. At these high temperatures, the viscous component of deformation in the asphalt mixture increases in relation to the elastic component and the use of elastic analysis for the pavement may be questionable. Although reasonable predictions of rut depth were reported, the distribution of vertical permanent strain with depth was not always well predicted. One reason for this was the relatively inaccurate computation of transient stresses even when using non-linear finite element analysis. Brown and Bell (2,3) also demonstrated the limitations of the axi-symmetric triaxial test for reproducing in situ stress conditions on elements away from the axis of symmetry of the wheel load even though they implemented the concept of using invariants for representing the stress conditions. However, they did develop a method for predicting surface permanent deformation for a loading regime involving a lateral distribution of wheel passes, but it was somewhat complex for routine design use.

The present project concentrated on granular materials as the main structural element in the pavement following research on another project at Nottingham which investigated the characteristics of well graded crushed limestone under repeated loading. The same subgrade

was selected as for the earlier work, being a silty clay whose strength could be controlled to some extent by changing its water content. Values of CBR between 2 and 8% were obtained.

Another reason for moving to unbound base construction was the opportunity it presented for investigating the behaviour of pavements with fabric inclusions. The use of non-woven material such as Terram 1000 (similar to Mirafi 140) had been demonstrated for haul roads (11) where large strains could be tolerated, but its use for improving the performance of granular bases in permanent roads, where deformations are necessarily smaller, had still to be demonstrated under realistic conditions. The approach to this aspect of the work was two-fold. Firstly the performance of pavement pairs which were identical save for the inclusion of fabric in one of them, was compared and, secondly, the mechanisms of fabric behaviour were investigated by making detailed in situ measurements of stress and strain.

Since the earlier project had included the development of a pavement test facility, only three pavement sections were tested in the time available. However, a considerable number of material characterisation tests were performed and a major effort was made on theoretical developments. In the new project the emphasis was on pavement testing and a total of seven pairs were constructed over the three-year period. In addition, the Pavement Test Facility was substantially improved. The theoretical work was restricted to a one-year effort due to shortage of funds and relatively little materials testing was done. However, the rolled asphalt surfacing, the crushed limestone base and the silty-clay subgrade had all been the subjects of previous testing programmes in related projects.

In summary, the overall aims of this research were to develop

analytical procedures to predict both the resilient and permanent strains in the tested pavements and to obtain a clearer understanding from in situ measurements of the mechanical behaviour of pavements with unbound bases including the effects of fabric inclusions.

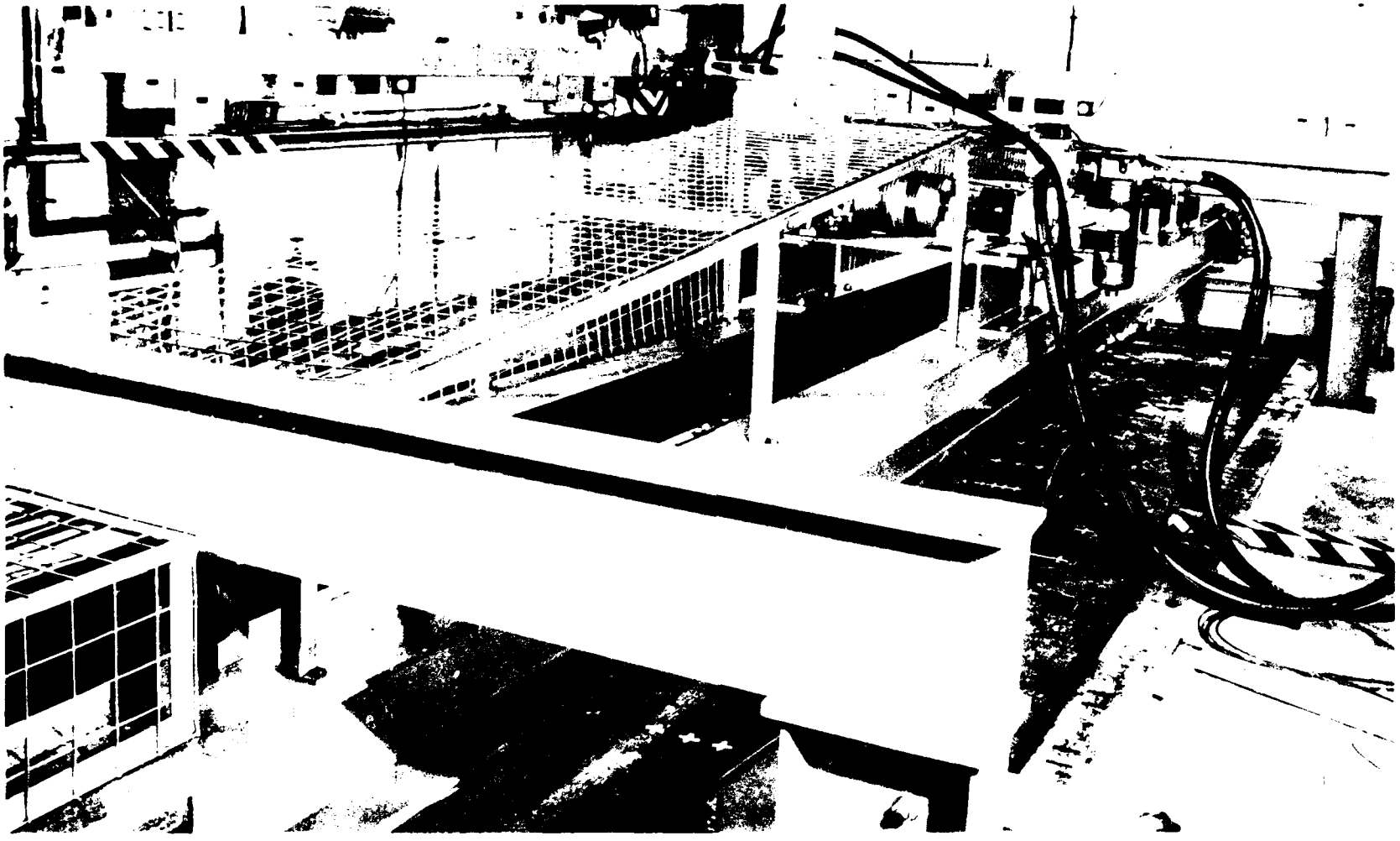

FIG. 2.1 GENERAL VIEW OF CONTROLLED TEMPERATURE ROOM CONTAINING PAVEMENT TEST FACILITY

# CHAPTER TWO

# EQUIPMENT DEVELOPMENTS

## 2.1 THE PAVEMENT TEST FACILITY

### 2.1.1 Introduction

The Pavement Test Facility was described in detail by Brown et al (1). During the present research, it has been further developed, so details of these improvements are described in this section. The loading wheel is fitted to a carriage, which runs on bearings between two beams spanning the long side of a rectangular laboratory (Fig. 2.1). This room is insulated to assist with temperature control and has access for pavement construction. The beams are mounted on end bogies which allow traversing of the wheel across the pavement in order to simulate the normal lateral distribution of wheel passes in real traffic. The main requirement of the facility is to apply a constant moving wheel load at a constant speed to a pavement structure maintained at a constant temperature.

### 2.1.2 The Original Loading System

At the beginning of 1979 a decision was taken to improve the loading system on the carriage. This originally consisted of a gear pump fitted on the carriage and driven by friction from a strip attached to the reaction beams. Pressure was maintained in an accumulator and applied to two loading rams which levered the wheel down onto the pavement (Fig. 2.2). Thus only "topping up" of the accumulator was necessary and the load on the wheel was continuously applied during testing in both directions of travel. This was an unrealistic situation as real traffic loading occurs in one direction only.

Another problem was that the system could not readily cope with variations in the surface level of the pavement so that some variations

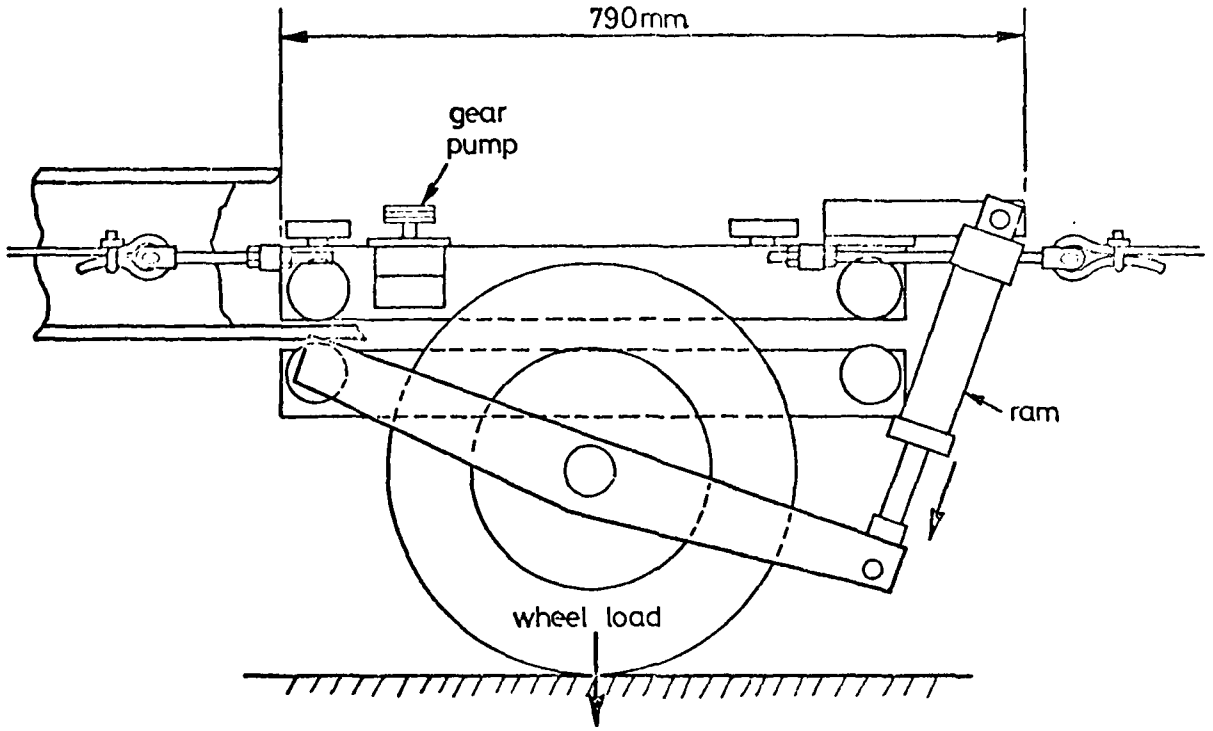


(a) LOADING SYSTEM

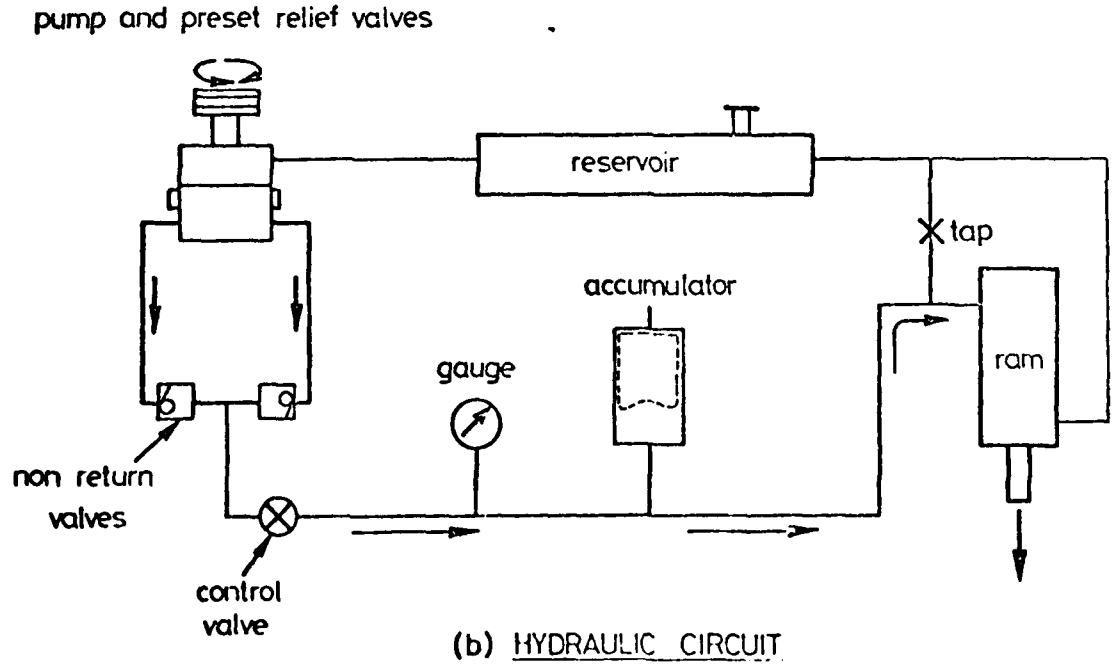


(b) HYDRAULIC CIRCUIT

FIG. 2.2 LOADING CARRIAGE

in load did occur. The improvements which were made allowed either one or two-directional loading and much better control of the applied load.

### 2.1.3 The Modified Loading System

A servo-controlled hydraulic system was chosen which could lift the wheel to a "no load" position in one direction, for unidirectional loading, but could also retain the ability to load in both directions for bidirectional loading. Load feedback in a servo loop maintained the constant load situation much better over unevenness in the pavement surface. The new components for this operation included two ultra low friction hydraulic rams, a servo valve and a "swinging arm" to carry hydraulic power hoses from the main pump to the moving carriage, Fig. 2.3. A command signal controlling the time of loading and a load signal controlling the magnitude of the applied load were required to operate the servo controlled rams which loaded the wheel (Fig. 2.4).

In Fig. 2.4, it can be seen that the command signal was derived from the velocity profile of the hydraulic motor rotation. The profile took the form of a ramp up (acceleration), a plateau (constant speed) and a ramp down (deceleration) before reversal. When this input was fed to the servo valve controlling the loading rams, the wheel load would increase, be held constant and then fall to zero in phase with the velocity. Although the signal changed sign on return of the wheel, it was conditioned to always be positive and the sequence was repeated. However, the signal reversal was used to advantage when the unidirectional control was selected. A diode was switched in before conditioning, effectively excluding the "negative going" part of the cycle, so that a zero voltage output was obtained for one direction of wheel travel (i.e. no load) (Fig. 2.4).

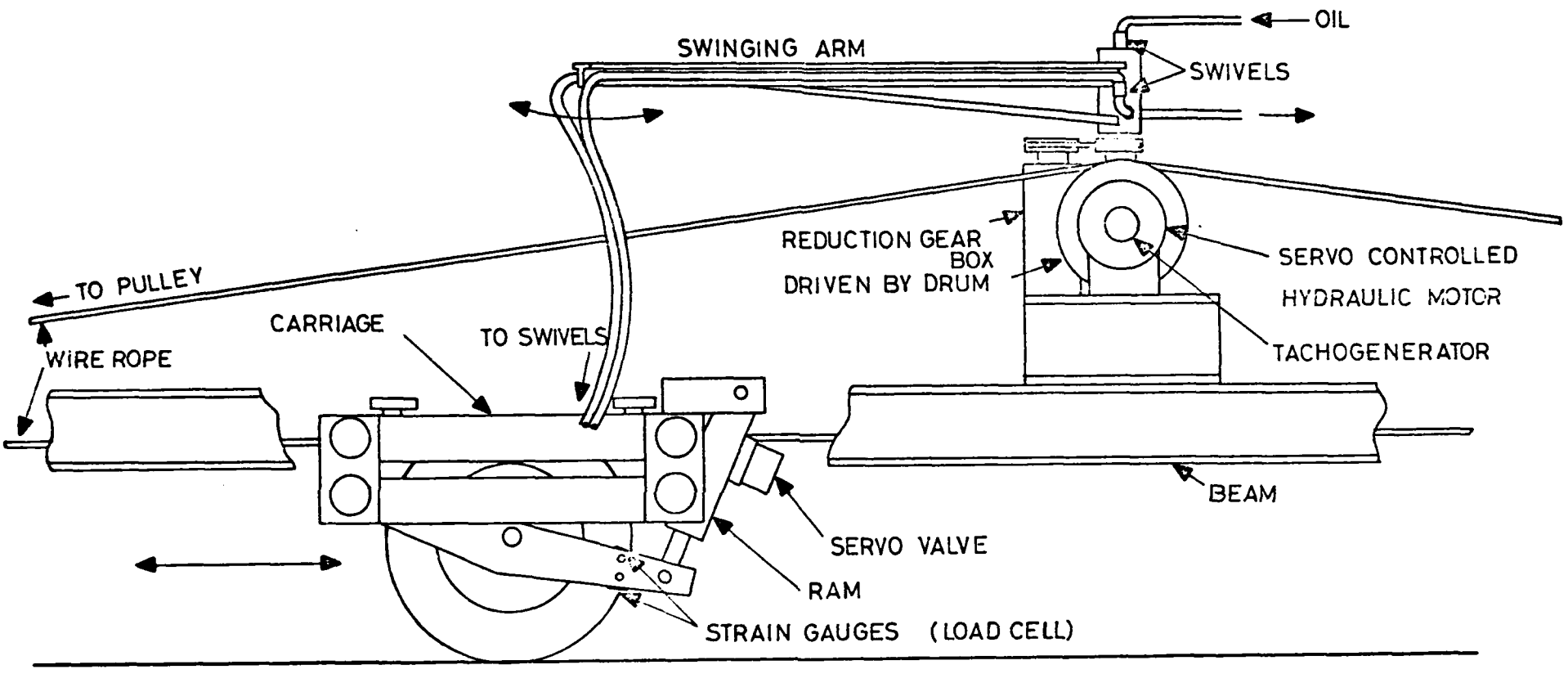


FIG. 2.3 ARRANGEMENT OF WHEEL LOADING SYSTEM

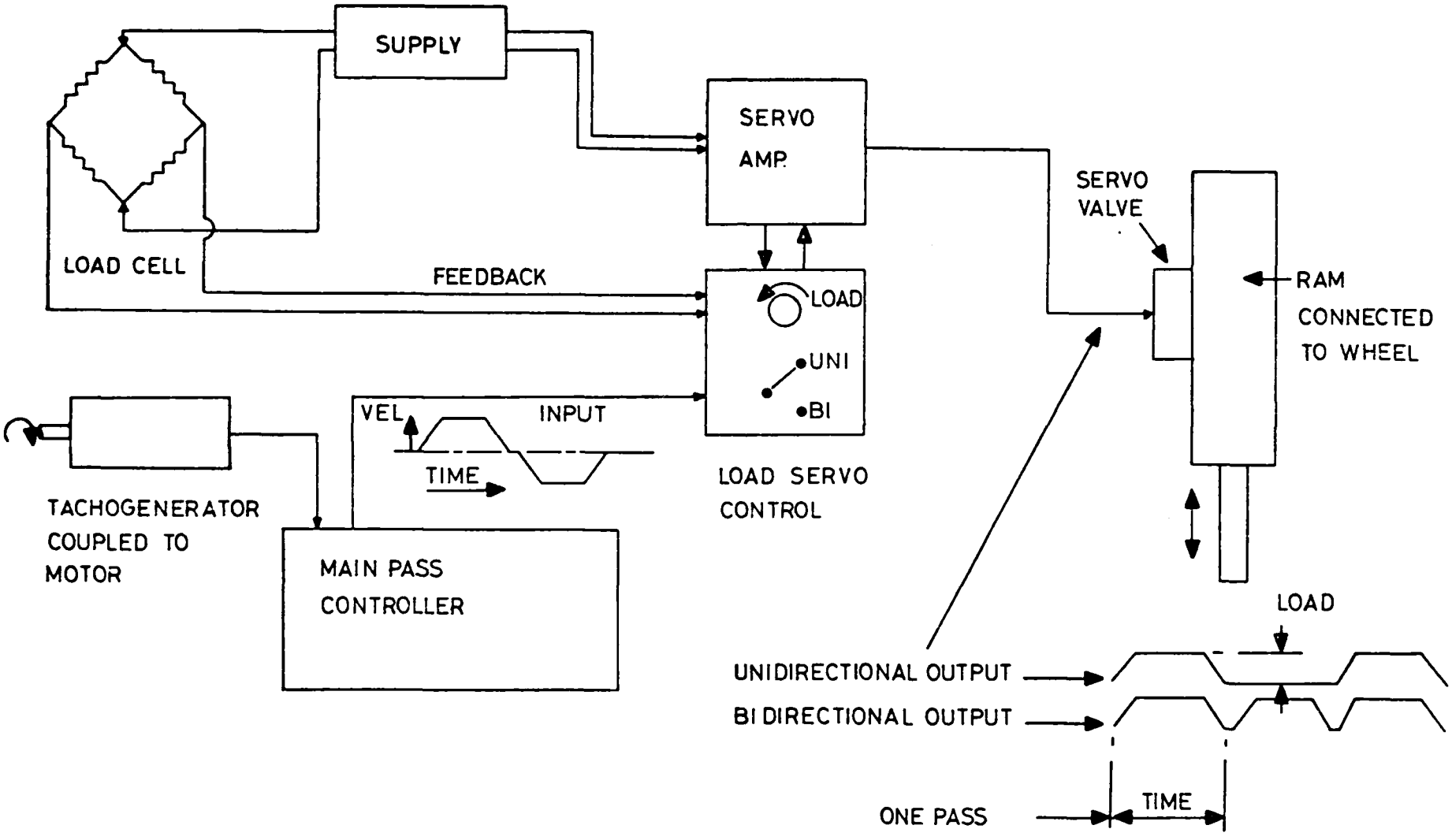


FIG. 2.4 ELECTRONIC LOAD CONTROL SCHEMATIC

The load magnitude was set by a potentiometer, the output from which was compared with that from a strain gauge bridge on the levers supporting the wheel (Fig. 2.3). Holes were drilled near the gauges to increase the local strain so that the gauge bridge output was compatible with the requirements of the servo amplifier. The gauges effectively formed a load cell, calibrated in volts per kN, and completed a feedback loop to the amplifier. If the distance between the beams and pavement surface increased, due to an uneven surface, then the load cell reading would decrease. The servo amplifier would sense the voltage discrepancy with the potentiometric setting and immediately command the servo valve to increase the pressure until the discrepancy was cancelled. A constant load was maintained by this means but the system response could not entirely eliminate the effect of sharp "bumps" in the surface. These could increase the load by 1 kN but generally it was maintained within ±0.5 kN for an applied load of 8 kN. It was clearly desirable to try and ensure a level finish to the pavement when constructed.

The introduction of a servo valve causes considerable pressure drop and some flow restriction so it was necessary to use the main hydraulic supply for the carriage drive system rather than the simple gear pump used originally. This was accomplished by using the arrangement shown in Fig. 2.5. A gearbox was coupled by means of bevels to the revolving drum about which the cable connected to the carriage was wound. The drum had the exact motion necessary to move a swinging arm smoothly and in sychronisation with the carriage movement. Eight revolutions of the drum were reduced to an arc of approximately $140^{o}$ by the gearbox whose output shaft was the point about which the arm pivoted. Swivel connections were used to transfer the oil through two flexible hoses at this point, and the hoses were continued along the arm and down

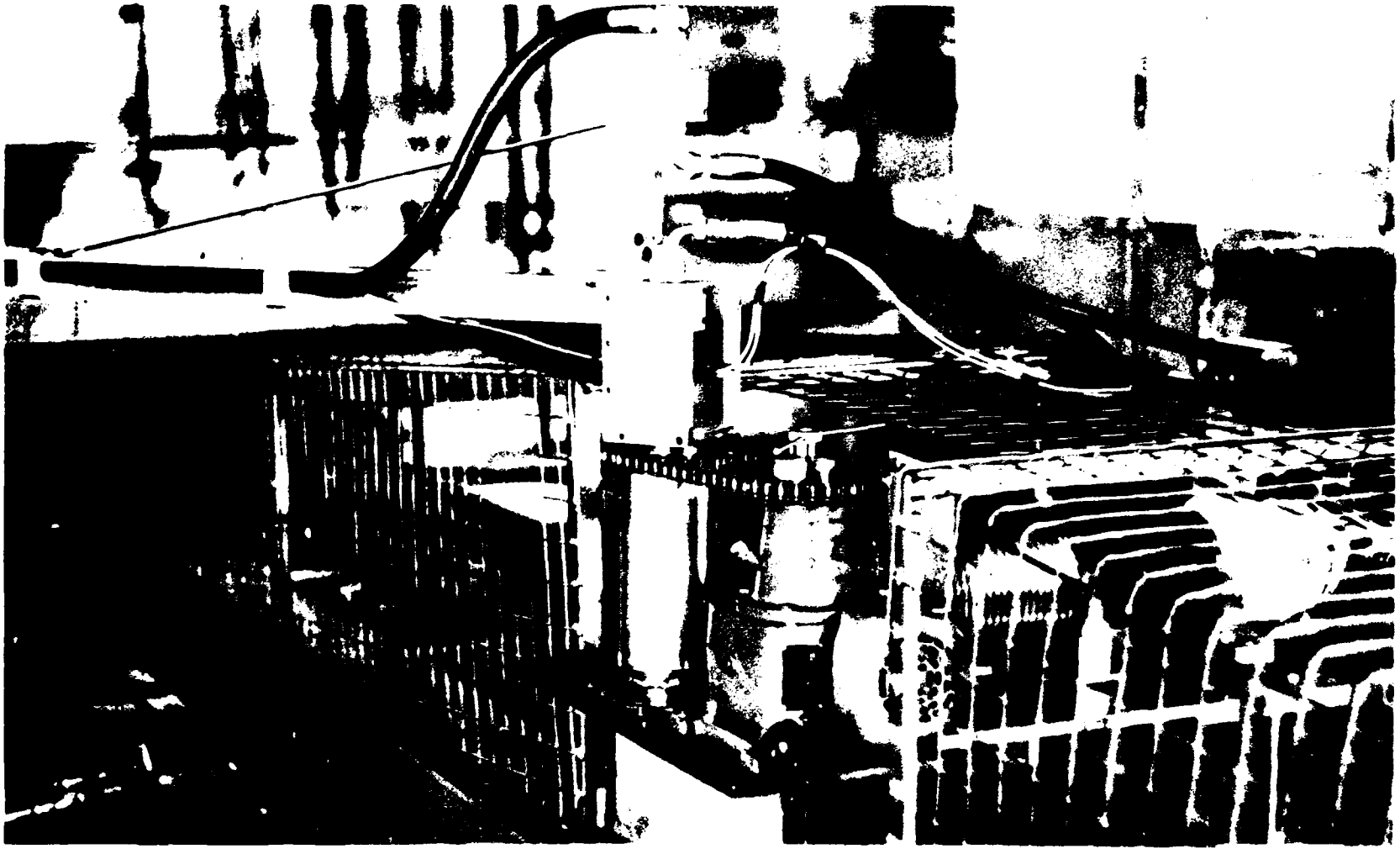

FIG. 2.5 SWINGING ARM DRIVEN BY GEARBOX COUPLED TO GROOVED DRUM

to swivels attached to the fixed hydraulic pipes on the carriage. The swivels allowed the hoses to take up a natural attitude as they had a tendency to swing and twist during reversal of the carriage. Electrical supply to, and output from, the strain gauge bridge plus connections to the servo valve were carried by two cables attached to the hose and arm. The completed loading facility is shown in Fig. 2.6.

During paving, the test facility was moved to one side of the laboratory and it was necessary to remove the arm. To facilitate this, the oil connections to the carriage were of a quick release, self sealing design, and plugs and sockets were used for the electrical cables. A warning light was fitted to the end of the arm, and a limit switch, connected to the main oil pump, was attached to the pivot to prevent arm overtravel should the cable slip on the drum. If the latter operated, the machine would shut down, causing the carriage to stop almost immediately.

### 2.1.4 The Pavement Test Facility Performance Specification

The specifications listed below represent the capabilities of the facility although the loads and speeds actually used during testing are detailed in Chapters 3 and 4.

| | | |
|---|---|---|
| Load range | = | 0-15 kN |
| Tyre pressure | = | 530 kPa |
| Contact area at 10 kN | = | 0.02 $m^2$ |
| Contact stress at 10 kN | = | 500 kPa |
| Speed range | = | 0-16 km/hr |
| Length of travel | = | 6.7 m |
| Length of assembly | = | 8.2 m |
| Temperature range | = | 20 to 35$^{o}$C |

Note: The difference between tyre pressure and contact stress is probably due to the stiffness of the side walls of the tyre.

## 2.2 PAVEMENT INSTRUMENTATION

### 2.2.1 Introduction

The parameters measured during testing were permanent and resilient strains, transient stresses, surface profiles and material densities. Subgrade vertical deflections were also measured for pavements constructed in the later stages of the work.

Specialised instrumentation for use in and on pavement materials has been developed to give representative results without disturbing the structural behaviour of the pavement. Bison strain coils and Nottingham pressure cells were installed to monitor strains and stresses and these have been described in detail previously (1,12). Reference has also been made previously to the use of strain gauges on fabric and deflectometers in the subgrade (13), for measuring horizontal strains and interface deflections respectively. A Troxler Nuclear Density meter was used, when available, during the testing programme. It was operated in a non-destructive mode (backscatter) primarily to measure the density of the asphalt and granular layers. Moisture content could also be determined with this device.

The stress and strain transducer outputs were analysed from Ultra Violet (UV) recorder traces and then calculations had to be made using calibration factors for each instrument. This was a time-consuming business which was speeded up by a number of developments described below.

### 2.2.2 The Strain Coil Lineariser

The strain coils (Fig. 2.7) operate as pairs of wire wound discs set approximately two diameters apart in the pavement and are

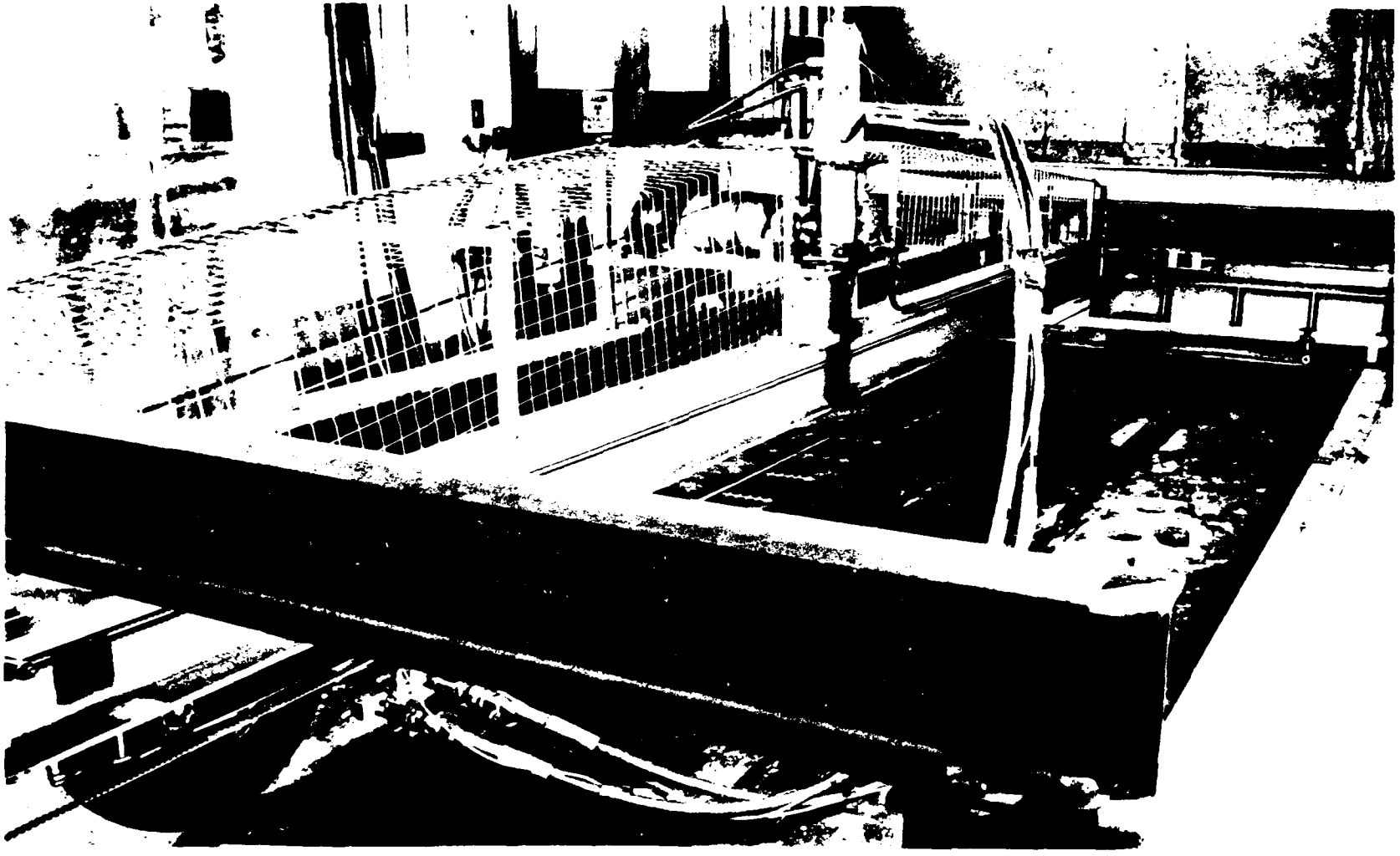

FIG. 2.6 PAVEMENT TEST FACILITY AFTER MODIFICATIONS

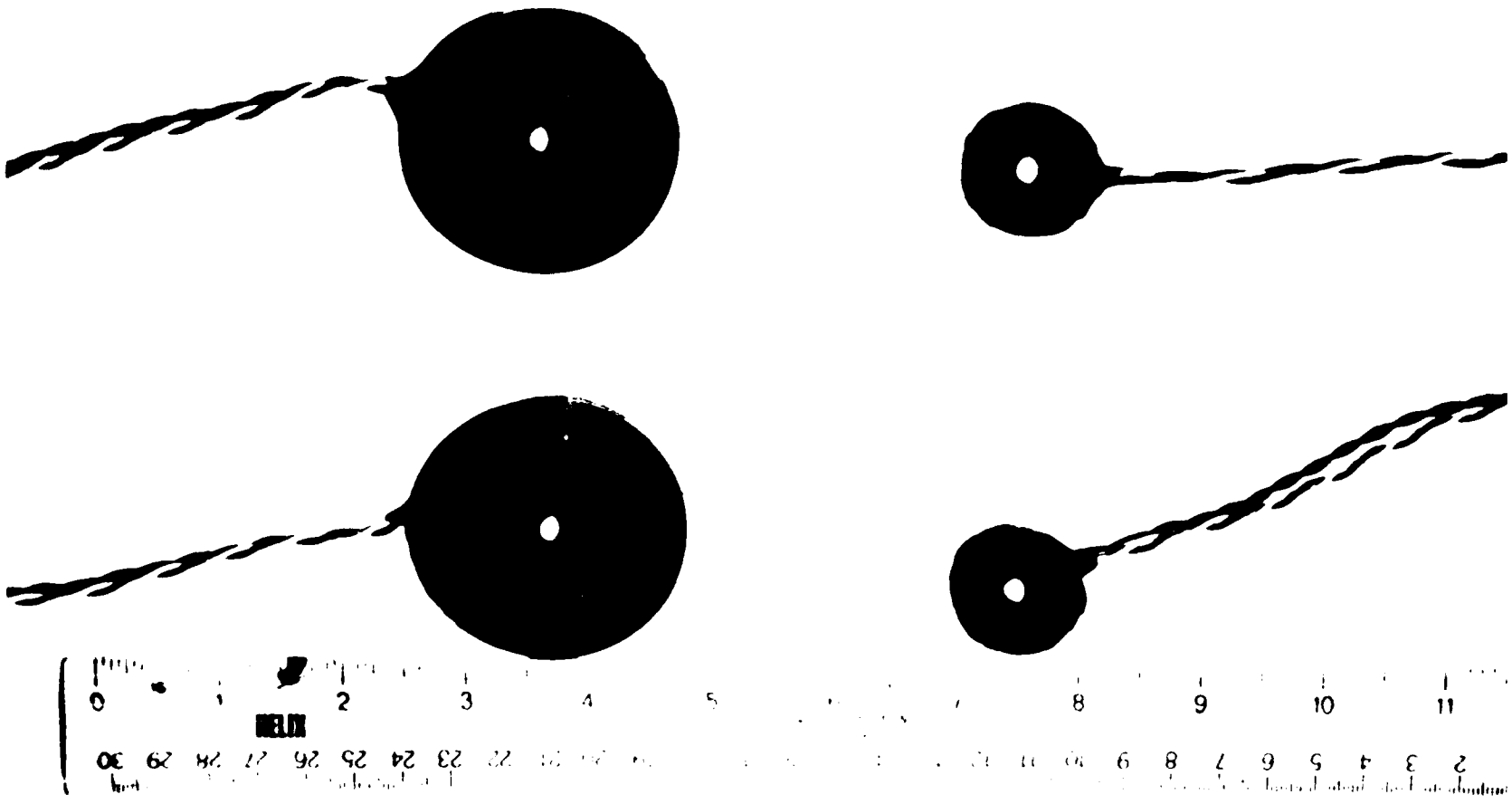

FIG. 2.7 BISON STRAIN COILS

electro-magnetically coupled so that their exact separation can be determined. This separation is related to readings on an amplitude dial control which, along with a phase balance and sensitivity control, is used to null the meter pointer on a Bison soil strain gauge instrument (Fig. 2.8). Hence, the readings at balance represent the permanent deformation which has accumulated, while the meter deflection responds to resilient deflections. Unfortunately, the output sensitivity is dependent on the coil spacing and varies in a non-linear manner (high when the spacing is small and low when the spacing is large), resulting in a curved relationship between gauge length and amplitude dial reading.

Permanent strain was still easily derived from these curves but it was necessary to scale all resilient strain responses on the UV record from a calibration pulse based on the amplitude dial reading. A lineariser was built to eliminate the need to scale and provide a calibrated output which was constant over the full amplitude dial range. This allowed resilient strains to be directly obtained from the UV record much more easily. This equipment is shown along with the Bison instrument, in Fig. 2.8, and a detailed description of its mode of operation is included in Appendix 1.

### 2.2.3 Pressure Cell Amplifiers

Originally, the strain gauged pressure cells had a d.c. supply and, because of current limitations, low outputs were obtained. The type of amplifiers which were introduced not only increased these outputs but gave considerable flexibility in terms of the required size of output signal. They were connected to the UV recorders by means of galvanometer matching units. The sensitivities of all the pressure cells were then adjusted to an identical level during calibration so that

the recorded pulses could be conveniently, quickly and easily converted to stresses.

### 2.2.4 Automatic Printing System

The ability to obtain scaled voltage outputs from the strain coils and pressure cells is part of an instrumentation system which will automatically print out transient stresses and strains caused by a moving wheel load. Items for this are at present being obtained and a block diagram of the system is shown in Fig. 2.9.

The pressure cell amplifiers and strain coil lineariser are individually selected by a scanner for consecutive wheel passes. Thus for one pass of the wheel the output of one transducer will be amplified, caught on a peak catcher, the peak voltage will be converted to a digital signal and then printed as a stress or strain. It is for this last operation that scale factor controls are necessary to produce a convenient reading such as 600 mV for 600 kPa. Calibration can be carried out through the system and adjustments made to compensate for "installation effects".

There are alternatives to this system such as digital transient recorders and digital storage oscilloscopes but it was felt that the selected arrangement could easily be expanded to add more channels and even increase the speed of printing such that several instruments could be monitored during one pass of the wheel. In the tests described in this report, transient stresses and strains reach reasonably uniform values after about the first 5,000 wheel passes and hence do not change significantly over the 10 or 20 passes required during scanning by the instrumentation.

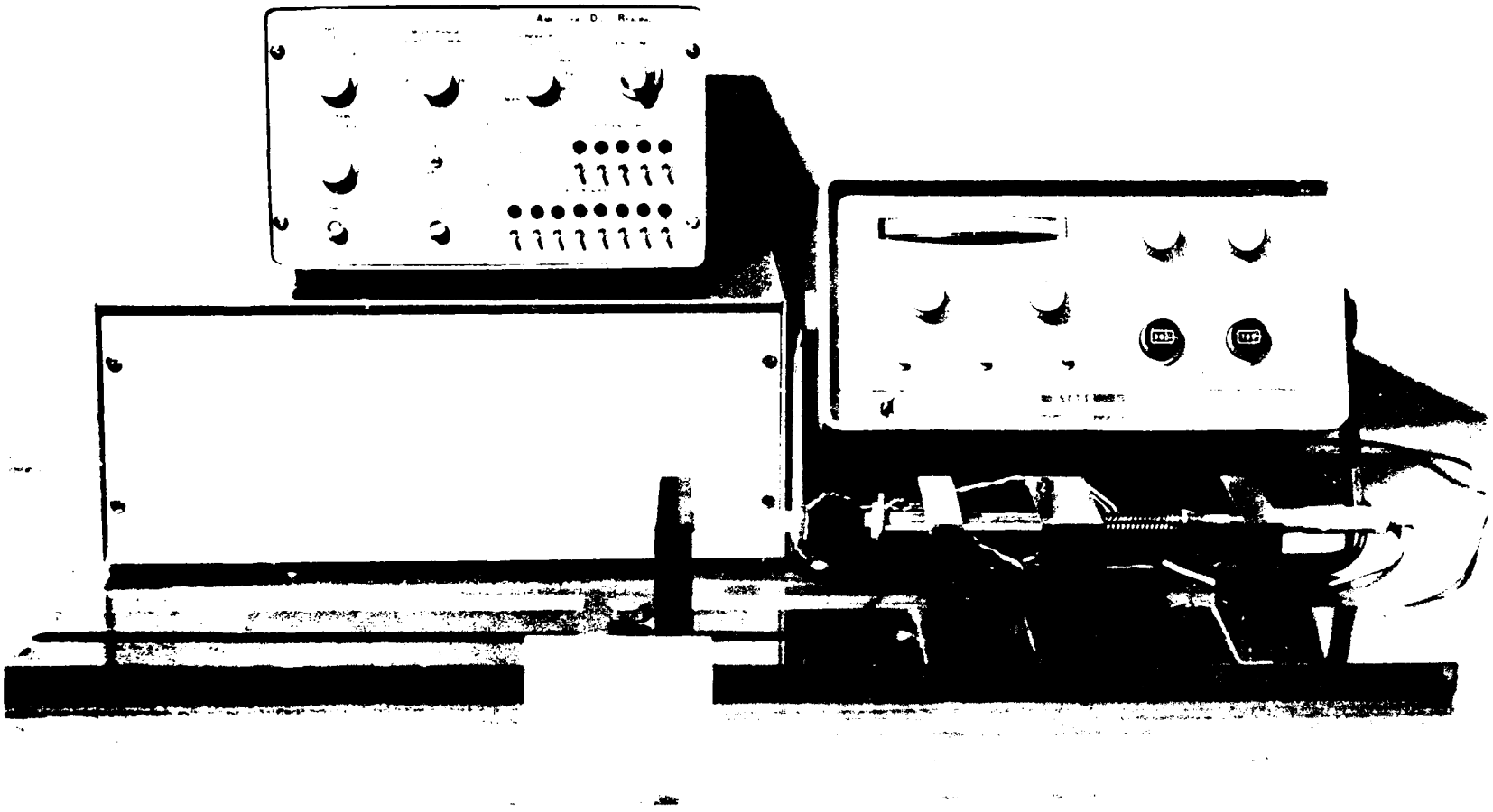

FIG. 2.8 STRAIN COIL CALIBRATOR, BISON INSTRUMENT AND LINEARISER

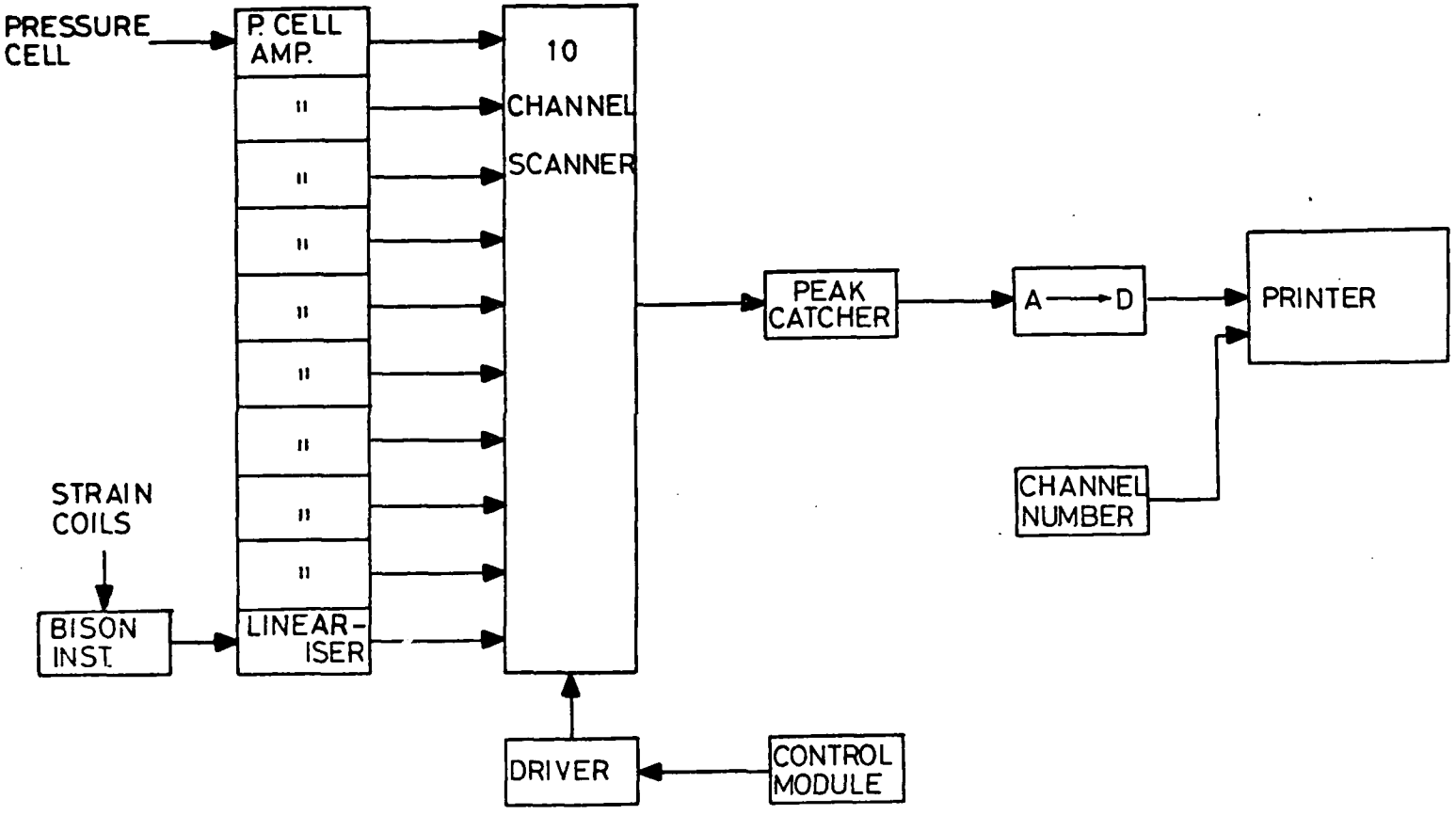


FIG. 2.9 AUTOMATIC DATA ACQUISITION SYSTEM

2.2.5 Additional Instrumentation

Surface profiles in the longitudinal and lateral directions were measured at points on a grid marked on the asphalt surface at intervals during each test. A displacement transducer running along a rigid beam was moved to each position on the grid and readings were obtained relative to the location of the end mountings of the beam (Fig. 2.10). Wheels were fitted to the plunger of the transducer so that it could be easily traversed across the pavement surface.

A displacement transducer was also used to measure the subgrade surface deflection both under transient loading conditions and for permanent deformation. In this case a core moving within the body of the instrument (transformer windings) was attached to a long rod located within a small diameter hole. The hole was drilled to a depth of 0.92 m which was below the zone of influence of the wheel load. The rod was held in position by screwing it into the soil. An output was obtained from the transducer which was proportional to the permanent or resilient deflection at the subgrade surface as appropriate.

Use of strain gauges on the fabric was predominantly experimental and controlling factors on their performance were the selection of adhesive and calibration technique. Strain coils were also attached to the fabric but these had the disadvantages of stiffening the material and were several times thicker than it. The strain gauges were of a post-yield type and, as such, could sustain high elongations. A gauge length of 60 mm was found to be most satisfactory. They are less likely to inhibit the local movement of the fabric and can be attached to the relatively flat melt bonded material with methyl-2-cyanoacrylate adhesive. Although not tried on woven fabric, problems would be anticipated with the uneven surface texture of these materials.

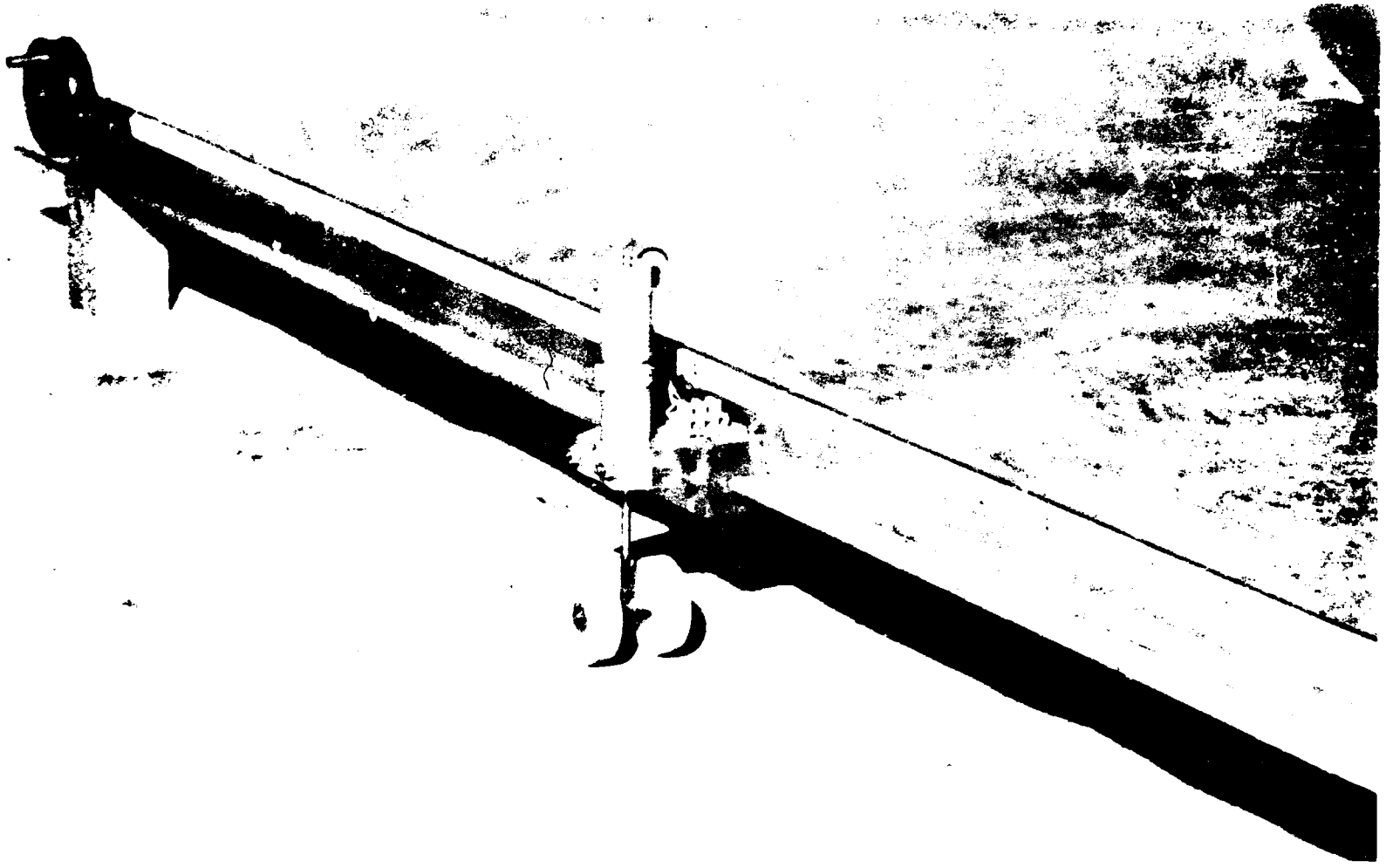

FIG. 2.10 PROFILOMETER

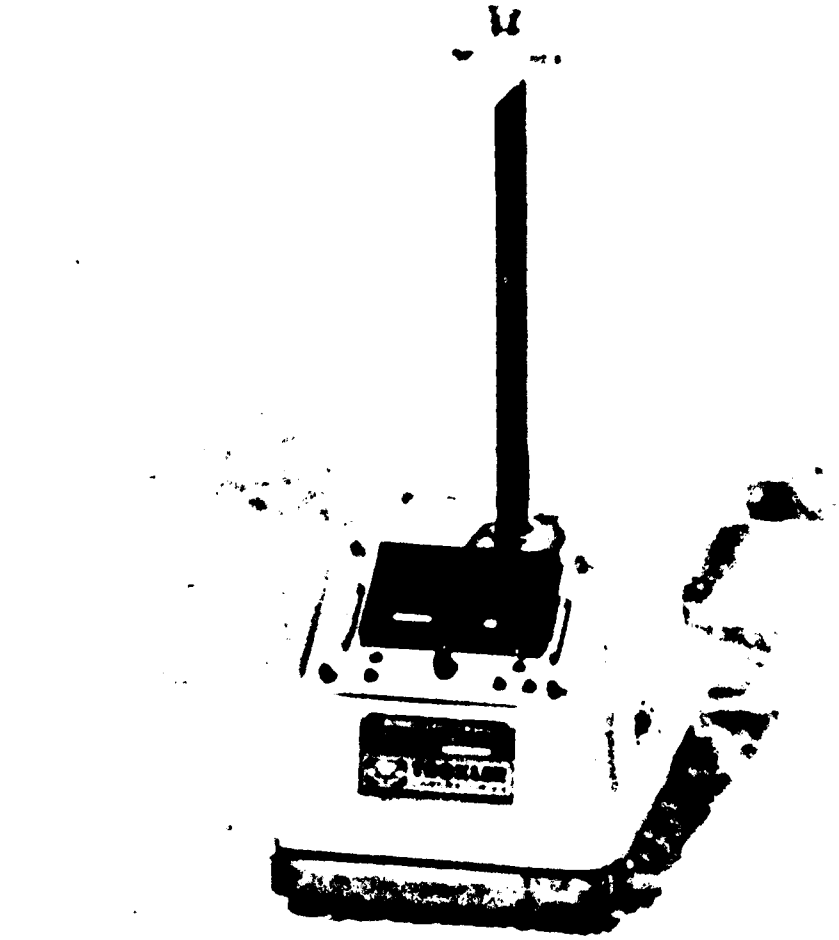

FIG. 2.11 TROXLER NUCLEAR DENSITY METER

Density measurements were taken with a "Troxler Nuclear Density Meter" loaned by the Transport and Road Research Laboratory. As this arrangement was dependent on availability, an identical meter was obtained on a permanent basis in the final year in conjunction with a project sponsored by Mobil Oil Co. Ltd.

This instrument (Fig. 2.11) can be used on the surface (backscatter), raised above the surface (airgap) or with its probe lowered into the pavement material (direct transmission). The probe contains a radioactive isotope (RA:BE) which emits (scatters) gamma photons and these are detected within the instrument and displayed as a count related to time. When the meter is placed above or on the surface of the material to be tested the detectors respond to the backscatter of the photons. When the probe is lowered into a prepared hole in the material, the detectors respond to the direct transmission of the photons.

The backscatter method was adopted for these tests as several readings could be taken over the relatively small test area and disturbance of the pavement materials was avoided. This technique is less accurate than the direct transmission method as the effect of surface voids and material composition is more severe. The voids result in a lower surface density and, as a large portion of the initial photon scattering takes place in the top 25 mm, the measurement tends to be heavily weighted by this lower density. Composition errors are compounded by the lower mean photon energy caused by the multiple scattering process. This results in greater photoelectric adsorption compared with the direct transmission mode in which the average photon energy is much higher.

These problems can be overcome to some extent by using fine material of known density in the surface voids. It may be possible to obtain a consistent error and then apply a correction factor.

# CHAPTER THREE

# PAVEMENT STRUCTURES

Seven pairs of pavements were tested, each consisting of a subgrade, a granular layer and a bituminous layer with a fabric incorporated in one or more of the pairs. The notation G indicates the inclusion of a granular layer and distinguishes these pavement tests from those in the previous project (1). Pavements containing fabric are signified by the letter T.

## 3.1 PAVEMENT MATERIALS

The subgrade was a silty clay known as Keuper Marl and obtained in the form of green (wet) bricks from two Leicestershire quarries owned by the Butterly Brick Co. Ltd. Material from Blaby was originally used but an upper layer of the subgrade was removed during the test programme and replaced by material from Desford. The details of these soils, given in Table 3.1, show them to be very similar. Repeated load triaxial testing of this material to determine resilient properties has been reported earlier (1).

The base layer of each pavement was made from a crushed limestone, graded to a "wet mix" base specification (15), Fig. 3.1. For the first five pavement pairs this material was placed in a dry state, since an earlier materials testing project had used it in this way (16,17) and valuable data was available on its resilient characteristics. As a result of placing the limestone dry, moisture migrated from the subgrade into the granular layer, changing the material characteristics slightly during testing. Consequently, for the final two pairs of pavements, it was placed at its optimum moisture content of 4.4% which is how it is

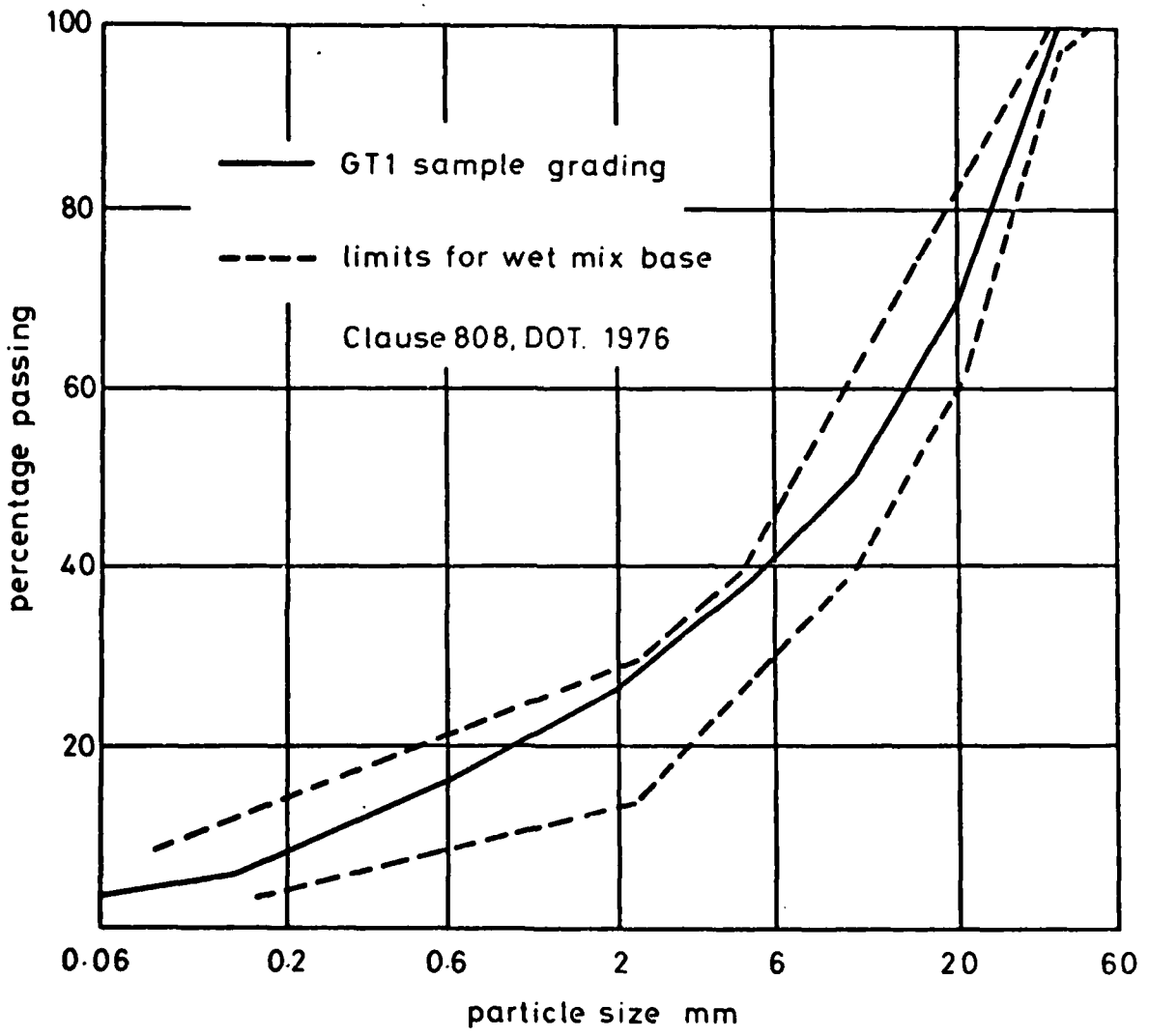


FIG. 3.1 GRADING CURVE FOR CRUSHED LIMESTONE BASE

Table 3.1 Results of tests on Keuper Marl

| Soil parameter | Blaby | Desford |
|---|---|---|
| Liquid Limit | 30% | 30% |
| Plastic Limit | 16% | 17% |
| Plasticity Index | 14% | 13% |
| Classification | Clay, low to medium plasticity | Clay, low to medium plasticity |
| *Maximum Dry Density | 1.88 $Mg/m^3$ | 1.84 $Mg/m^3$ |
| *Optimum Moisture Content | 15.2% | 16.8% |

* British Standard, light compaction (14).

normally used on site. The limestone was supplied by the Amalgamated Roadstone Corporation of Chipping Sodbury, Gloucestershire.

Hot rolled asphalt mixes prepared in accordance with BS 594 (18) were used for each pavement. A basecourse mix with, nominally, 65% coarse aggregate and 5.7% binder content of 50 pen bitumen, was used in the first pair of pavements. This was changed to a wearing course mix (schedule 1A in BS 594) which contained 30% coarse aggregate and had a binder content of 7.9% of the same binder for the remaining pavements. It was found that the finer mix facilitated the installation of strain coils, the performance of which may be inhibited by the interposition of large aggregate particles. Grading curves from samples of each type of mix are presented in Fig. 3.2. The dynamic stiffness and fatigue characteristics of hot rolled asphalt have been well documented (19) so the only check test carried out was on a simply supported beam cut from the pavement to determine stiffness. More tests had been planned, but the cores taken from each pavement were rather short (40 to 50 mm) and equipment for handling these was not developed in time to be utilised.

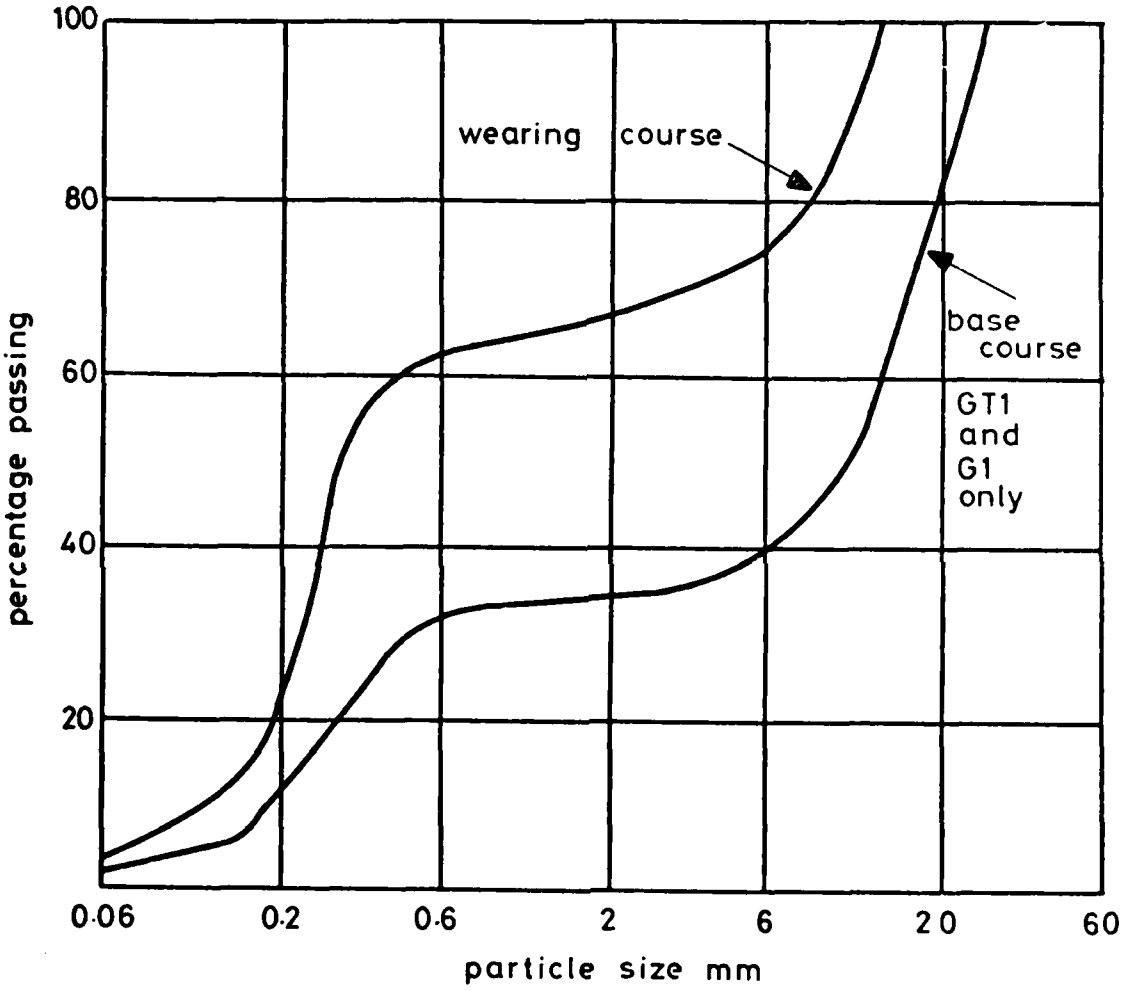


Fig. 3.2 GRADING CURVE FOR AGGREGATE IN HOT ROLLED ASPHALT MIX

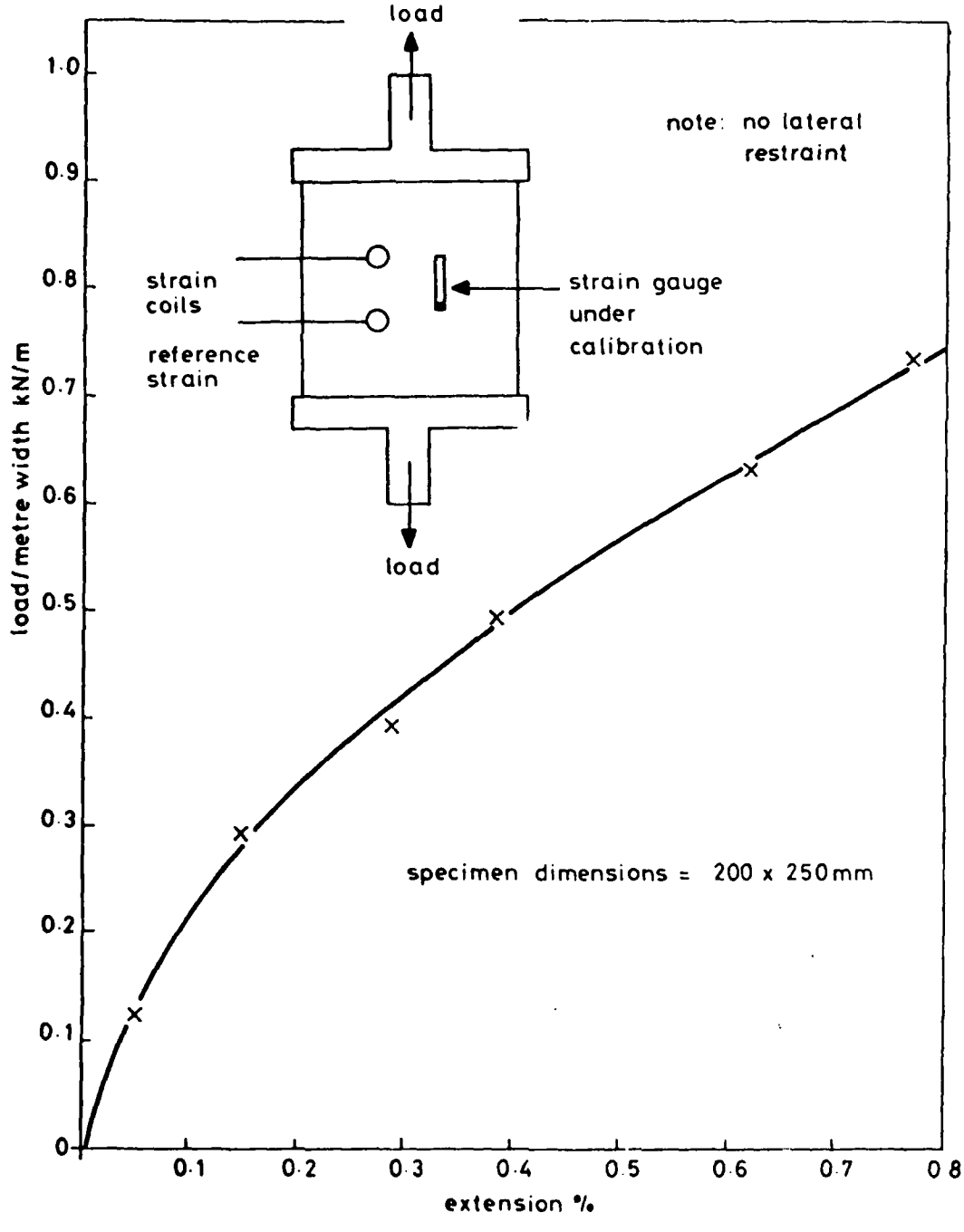


FIG. 3.3 LOAD-EXTENSION CURVE FOR TERRAM 1000

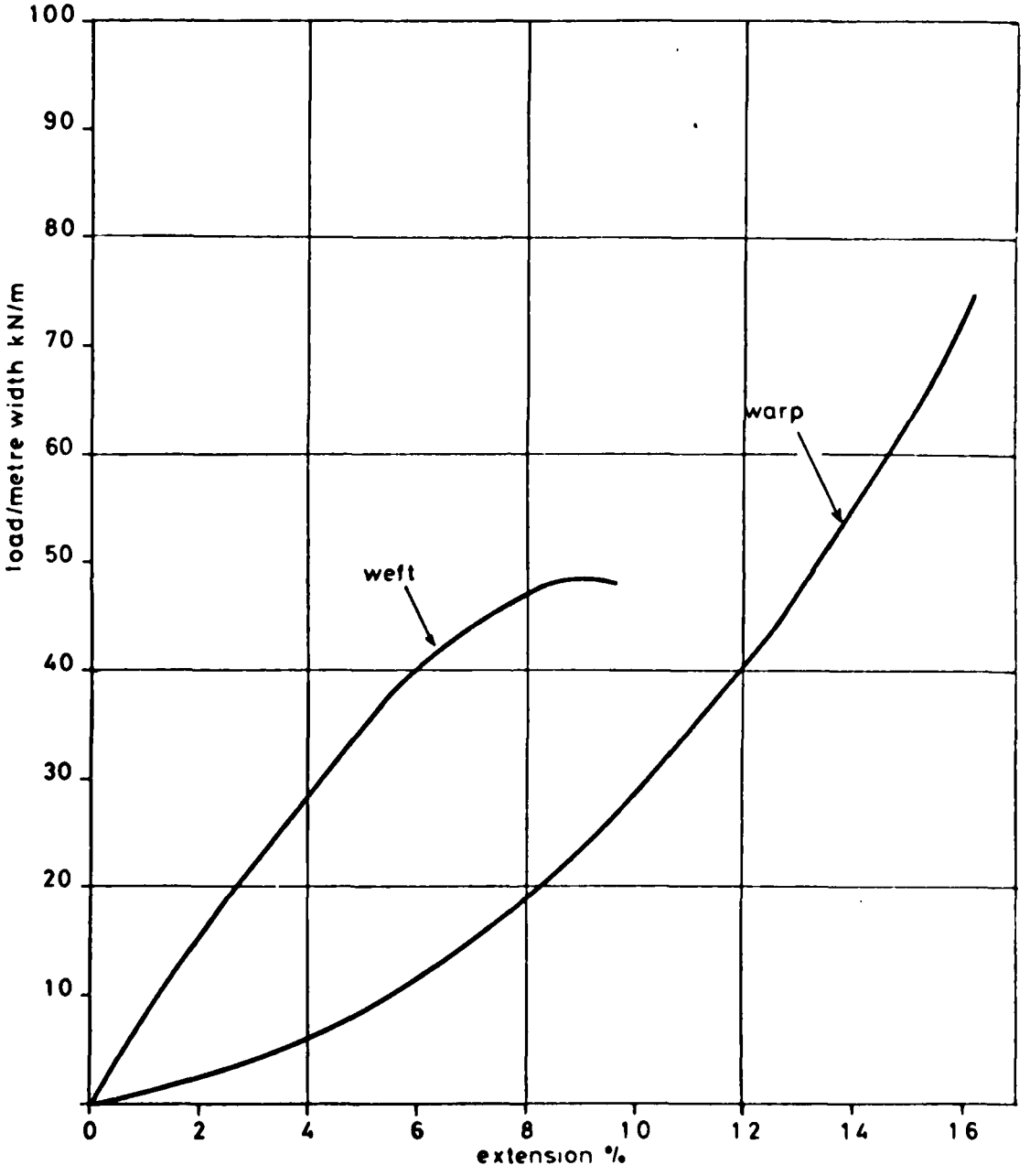


FIG. 3.4 LOAD-EXTENSION CURVE FOR TERRAM 7M7

Two types of fabric manufactured by ICI Fibres Ltd were tested. The first was Terram 1000 which is a melt bonded material comprising 67% polypropylene and 33% polyethylene. Terram 7M7 was also used and this consisted of Terram 1000 reinforced with Terylene yarn (Polyester), chain stitched in the warp direction through the Terram, and over straight laid strands in the weft direction. Fig. 3.3 shows the load extension curve at relatively low strains for Terram 1000 taken from a calibration exercise for strain gauges on the fabric. No such experiment was performed on the Terram 7M7 and the curves in Fig. 3.4 were taken from information supplied by ICI Fibres (20).

## 3.2 PAVEMENT SPECIFICATION

The seven pairs of pavements were arranged in the manner shown by Fig. 3.5. The changes were made so as to achieve repeatability between pairs, only one of which contained fabric, so that direct comparisons could be made. For single pavements this was difficult, because of construction variations so, following testing of the first pair (G1 and GT1), it was decided to operate a parallel arrangement with fabric under one side in an otherwise identical structure. The two halves were considered as separate pavements, i.e. one pair. Experience showed, however, that loading effects in one pavement carried across to the other, and, hence, independent results were not always obtained. The last four pairs were tested in a series arrangement which was more satisfactory, although wheel speed had to be reduced so that the constant speed length of the loading facility could be lengthened. Despite these changes, useful results were obtained from all pavements.

Sections through each pavement and the position and type of fabric are shown in Fig. 3.6. It can be seen that fabric was used in each

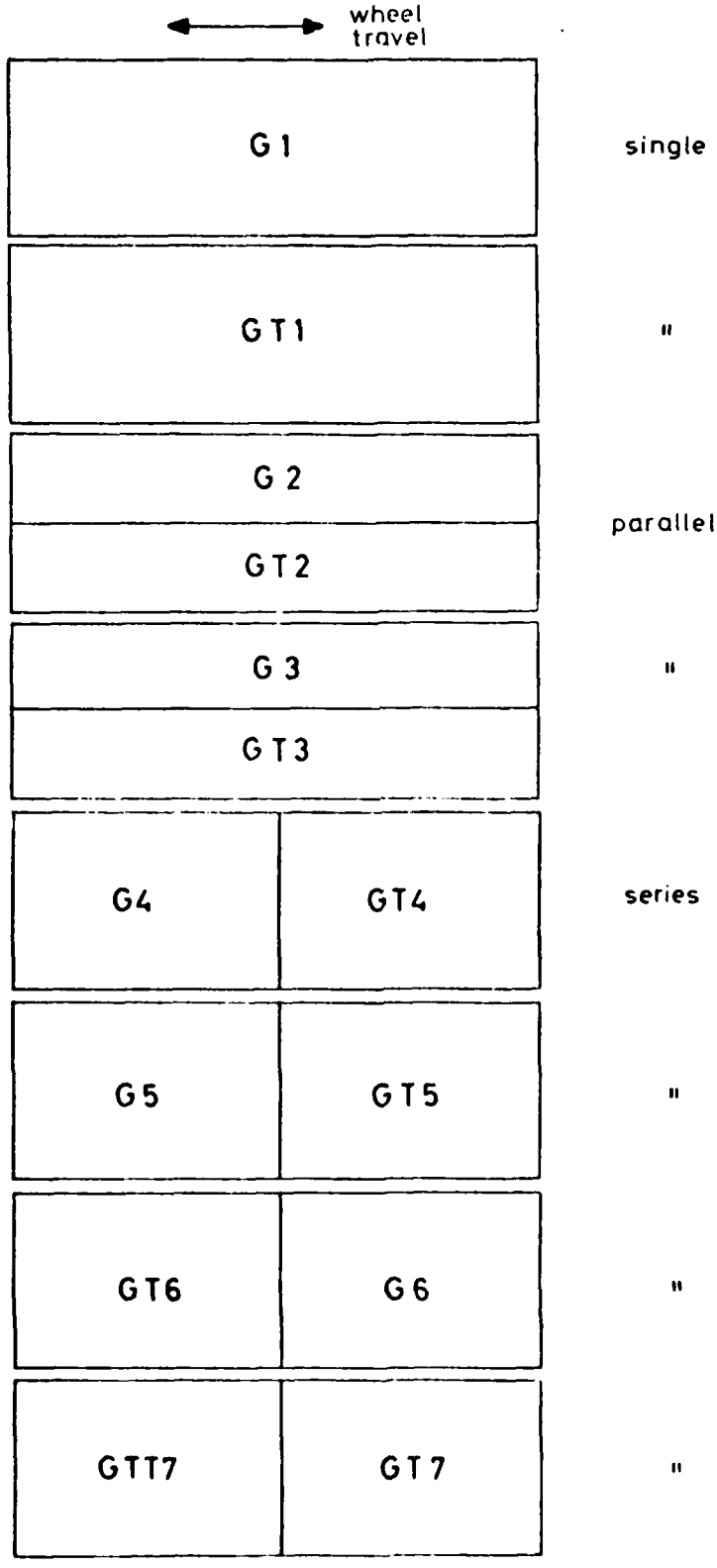


FIG. 3.5 PLAN VIEW OF PAVEMENTS

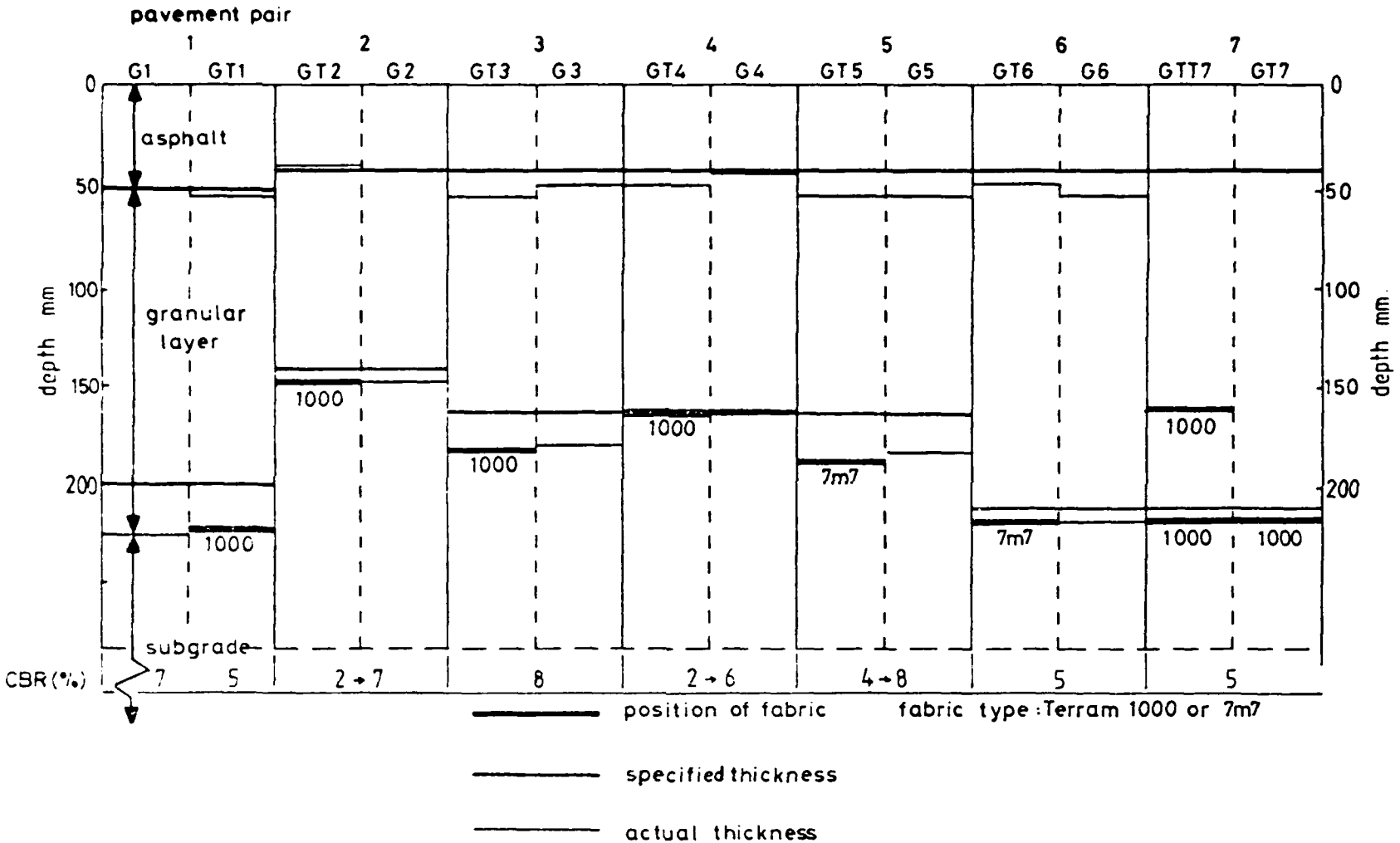


FIG. 3.6 RELATIVE THICKNESSES OF ASPHALT AND GRANULAR LAYERS

half for GTT7 and GT7. The heavy solid line represents the specified construction and the lighter lines indicate the thicknesses actually achieved. A general idea of the relative strengths of each structure can be obtained by considering the layer thicknesses and subgrade CBR's shown in Fig. 3.6. The CBR changed as a consequence of changes in moisture content between one test and the next. Pairs of pavements 1, 6 and 7 were strong, 3, 4 and 5 were medium and 2 was weak.

The basic arrangement of instruments installed in each pavement to monitor performance was similar. Details for each pair are shown in Figs 3.8 to 3.12 with a key provided in Fig. 3.7. The upper half of each diagram represents a longitudinal section through the pavement below the constant speed run of the wheel and a plan is shown in the lower half. All instruments were covered at some stage during each test by the wheel as they were within its lateral traversing range. The vertical and horizontal scales in Figs 3.8 to 3.12 differ, to provide a clearer idea of the layout in the sections. This tends to give the impression of an unacceptable concentration of instruments but this was not the case as care was taken to provide sufficient space to minimize transducer interaction.

A stack of strain coils placed coaxially provided readings of vertical strain at various depths and further coils linked to a driving coil in the main stack monitored horizontal strains at each interface with the coils operating in the coplanar mode. Strain coils and in one case, strain gauges, were attached to the fabric. These were complemented with strain coils above and below the fabric, to establish the extent of the continuity of horizontal strains across this interface. Pressure cells were installed to measure vertical and horizontal transient stresses in the granular layer and subgrade. Thermocouples were positioned to determine the temperature distribution with depth as

The direction of wheel travel on the following diagrams is as shown below:-

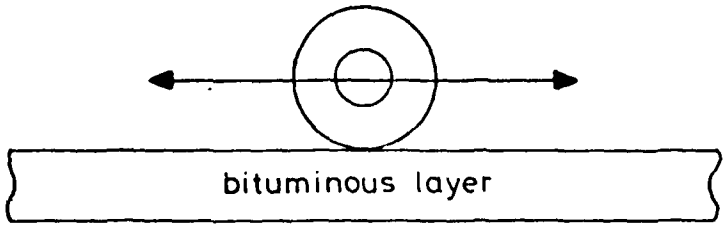


The symbols used on the following diagrams are as follows:-

b = bituminous layer
g = granular layer
s = subgrade

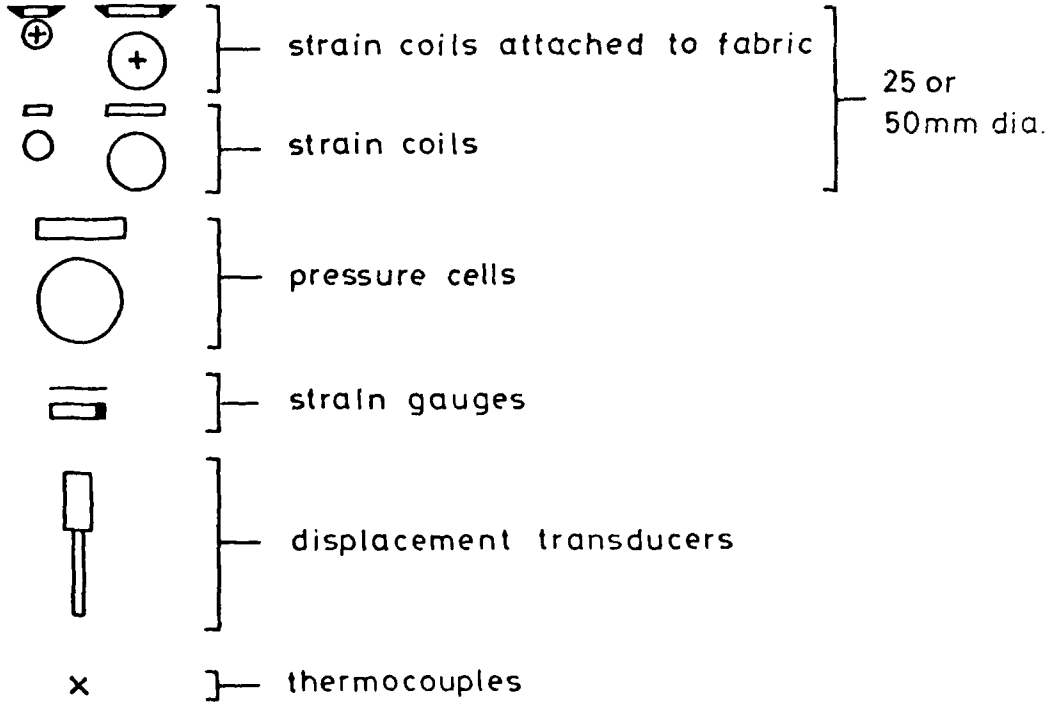


FIG. 3.7 KEY TO INSTRUMENTATION LAYOUT

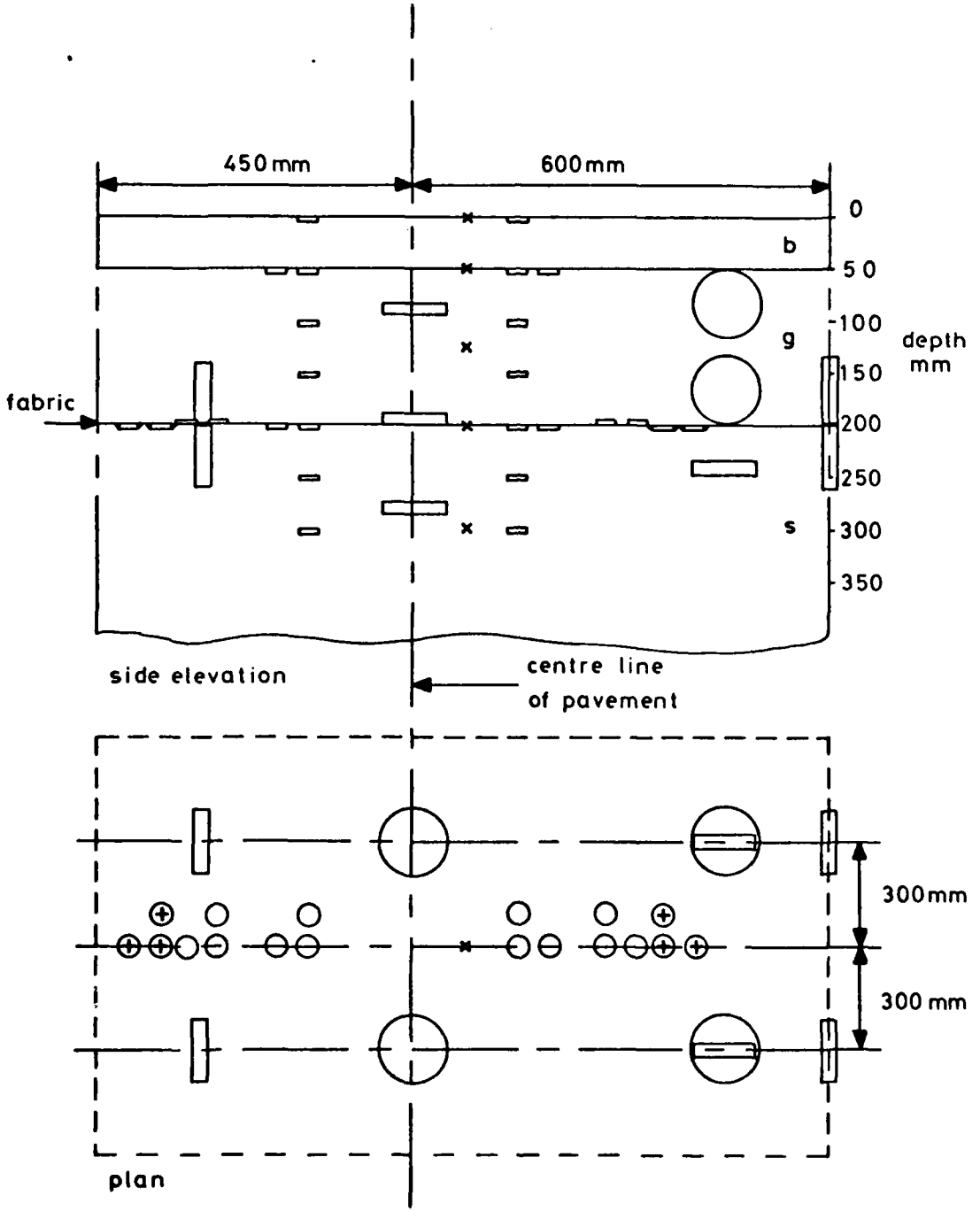


GT1 as shown above

G1 as above less coils attached to fabric

FIG. 3.8 INSTRUMENTATION LAYOUT FOR GT1 AND G1

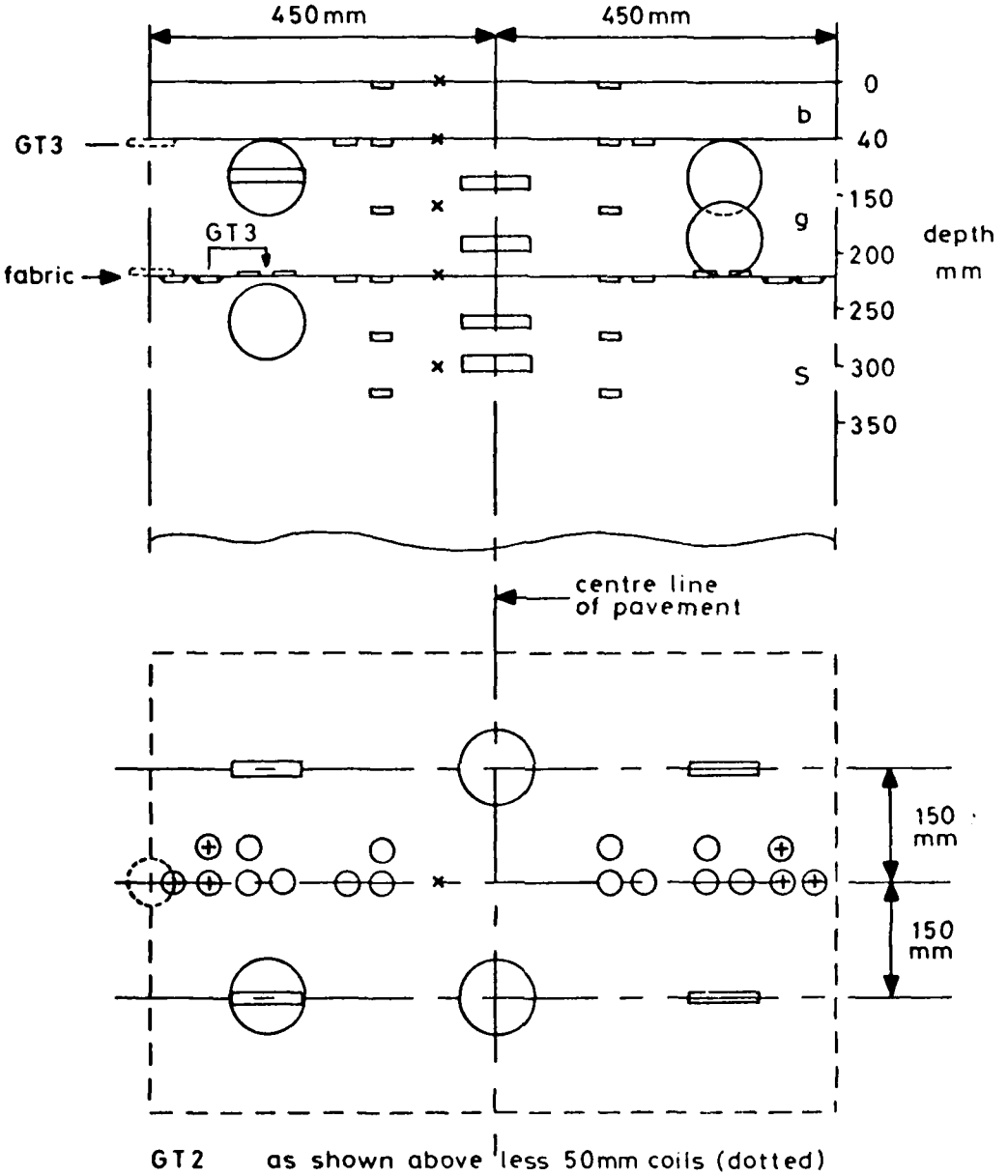


GT2 as shown above less 50mm coils (dotted)

G 2 as above less coils attached to fabric

GT3 50mm coils added (dotted) and coils attached to fabric replacing coils in granular layer for left hand stack

G 3 as above less coils on fabric

FIG. 3.9 INSTRUMENTATION LAYOUT FOR GT2, G2, GT3 AND G3

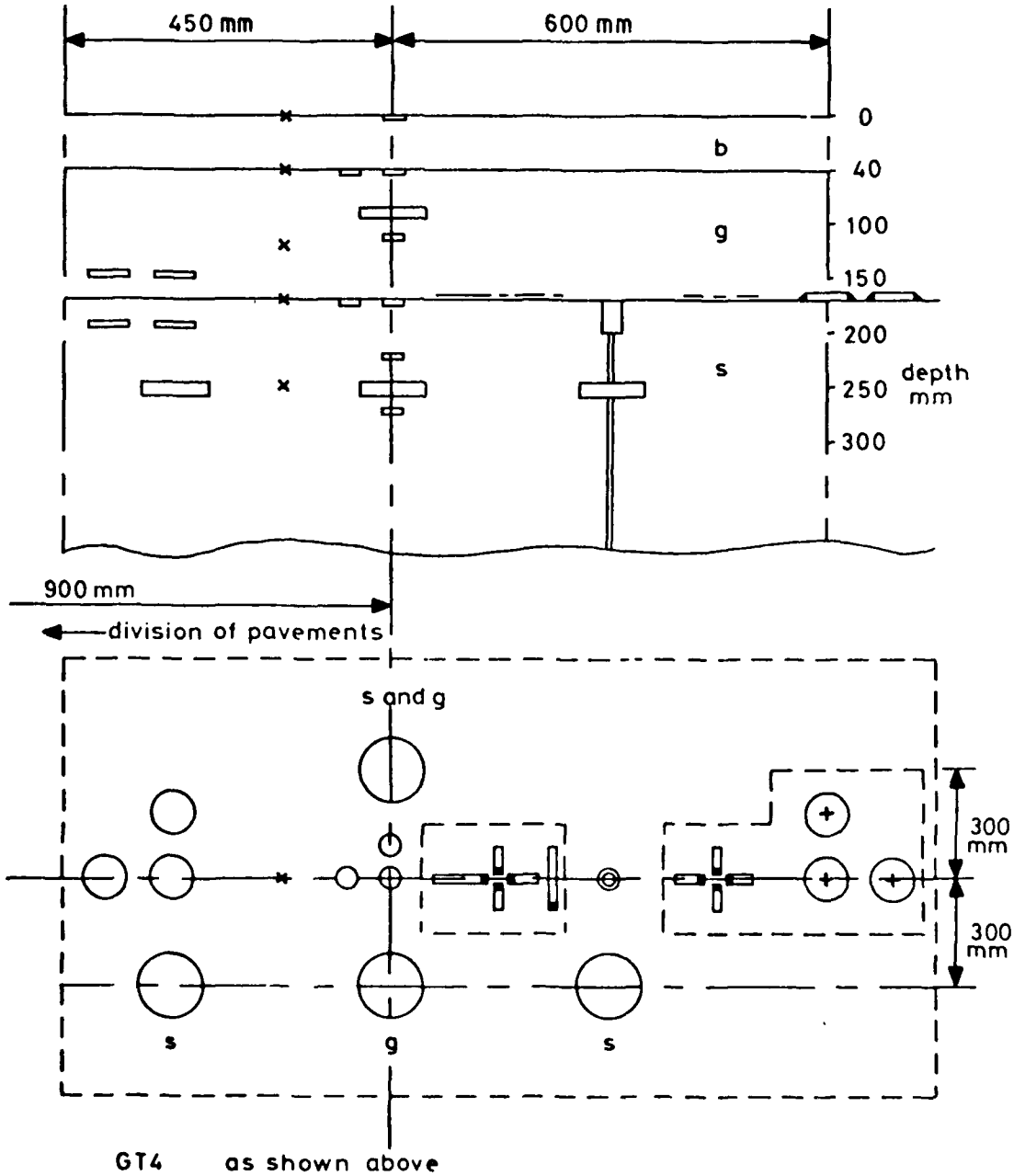


GT4 as shown above

G4 mirror image of above less gauges in inner dotted surrounds

FIG. 3.10 INSTRUMENTATION LAYOUT FOR GT4 AND G4

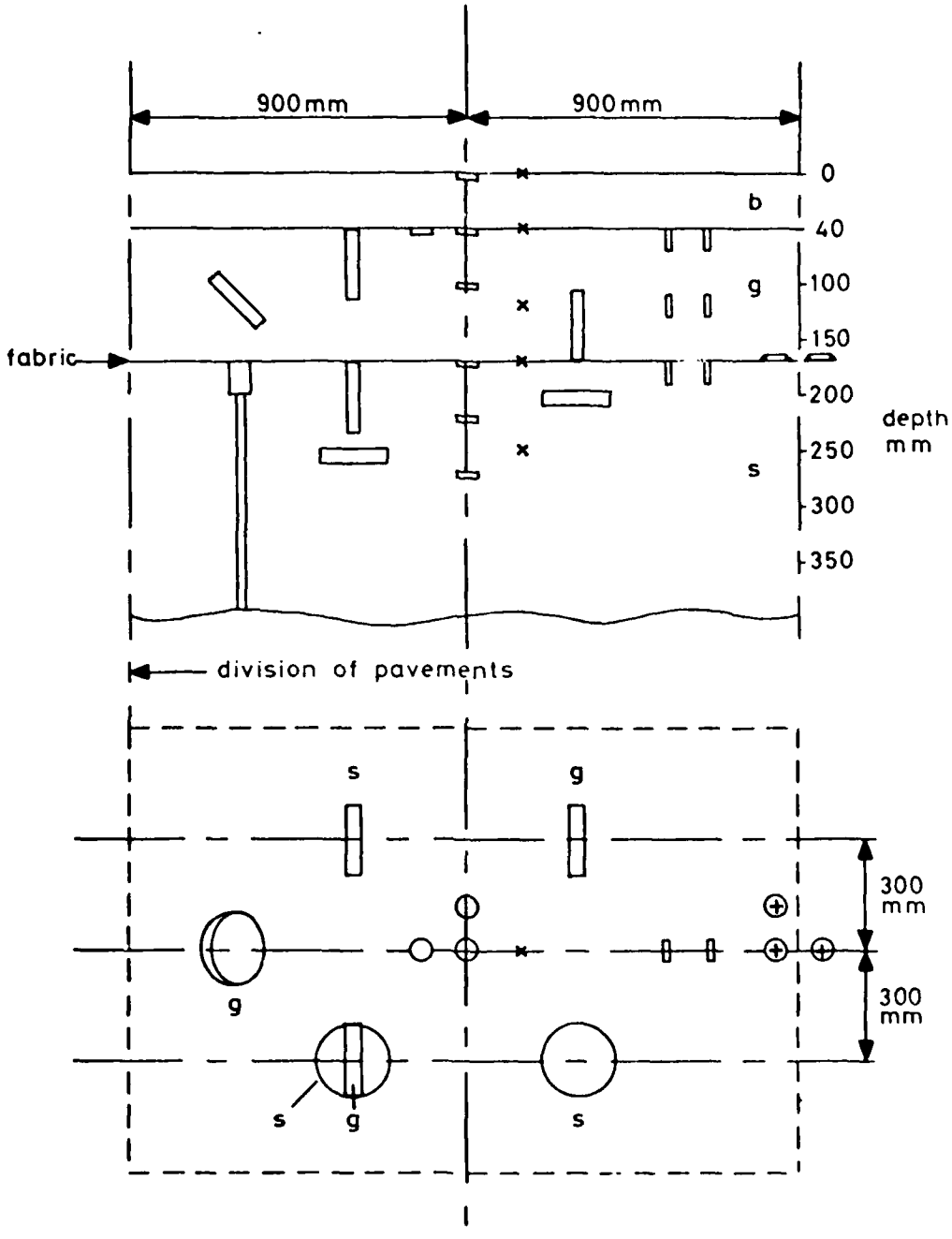


GT5 as shown above

G5 mirror image of above

FIG. 3.11 INSTRUMENTATION LAYOUT FOR GT5 AND G5

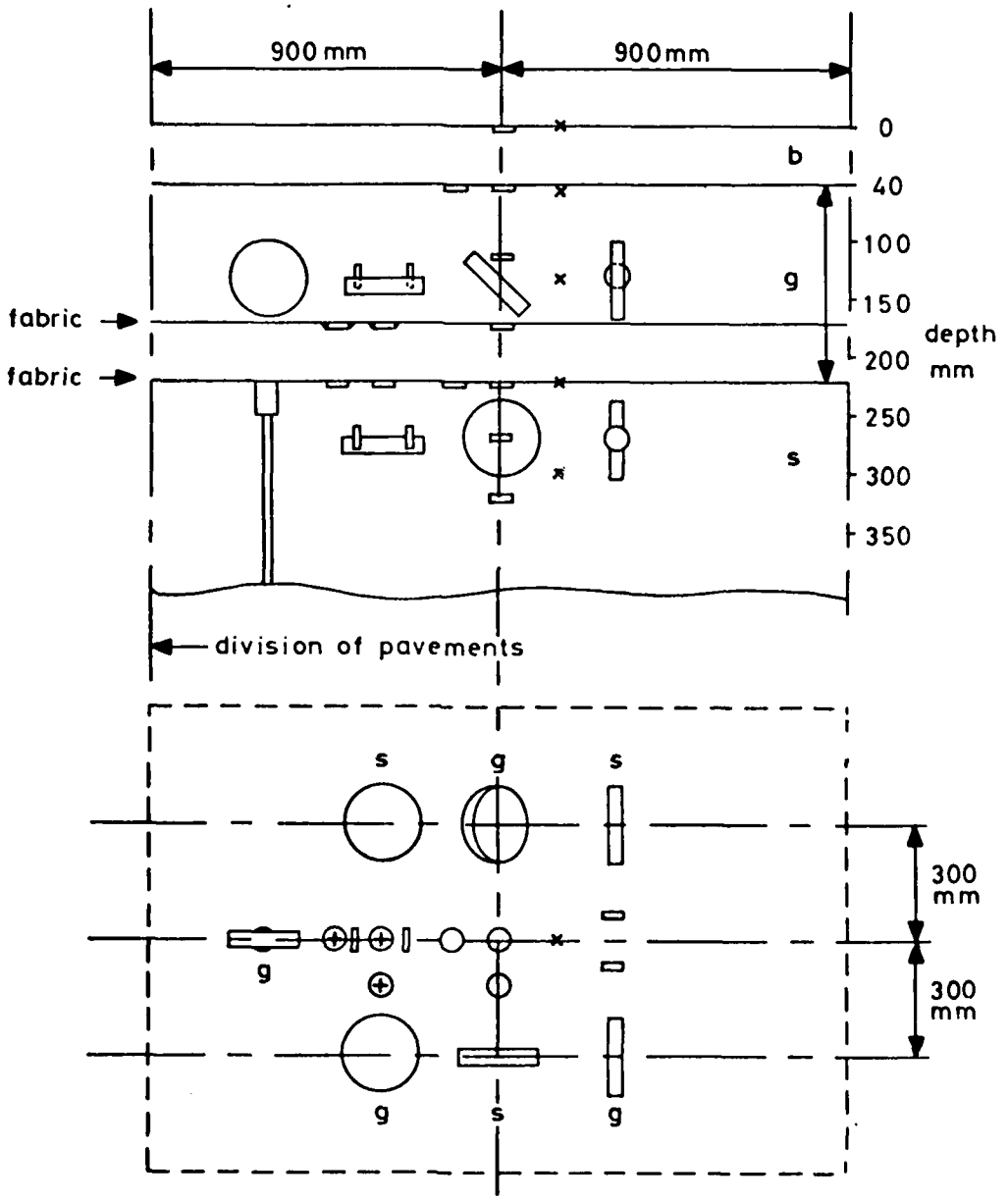


GTT7 as shown above

GT7 and GT6 fabric on subgrade

G6 *no fabric*

instrumentation for GT7 and G6 mirror image of above

FIG. 3.12 INSTRUMENTATION LAYOUT FOR GTT7, GT7, GT6 AND G6

equilibrium of this parameter was required prior to testing.

Information from the instruments was required to provide validation data for the theoretical analyses and to indicate the in situ behaviour of the fabric. Decisions on the positions of the instruments were related to these requirements which, fortunately, were complementary. Pavements GT4 and G4 (Fig. 3.10) had arrangements which were specifically designed to examine the performance of the fabric by using pressure cells installed to measure vertical stresses only, with some emphasis on the subgrade as it was felt that the presence of the fabric would reduce this parameter if the granular layer was being appreciably stiffened. This pair of pavements also incorporated strain gauges and coplanar 50 mm coils attached to the fabric instead of the usual coplanar 25 mm coils which sometimes had a tendency to tilt during compaction. Displacement transducers measuring the subgrade surface deflection were also introduced and used in subsequent pavements. A coaxial arrangement of coils for measuring horizontal strains was introduced for pavements 5 (Fig. 3.11) and used subsequently as an alternative to the coplanar alignment in an attempt to provide more accurate measurements.

An important aspect of pavement instrumentation technique is to obtain replicate measurements in order to verify transducer readings. This was possible for the strain coils shown in pavement pairs 1 to 3, i.e. the single and parallel pavements (Figs 3.8 and 3.9). In the case of the pavement pairs in series and for the pressure cells in general, duplication of instruments was difficult because of limited space. Fortunately, previous experience (1,12) could be called on to reduce errors arising from installation techniques. Furthermore, confirmation of the final strain coil readings was provided by physical measurements of their spacing made during excavation, and by simulating their elastic

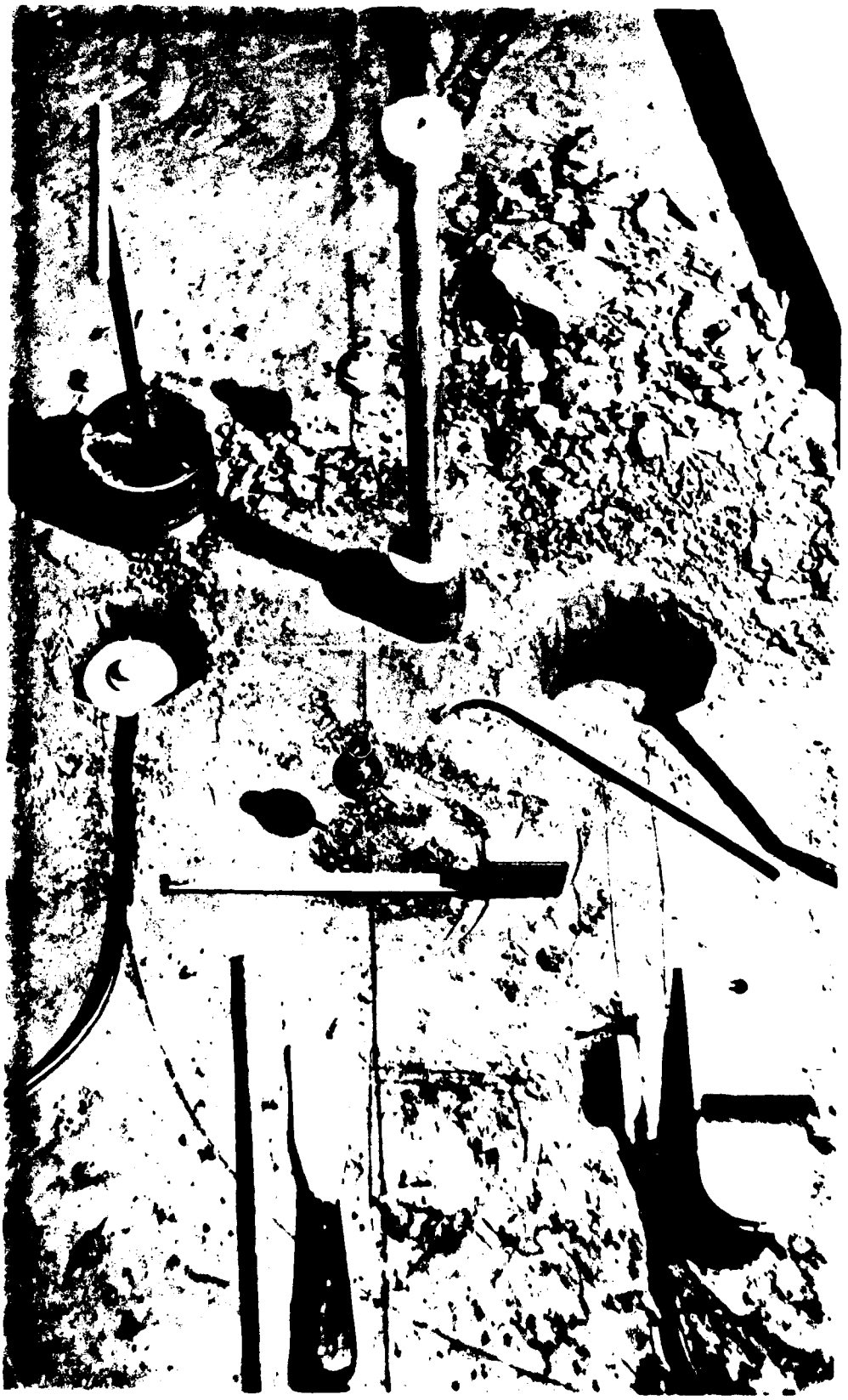

FIG. 3.13 INSTALLATION TOOLS

response on a calibrator. A discussion of the installation techniques follows as an integral part of the next topic.

## 3.3 PAVEMENT CONSTRUCTION

The clay subgrade had been installed previously (1) as layers of wet bricks in a waterproofed concrete lined pit 4.9 m long, 2.4 m wide and 1.5 m deep. A triple legged pneumatic tamper was used to compact each layer and this had enough energy to destroy the brick interfaces. The final level was dependent on the thickness of the granular and bituminous layers as it was convenient to finish the pavement flush with the top of the pit. New, softer clay was introduced for pavement pairs 2 and 4 replacing a 0.5 m depth of the original clay which had partially dried out. It is important to scarify between layers to improve the bond and also achieve a level finish as this will affect the control of the level of subsequent layers.

Pressure cells and coils were placed in holes in the clay which were cut with special tools, shown in Fig. 3.13, designed to ensure minimum disturbance around the instruments. Excavated soil was tamped in layers round the instruments and the holes and layer surfaces were scarified as installation proceeded. A much deeper, small diameter, hole was required for the deflectometer and this was cored with a sharpened polished steel tube to a depth of 0.92 m. A greased rod with a coarse threaded end was placed in this clearance hole and screwed firmly into the clay at its base. This datum was considered to be remote from the loading effects of the wheel so that the displacement transducer attached to the upper end of the rod could provide a measure of the subgrade surface deflection. The core of the LVDT was attached to the reference rod and the body keyed into the soil with the aid of an annular ring screwed to it.

A copper-constantan thermocouple was set in a small hole, 150 mm deep and a second one was laid on the subgrade surface. The fabric was rolled across the subgrade and, in the case of the pavements in series, pinned down across the lateral centre line. It was slightly oversize and was folded up at the pavement edge. Any coils or strain gauges which were to be attached to the underside of the fabric were glued in position with the fabric rolled back or placed on the subgrade with the adhesive at the tacky stage and the fabric rolled over them. This latter technique was only suitable for coils but it was necessary to lightly glue them to a piece of Terram 1000 initially in order to retain their alignment. In fact, each gauge and coil was covered with a piece of fabric for protection and the elimination of artificial interlocking with the subgrade or granular material in the case of the coils. Hence, the same surface texture was in contact with the adjacent pavement materials although there may have been some local stiffening from the double thicknesses of fabric. Strain coils were glued with "Araldite Rapid" epoxy resin and the strain gauge adhesive was M bond 200 methyl-2-cyanoacrylate (Micro Measurements), Fig. 3.14. The fabric was pinned to the subgrade across the lateral centre line for pavements 4, 5, 6 and 7 as shown in Fig. 3.15 using some purpose-made staples. Dry crushed limestone was then placed in either two or three layers for the thinner and thicker constructions respectively.

The dry material was delivered as coarse and fine mixes with the grading split halfway by mass at the 10 mm particle size. This was to limit separation of the aggregate during transport in the dry state. Coarse material was placed first in a full width section of about 0.75 m length. The same weight of fines was then placed over this to a constant depth set by a straight edge. This procedure was continued until the

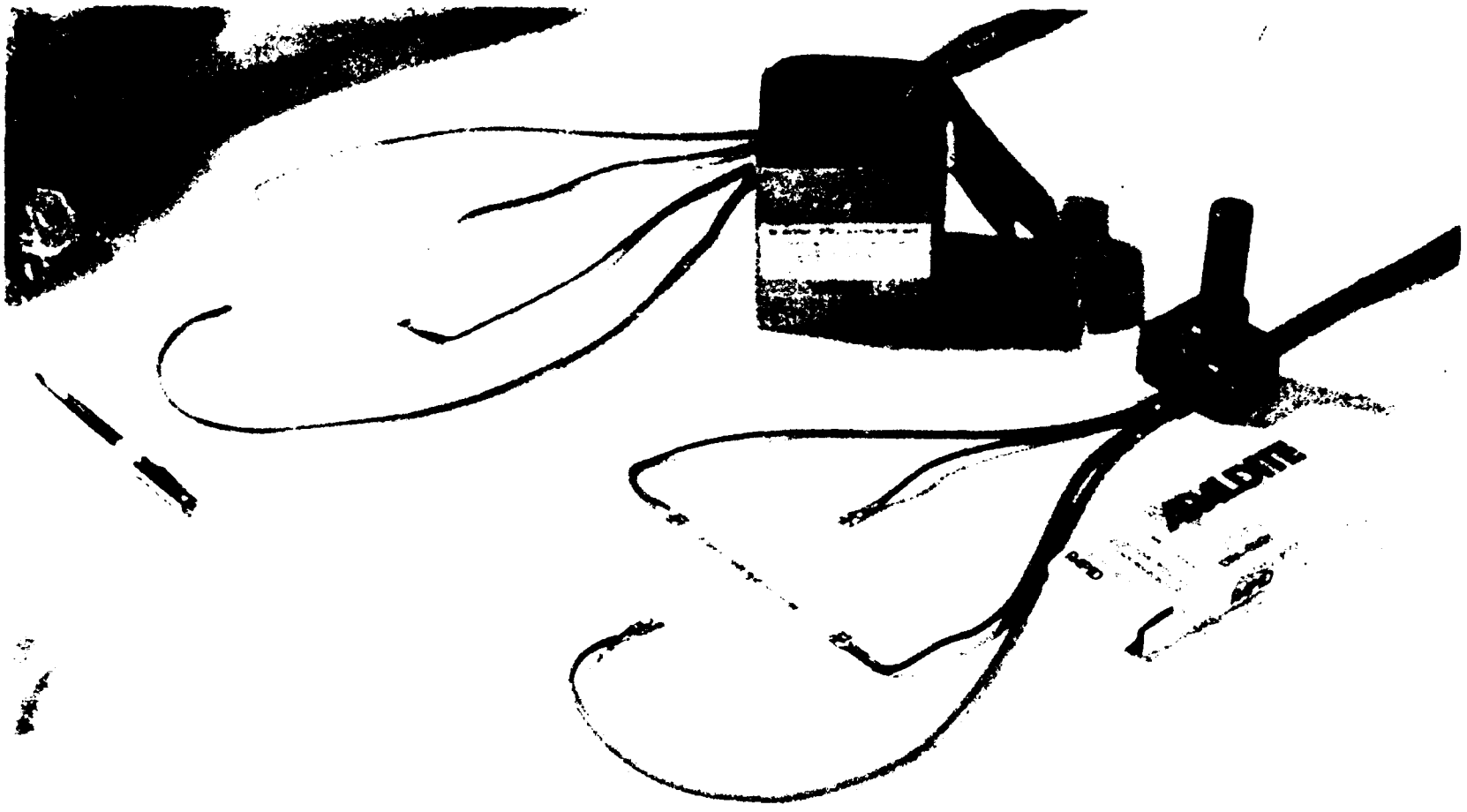

FIG. 3.14 STRAIN GAUGES ATTACHED TO TERRAM 1000

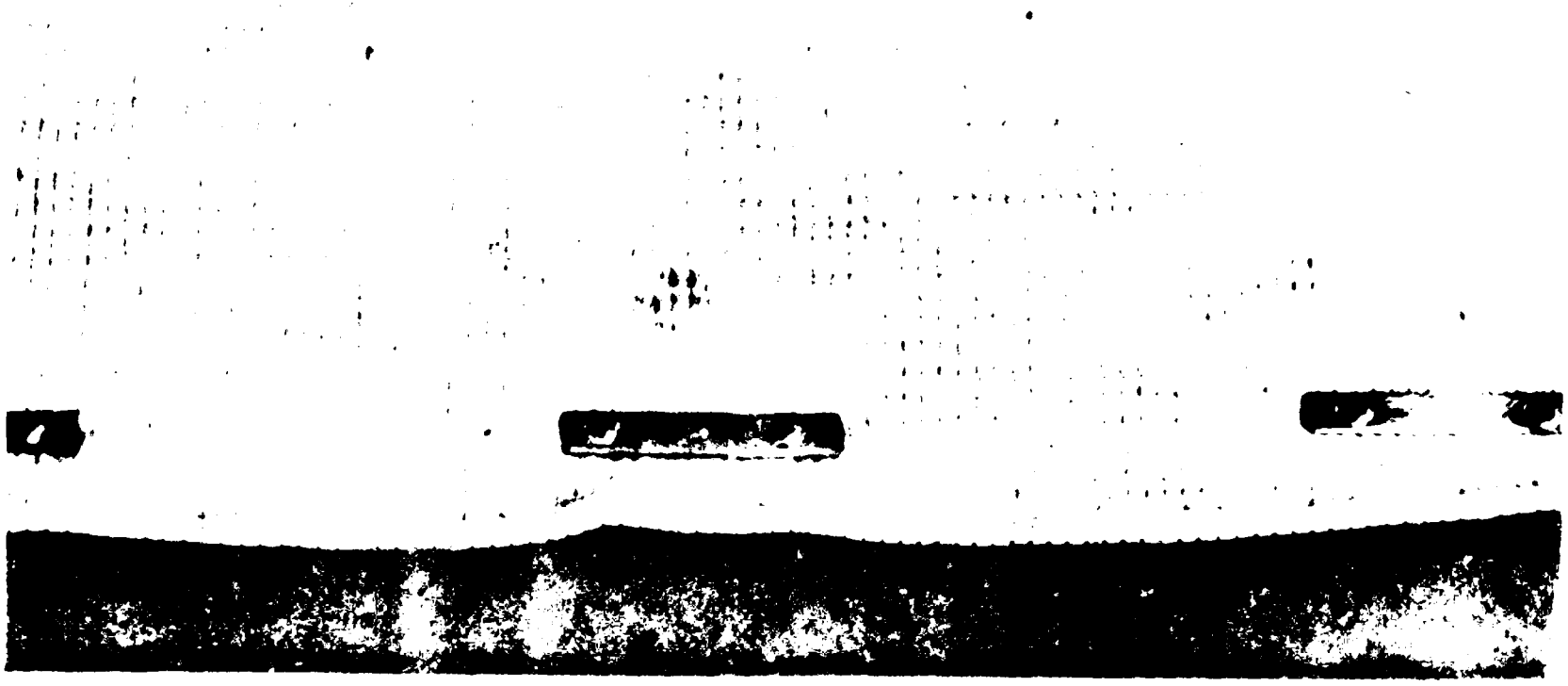

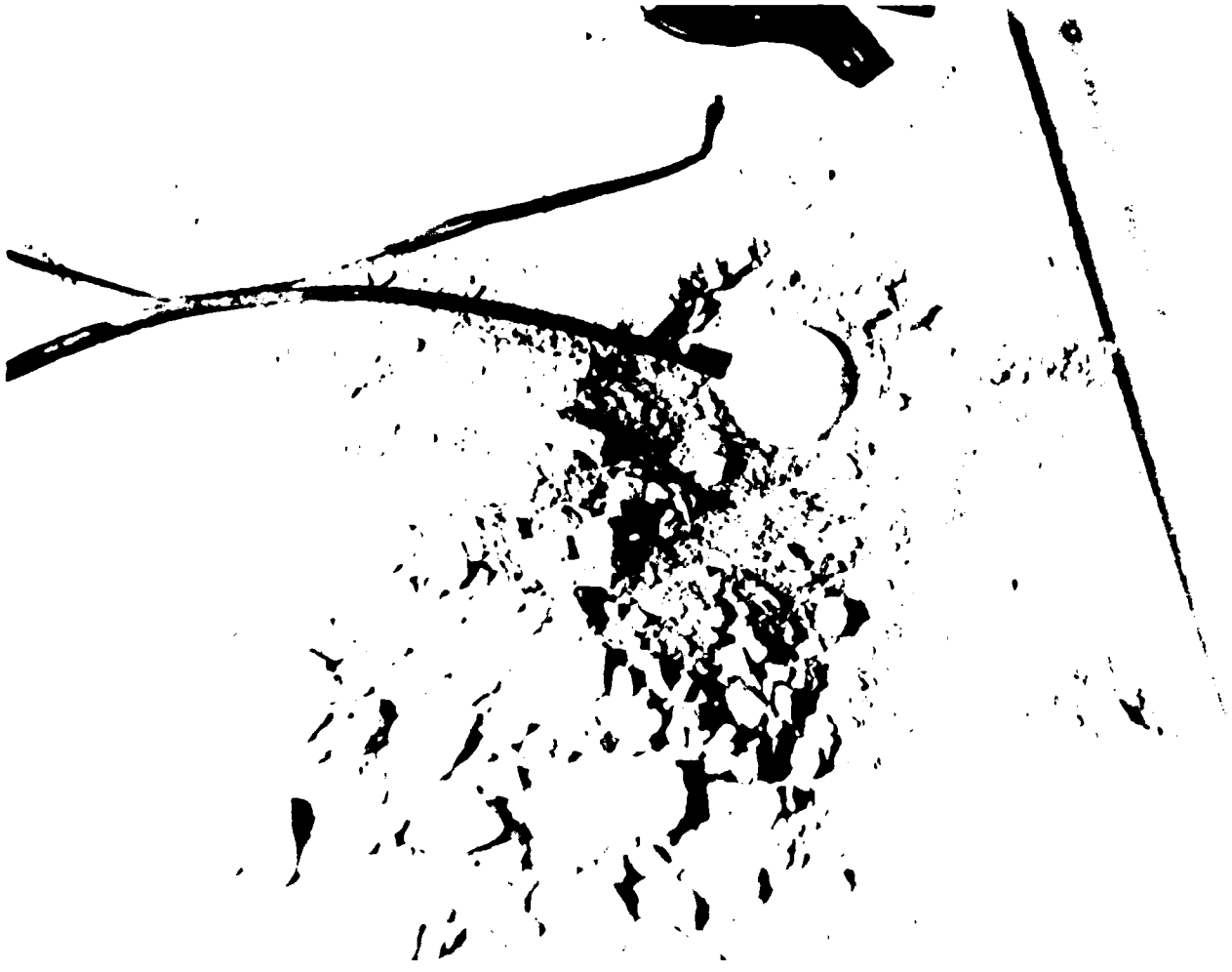

FIG. 2.16 INSTALLATION OF PREPACKED PRESSURE CELL IN GRANULAR LAYER

full depth of the subgrade was covered. A 380 kg pedestrian vibrating roller was used to vibrate the fines into the coarse matrix. It was found from a previous trial that 10 passes were sufficient to achieve a satisfactory level of compaction, and this was usually indicated by the inability of the surface fines to penetrate further into the compacted material.

Holes were excavated at the pressure cell locations, Fig. 3.16, and the cells were placed in a prepacked condition with fine material having particles no larger than 1/50 of the diaphragm diameter held in position over the diaphragm with thin plastic film. A quantity of fines was then tamped around the instrument and excavated material was used to complete the installation. It is recognised that this procedure may introduce a local reduction in the granular material stiffness but calibration exercises on the pressure cell in a 230 mm diameter triaxial specimen of the crushed limestone at low confining stresses, indicated that this technique led to a true representation of the in situ stress, Fig. 3.17. The procedure is described elsewhere (12). A reduction in the measured output occurred as the confining stress was increased but the calibration conditions shown in Fig. 3.17 are compatible with the pavement tests.

Strain coils were also positioned in or on selected fines, depending on their orientation, in order to more easily control their alignment. This was initially accomplished with plumb lines (Fig. 3.18) and, more precisely, by obtaining a maximum output from the Bison instrument as the coil was moved to its optimum position.

Compaction of further material and instrument installations were continued until the granular layer was complete. For the last two pairs of pavements the limestone was placed moist and it was thus not

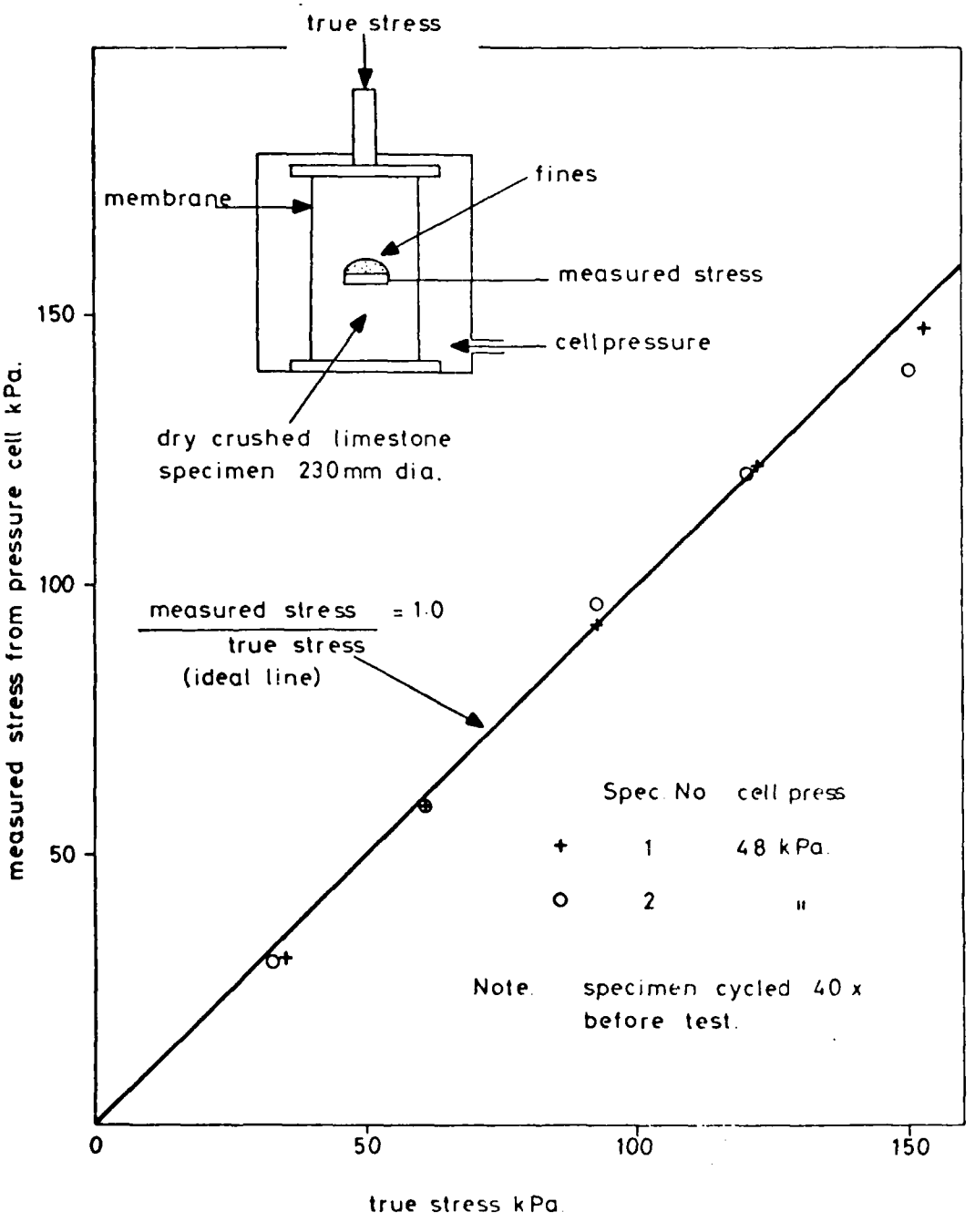


FIG. 3.17 CALIBRATION OF PRESSURE CELL IN CRUSHED LIMESTONE SPECIMEN

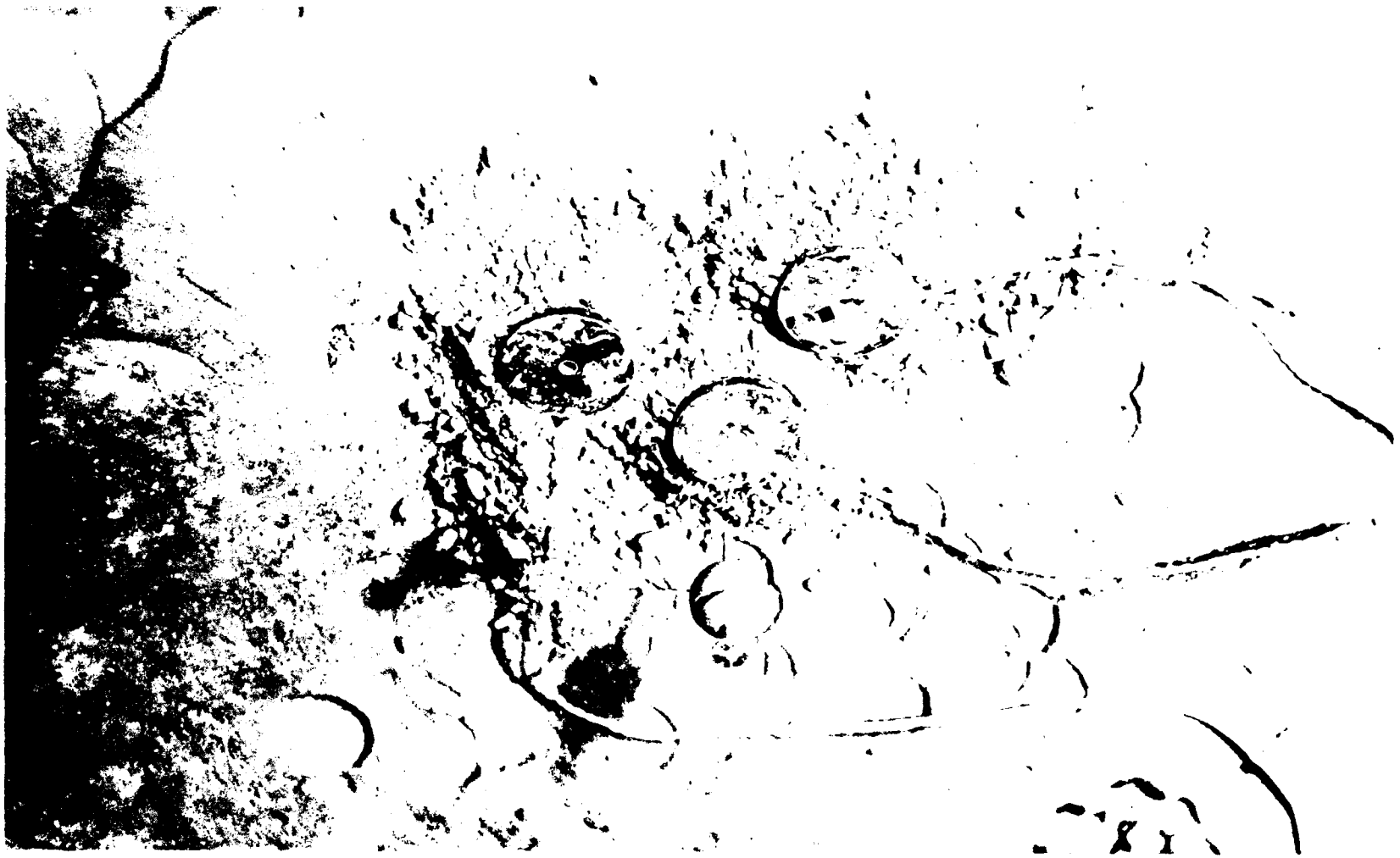

necessary to split the grading. Coils placed on top of the granular layer were covered with a fine hot asphalt mix (sandsheet with 8% binder content).

When the bituminous mix arrived, any exposed cables were covered with carefully selected hot mix from which relatively large aggregate was removed. This was particularly necessary for the basecourse mix used in the first pair of pavements. Tarmac Roadstone Limited kindly supplied and laid this layer as laboratory mixing facilities could not cope with the required quantity, and their expertise ensured a reasonable consistency of thickness and compaction. The same pedestrian vibrating roller was used as for the base, the first pass being without vibration. When the material had cooled, the final strain coils were let into the surface, glued in position with Araldite epoxy resin, and their associated cables run out through shallow trenches cut into the asphalt. These cables were sealed with hot sandsheet.

## 3.4 FINAL STRUCTURES

The data in Fig. 3.6 shows that the finished pavement thicknesses were not exactly as specified. This was a result of difficulties in judging the amount of material necessary to achieve a certain final thickness. However, this did not affect the required variation in pavement strengths which was required.

Table 3.2 has been compiled in order to summarise the compacted state of all materials in each pavement. Details of the wheel loads are also included. For all tests, the inflation pressure of the tyre was 530 kPa, though the actual contact pressure varied somewhat with the applied load. The wheel speed was 14.5 km/hr for pavement pairs 1 to 3 but was reduced to 8 km/hr for the remainder. All tests were performed at 25$^{o}$C.

## Table 3.2 Details of pavement materials

| Pavement No. | Wheel load (kN) | Subgrade | | | | | | Limestone Base | | | | | Rolled Asphalt | | | |
|---|---|---|---|---|---|---|---|---|---|---|---|---|---|---|---|---|
| | | CBR (%) | | w (%) | | $\rho$ | $\rho_d$ | $\rho$ | $\rho_d$ | w (%) | | h | $\gamma_m$ | $M_B$ | $V_V$ | h |
| | | before | after | before | after | ($kg/m^3$) | | ($kg/m^3$) | | before | after | (mm) | ($kg/m^2$) | (%) | (%) | (mm) |
| GT1 | 11 | 5 | - | 16.1 | - | 2160 | 1860 | 1965 | | 0 | - | 170 | 2310 | 5.1 | 6.1 | 52 |
| G1 | | - | 7 | - | 14.5 | 2190 | 1910 | 1890 | | 0 | - | 174 | 2030 | 5.3 | 8.5 | 50 |
| GT2 | 11 | 2 | 7 | 16.3 | 14.4 | 2090 | 1800 | 1860 | | 0 | 1.3 | 110 | 2180 | 7.0 | 5.8 | 37 |
| G2 | | | | | | | | 1950 | | 0 | 1.5 | 107 | 1980 | | 5.8 | 40 |
| GT3 | 8 | 8 | | 14.4 | | 2135 | 1867 | 2072 | | 0 | 0.5 | 128 | 2020 | 6.8 | 4.3 | 53 |
| G3 | | | | | | | | | | 0 | 0.4 | 131 | 1810 | | 4.6 | 46 |
| GT4 | 5 | 2 | 6 | 21.0 | 19.2 | 2018 | 1668 | 1980 | | | | 117 | - | 8.1 | 8.2 | 47 |
| G4 | | | | | | | | 1944 | | | | 122 | | | 9.6 | 41 |
| GT5 | 8 | 4 | 8 | | 18.2 | 2090 | 1750 | | | | | 135 | - | 7.9 | 7.7 | 52 |
| G5 | | 4 | 8 | | 19.2 | 2070 | 1753 | | | | | 130 | - | | 7.5 | 52 |
| GT6 | 8 | 5 | 5 | | 19.8 | 2082 | 1738 | 2103 | 2038 | 4.4 | 2.0 | 171 | - | 7.9 | 5.2 | 51 |
| G6 | | | | | 18.5 | 2079 | 1754 | 2223 | 2154 | 4.4 | 2.0 | 164 | | | | 49 |
| GTT7 | 8 | 5 | 6 | | 20.2 | 2067 | 1720 | 2314 | 2210 | 4.7 | 2.6 | 170 | 2150 | 7.9 | 9.6 | 38 |
| GT7 | | | | | 19.0 | 2102 | 1766 | 2118 | 2022 | 4.7 | 2.6 | 175 | | | | 44 |

$\rho$ = bulk density  w = moisture content  $\gamma_m$ = mix density from Troxler  $M_B$ = binder content

$\rho_d$ = dry density  h = layer thickness  $V_V$ = void content

All the information on the subgrade in Table 3.2 was taken from CBR cores with supplementary samples taken to confirm the moisture content readings. The moisture content at the end of one test can be assumed to be equal to the moisture content at the start of the next. Where new clay was added, the moisture content at the beginning and end of each test is given. This applies to pavements 2 and 4 which were deliberately weakened by a replacement layer of softer clay. The reduction in CBR was a direct result of this change, but for other pavements the difference in CBR between the end of one test and the beginning of the next was due to the trimming of the subgrade surface, the top of which hardened during a test as a result of moisture migration into the limestone. This indicates that the top 25 mm of the subgrade is most sensitive to the drying out process and this was not reflected in the moisture content samples which were taken from below this level. The introduction of the moist limestone in pavement 6 appeared to stabilise this situation. The bulk densities are the means from three cores in each case, with little variation being noted.

A Troxler Nuclear Density Meter was used to obtain the bulk density readings for the granular layer. This is equivalent to the dry density for the dry crushed limestone. It was hoped that the compaction of this layer would be improved by the presence of the fabric, but no such trend emerged. A greater number of readings was taken from Pavement GT6 onwards when a meter was made available for continuous use by Mobil Oil Co. Ltd. This gave scope for variations in technique aimed at improving the accuracy of the measurements. Some moisture contents were measured in the dry granular layer during excavation and indicated a significant movement of moisture from the subgrade. The reverse appeared to occur for the wet limestone (Pavements 6 and 7). The presence of fabric did not affect this moisture migration.

Density measurements for the bituminous layer are likely to be more reliable as the surface texture was more consistent and the layer thickness was compatible with the depth of material which the instrument can operate on. The asphalt density values quoted in Table 3.2 all came from measurements with the Troxler meter, while the void contents were calculated from the weighing of cores. The discrepancies indicate that techniques for using the nuclear density meter need further development or that insufficient measurements were taken. The void contents are considered rather high for rolled asphalt; figures in the range 3 to 5% would be expected normally. These high voids may be attributable to the condition of the cores extracted from the bituminous layer as this was considerably pitted by the granular material and the cores were too short to trim. Specified binder contents for the basecourse and wearing course were 5.7% and 7.9% respectively with an allowable variation of ±0.6%. Hence, only pavements 2 and 3 could be considered out of specification in this respect.

The reduction in wheel load for pavements 3 arose as a result of the premature failure of the previous pair which had a low initial subgrade CBR (2%). A nominal 8 kN load was then introduced, but this was reduced to 5 kN for pavements 4 as these also had a low initial subgrade CBR. The reduction in speed was necessary to increase the length of the constant speed run for the series arrangement of pavements.

# CHAPTER FOUR

# PAVEMENT TEST PROCEDURE

After each pavement had been constructed, a grid was marked out on the surface as shown, for the various configurations, in Fig. 4.1. Initial measurements were taken at all the node points using the profilometer (Fig. 2.10) and all the instruments were zeroed when the pavement temperature had reached 25°C.

## 4.1 THE LOADING PROGRAMME

Table 4.1 summarises the loading programme, indicating the increase in wheel passes at nine positions at 75 mm spacing across the pavement for the single and series pavements while five positions were used for the parallel pavements. Two histograms have been plotted in Fig. 4.2 to indicate the lateral distribution of accumulated wheel passes across the pavements intended to simulate the wheel path variation of real traffic. The lateral increments allow for a 50% overlap of the tyre contact width. The loaded contact area approximates to a 150 mm diameter circle. It is, however, slightly elliptical but of the same area at 8 kN load while at 11 kN, the area is somewhat greater.

The first two pairs of pavements were tested at 11 kN (Table 3.2). This resulted in premature failure of the second pair (GT2 and G2) which were weak structures and the number of load applications for these pavements are shown by the dotted line in Fig. 4.2.

The load and velocity were set through the electronic control system by means of calibrated potentiometers and the number of passes for each lateral position was programmed into the traverse control. Automatic loading was then switched on and a traverse of all the lateral positions in the sequence shown at the bottom of Table 4.1 was completed, giving the

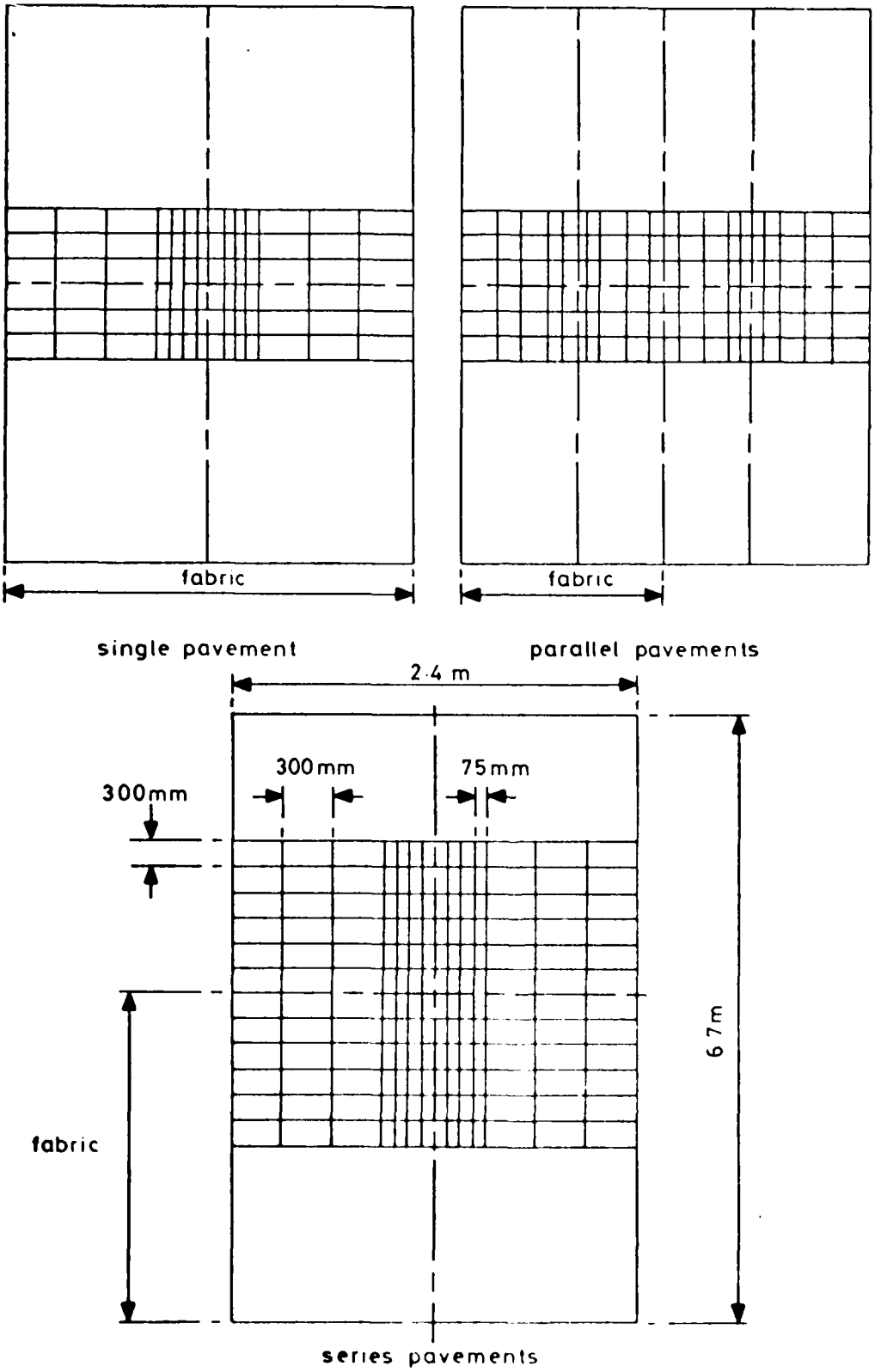


FIG. 4.1 GRID SYSTEMS FOR SURFACE DEFORMATION MEASUREMENTS

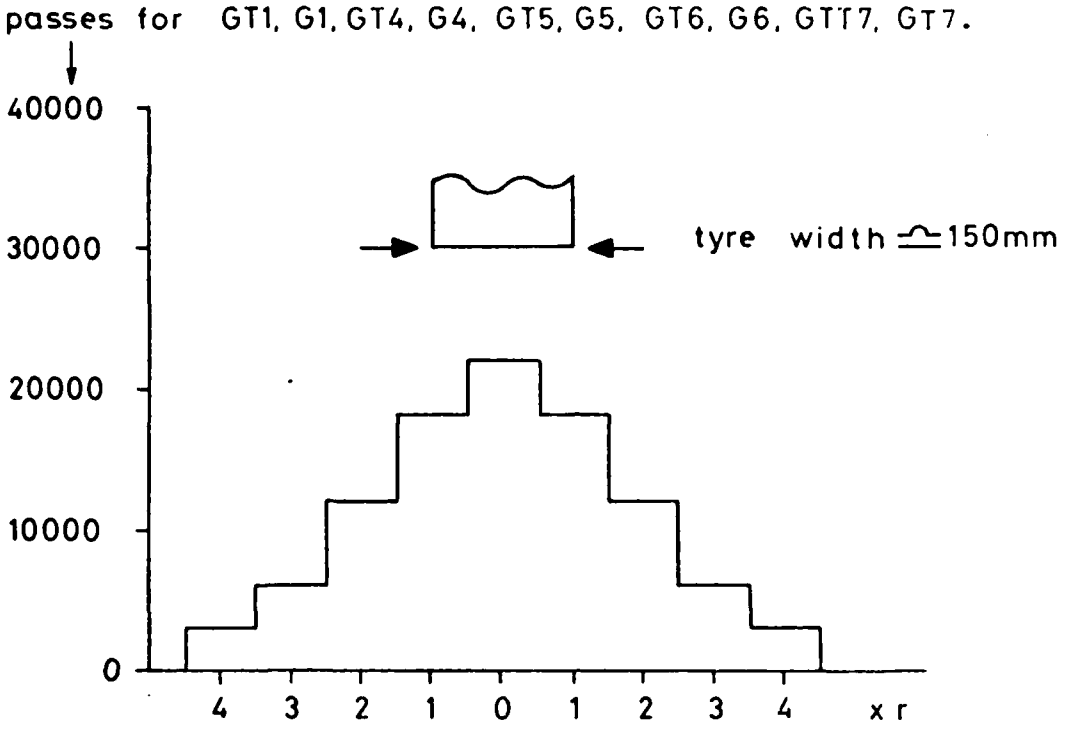


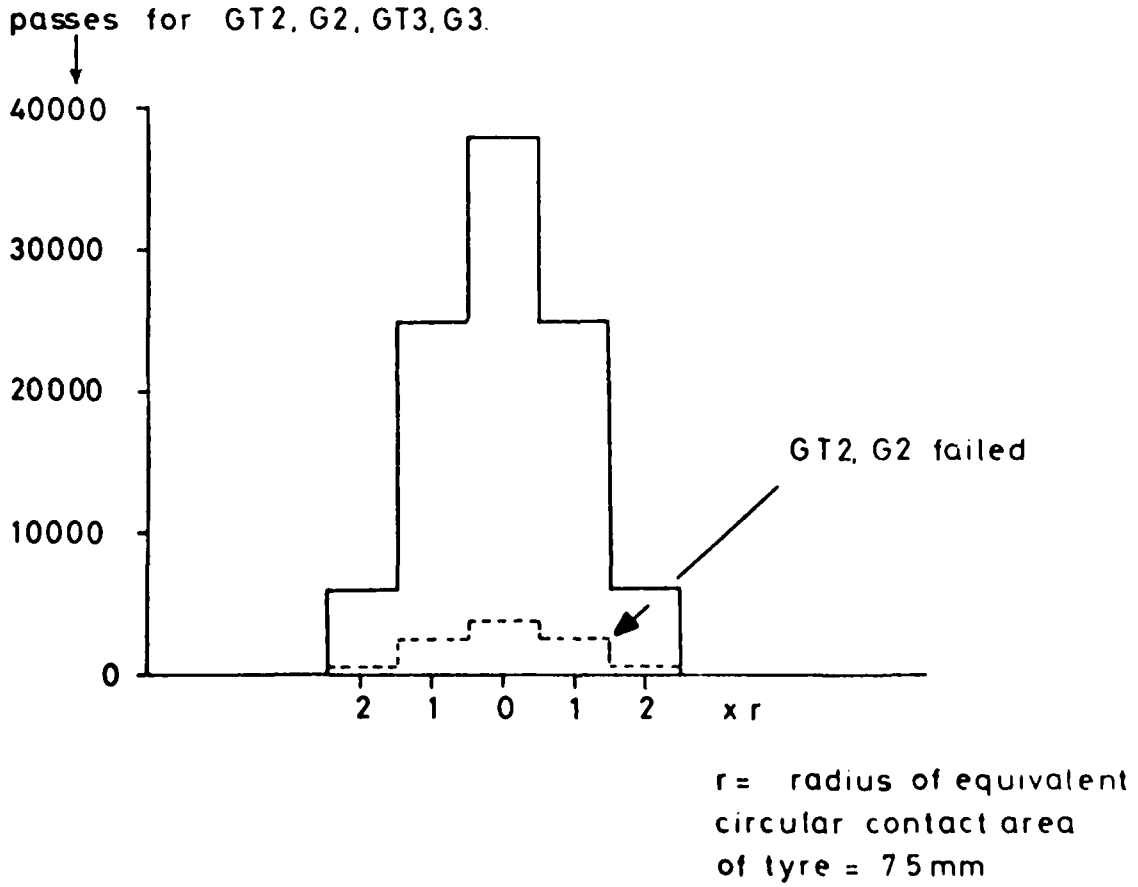


FIG. 4.2 DISTRIBUTION OF PASSES APPLIED TO EACH PAVEMENT

Table 4.1 Details of the loading procedure

| Total for all 9 (or 5) positions | Passes for pavements 1, 4, 5, 6 and 7 | | | | | | | | | Passes for pavements 2 and 3 | | | | |
|---|---|---|---|---|---|---|---|---|---|---|---|---|---|---|
| | 1 | 2 | 3 | 4 | 5 | 6 | 7 | 8 | 9 | 1 | 2 | 3 | 4 | 5 |
| 1000 | 30 | 60 | 120 | 180 | 220 | 180 | 120 | 60 | 30 | 60 | 250 | 380 | 250 | 60 |
| 2000 | 30 | 60 | 120 | 180 | 220 | 180 | 120 | 60 | 30 | 60 | 250 | 380 | 250 | 60 |
| 5000 | 90 | 180 | 360 | 540 | 660 | 540 | 360 | 180 | 90 | 180 | 750 | 1140 | 750 | 180 |
| 10000 | 150 | 300 | 600 | 900 | 1100 | 900 | 600 | 300 | 150 | 300 | 1250 | 1900 | 1250 | 300 |
| 20000 | 300 | 600 | 1200 | 1800 | 2200 | 1800 | 1200 | 600 | 300 | 600 | 2500 | 3800 | 2500 | 600 |
| 50000 | 900 | 1800 | 3600 | 5400 | 6600 | 5400 | 3600 | 1800 | 900 | 1800 | 7500 | 11400 | 7500 | 1800 |
| 70000 | 600 | 1200 | 2400 | 3600 | 4400 | 3600 | 2400 | 1200 | 600 | 1200 | 3000 | 7600 | 3000 | 1200 |
| 100000 | 900 | 1800 | 3600 | 5400 | 6600 | 5400 | 3600 | 1800 | 900 | 1800 | 7500 | 11400 | 7500 | 1800 |
| Accumulated total | 3000 | 6000 | 12000 | 18000 | 22000 | 18000 | 12000 | 8000 | 3000 | 6000 | 25000 | 38000 | 25000 | 6000 |

The above passes were applied in the following sequence for the pavements in the top column.

| Sequence | 9 | 6 | 7 | 3 | 1 | 4 | 2 | 5 | 8 | 5 | 3 | 1 | 2 | 4 |
|---|---|---|---|---|---|---|---|---|---|---|---|---|---|---|

individual numbers shown in the first line of the table and totalling 1000 passes. In detail, this involved 30 passes at position 9 followed by 180 passes at position 6, 120 at 7, etc. This gave a semi-random lateral distribution during the 1000 passes. This procedure was repeated once to accumulate 2000 passes, three times to achieve 5000 passes and so on, until 100,000 passes had been completed which was considered sufficient in the time available to accumulate enough data for analysis.

## 4.2 RECORDING PROCEDURE

Profilometer and permanent strain readings were taken after the numbers of passes shown in Column 1 of Table 4.1. During the actual loading, resilient strains and transient stresses were recorded on two Ultra Violet Oscillographs. Pressure cells could be recorded continuously but it was only possible to select one strain coil pair at a time. However, it was found that the transient response from each of the instruments settled down to a reasonably constant value after 5000 passes so that, beyond this point, there was no significant variation in the resilient strains over the short period required to individually select and record the strain coil outputs. The output from the thermocouples measuring the temperature at various depths was monitored on a chart recorder and the values were regularly checked.

The wheel load and position were marked on the UV Oscillograph paper, the position being taken from the appropriate feedback LVDT and related to marker outputs set for 1 m and 300 mm either side of the lateral centre line. This established the relationship between wheel load position and transient stress-strain peaks. Pulse length in terms of distance as the wheel approached and passed could also be obtained.

## 4.3 SINGLE TRACK TESTS

On completion of the main multi-track tests on pavements 4 to 7, single track tests were carried out on either side of the main test area. These included a total of 22,000 passes, being equal to the number applied to the central position in the multi-track tests (Table 4.1). Profilometer readings on a reduced grid system were taken at the appropriate intervals but, as there were no instruments at the single rut locations, stress and strain measurements could not be recorded. The object of these tests was to confirm the trends in permanent deformation observed for the "with and without fabric" situation and to simplify the loading system. This is a necessary step as the accumulation of permanent deformation in the centre of the multi-track test is influenced by the wheel in its various lateral positions.

An important variation on the single rut test was the introduction of unidirectional tests from pavements 4 onwards. This allowed single track tests to be carried out on either side of the main test area to additionally examine the difference in pavement performance due to one way or two way loading.

# CHAPTER FIVE

# TEST RESULTS

## 5.1 INTRODUCTION

This section presents a summary of all the measured pavement performance data. Each parameter is dealt with on just one or two figures, which include data from all the pavements that were tested. Permanent strain results were taken from strain coil measurements at 70,000 passes except for the second pair of pavements, which failed prematurely. Resilient measurements were taken after at least 10,000 passes had been completed (5,000 in the case of pavements 2) as their magnitudes levelled off beyond this point. The number of passes applied in the single track tests equalled the number of passes at the central position for the multitrack tests.

The data presented in this chapter is used to compare with theoretical predictions in Chapter 6. It was also used to study the effects of the fabric inclusions and the discussion of this subject is included in Section 5.7.

## 5.2 PERMANENT DEFORMATION

The accumulation of surface permanent deformation during the course of all tests is shown in Figs 5.1 and 5.2 and the transverse profiles of the ruts in Fig. 5.3.

The need to change from the parallel to the series arrangement of pavement pairs is demonstrated by the data in Fig. 5.3 for pavements 2 and 3. The two ruts are close together and there was clearly interference between loading of one section and the other. The rut depths in Fig. 5.3 reflect the relative strengths of the pavements as noted in Section 3.2 when

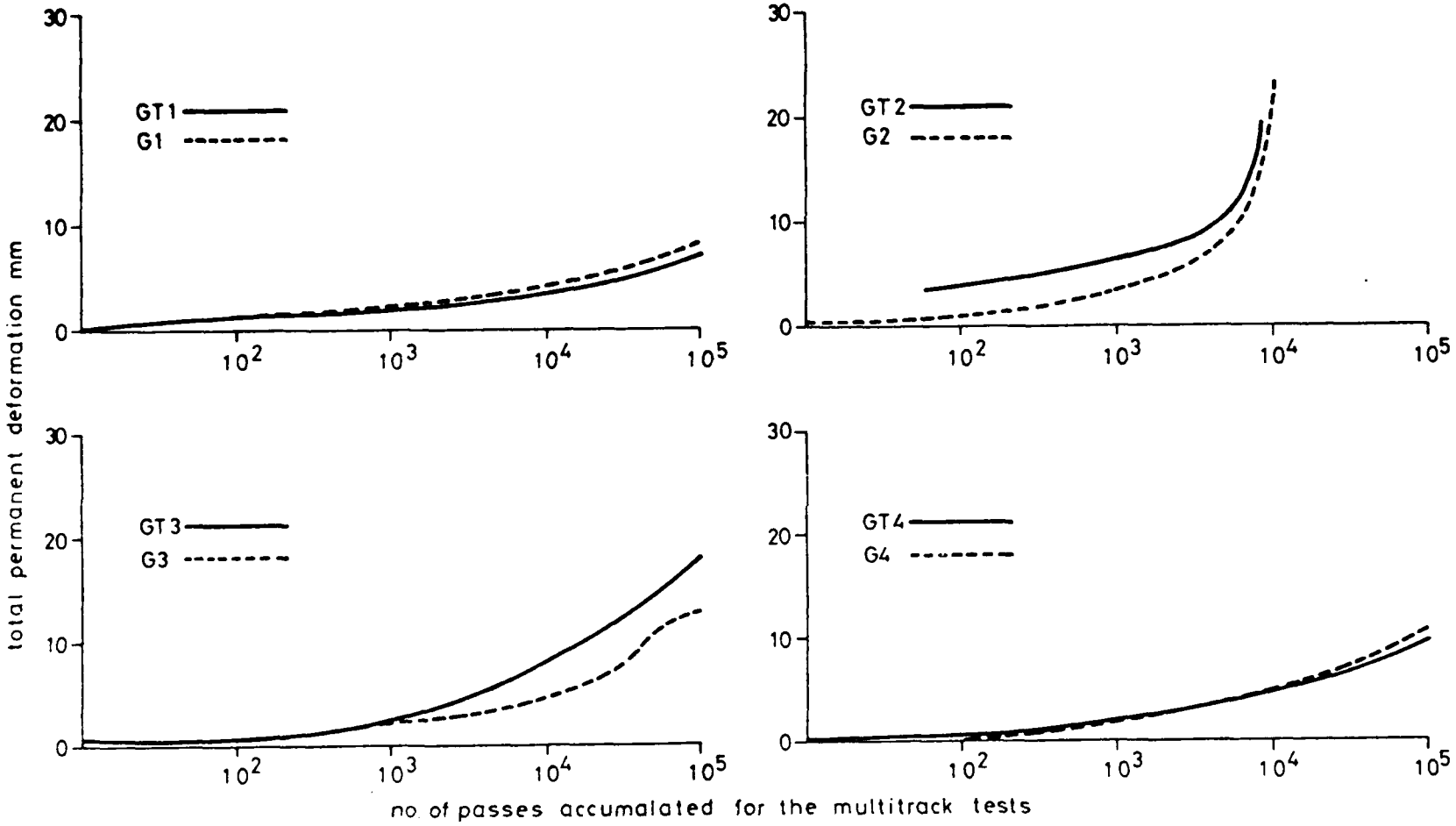


FIG. 5.1 ACCUMULATION OF PERMANENT DEFORMATION AS MEASURED BY THE PROFILOMETER (PAVEMENTS 1 TO 4)

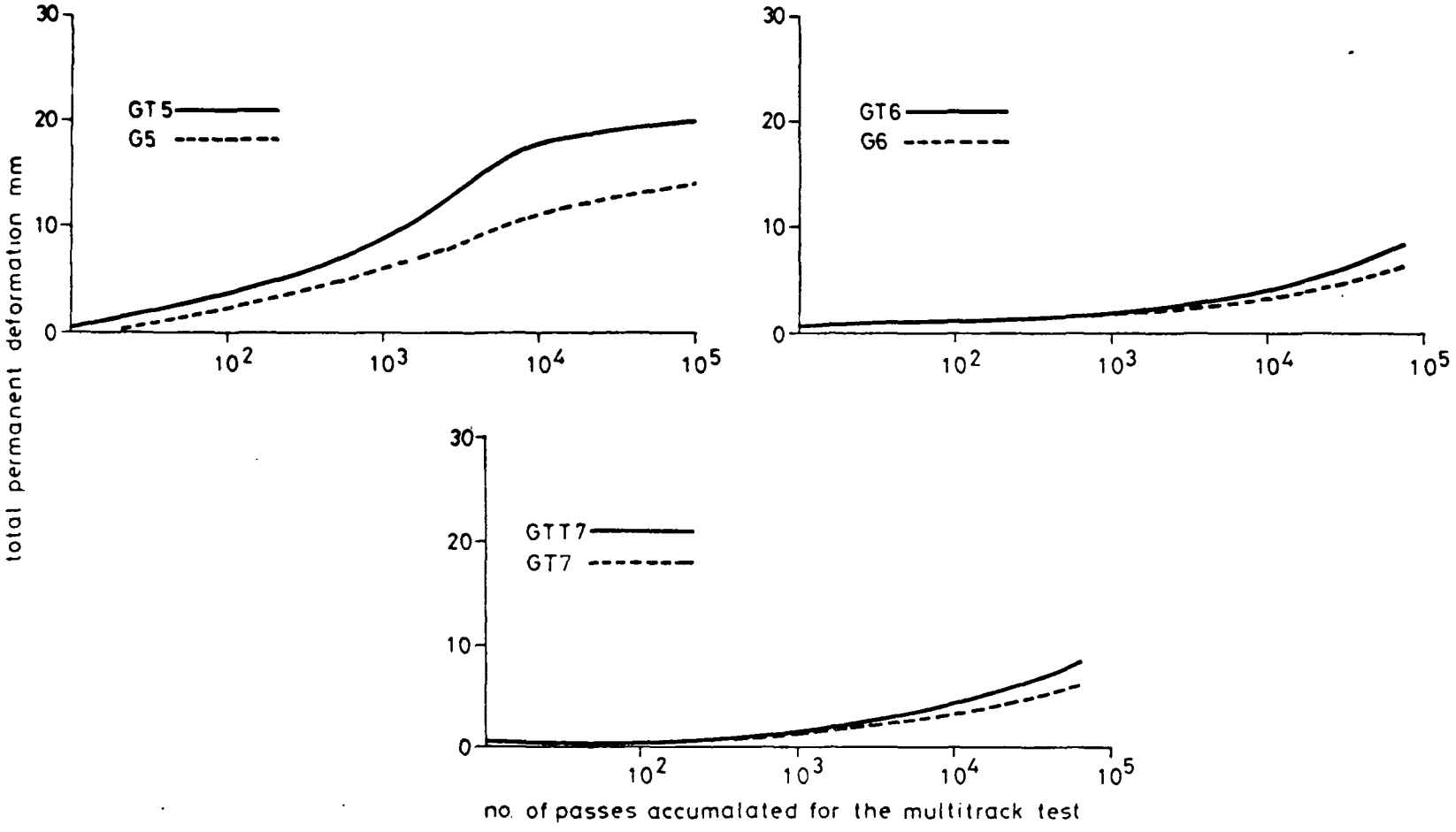


FIG. 5.2 ACCUMULATION OF PERMANENT DEFORMATION AS MEASURED BY THE PROFILOMETER (PAVEMENTS 5 TO 7)

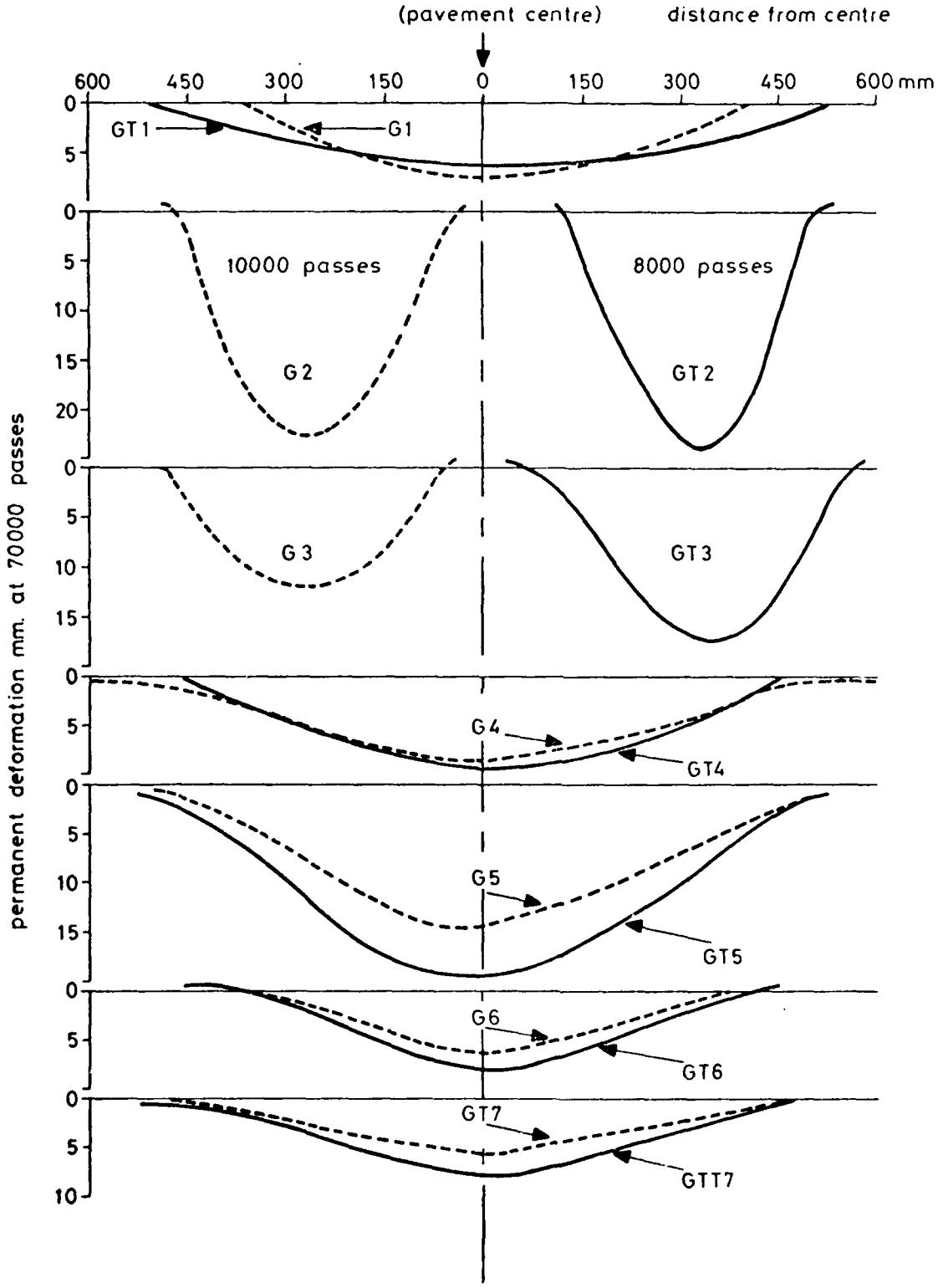


FIG. 5.3 LATERAL SURFACE PROFILES AFTER 70,000 PASSES

considered in relation to the applied wheel loads.

## 5.3 PERMANENT STRAINS

The variations of measured permanent strain with depth are shown in Figs 5.4 to 5.6. The values have been plotted at the centre of the appropriate gauge length, being the separation of the strain coil pairs.

It is important to determine the way in which the vertical permanent strain in each layer contributes to the surface deformation and this is illustrated in Fig. 5.4. The strong pavement pairs (Nos 1, 6 and 7, Section 3.2) show gradually decreasing strain with depth reaching an insignificant level in the subgrade. It should be noted that an exception to this is observed above the fabric in the granular layer of GTT7. Another exception is the high strain in the bituminous layer of G1 which is related to its poor compaction as evidenced by high void content (Table 3.2). The strains in the granular layer and subgrade were larger for the medium strength pavements (Nos 3, 4 and 5) and the weakest pavement pair (No. 2) exhibited very large strains in the subgrade. All pavements developed significant strains in the asphalt and a tendency for increased strains in the upper half of the granular layer.

Horizontal, lateral permanent strains are presented in Fig. 5.5 and are seen to increase to high tensile levels at the bottom of the bituminous layer for all except pavements 1. An apparently compressive strain in this layer for GT1 may be a result of strain coil tilt which can reverse the sense of the output in this coplanar mode. Crosses at the lower interfaces are measurements on the fabric and these should be compared with the readings above and below to examine continuity. The measurements plotted immediately above and below the fabric were obtained by superposition since it was not possible to take measurements at points in such close proximity to one another (see instrumentation layouts in

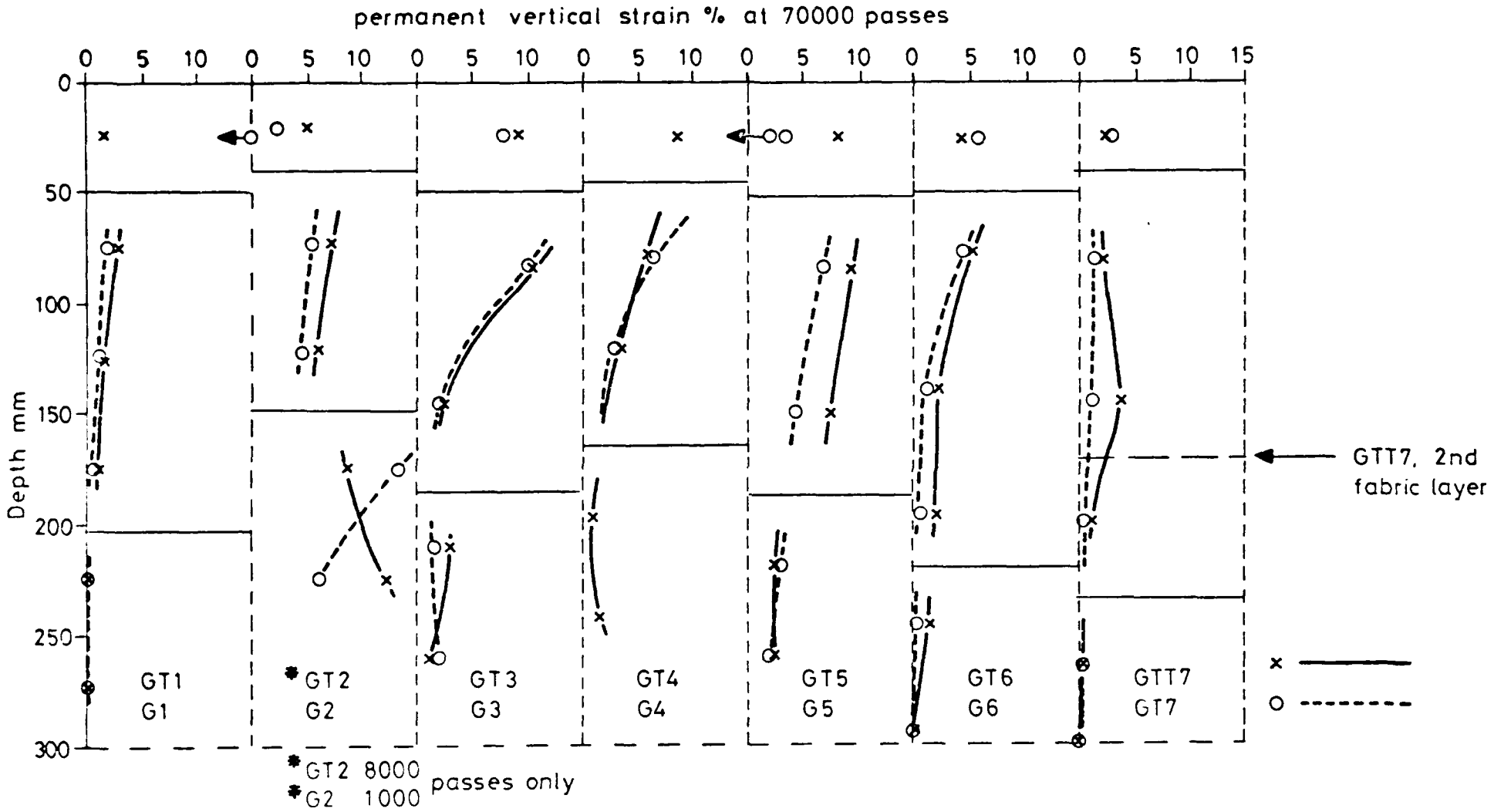


FIG. 5.4 PERMANENT VERTICAL STRAIN AGAINST DEPTH

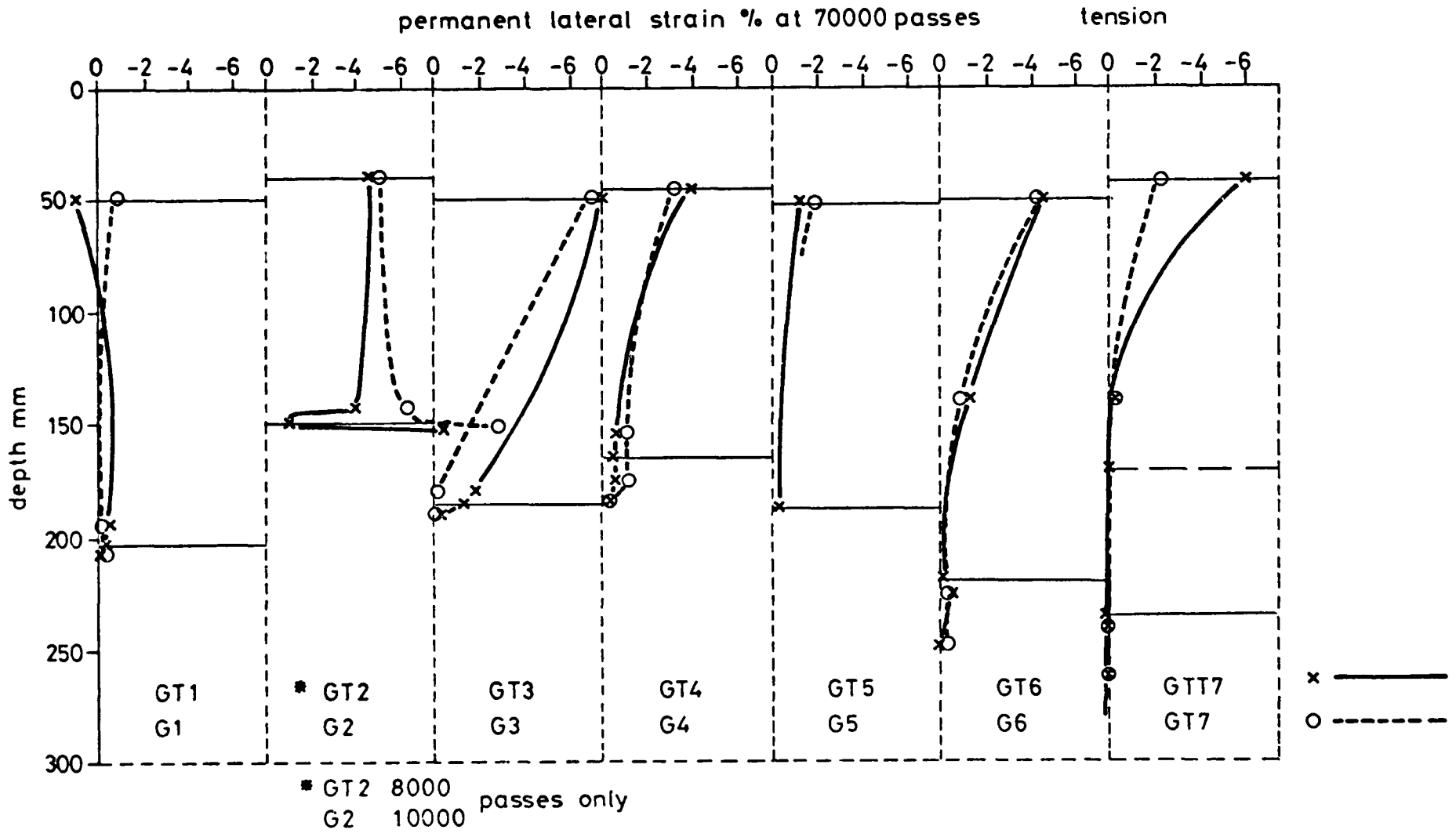


FIG. 5.5 PERMANENT LATERAL STRAIN AGAINST DEPTH

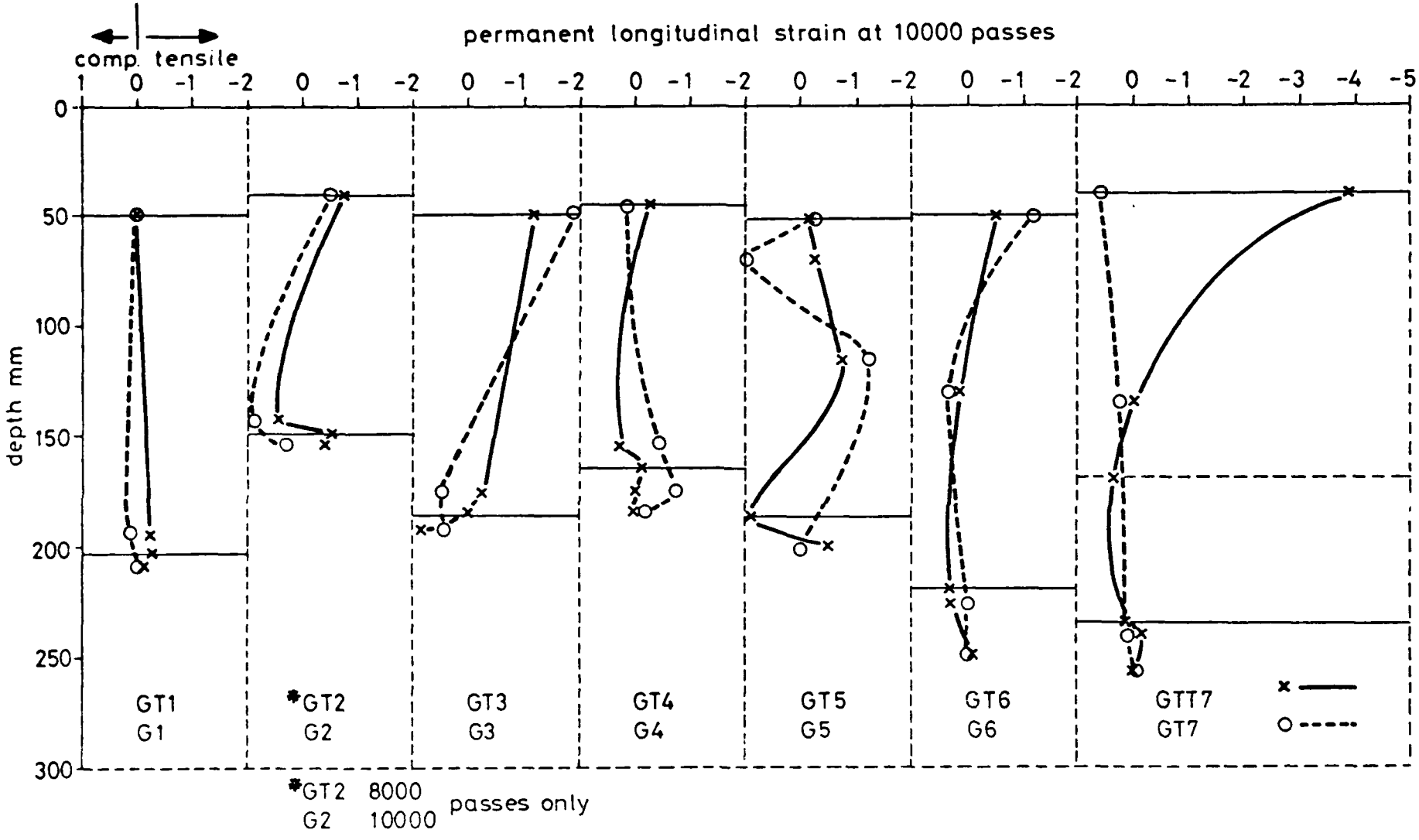


FIG. 5.6 PERMANENT LONGITUDINAL STRAIN AGAINST DEPTH

Figs 3.7 to 3.12).

The longitudinal strains (Fig. 5.6) were somewhat inconsistent but this may be due to their low magnitudes. A very high strain reading was obtained at the bottom of the asphalt layer for GTT7 and this may have been due to a loose coil installation or, less likely, a crack between the coils. Theoretically, the permanent strain in this direction should be zero (Chapter 6) but, in practice, one location may sustain compressive deformation and another tensile, causing a resultant zero strain over a length of pavement.

## 5.4 RESILIENT STRAINS

Fig. 5.7 shows that the resilient strains reached steady values after the first 20,000 passes, and it is these values that are generally shown in the following figures (5.8 to 5.10). For pavements 2, which failed prematurely, values were taken after only 5,000 passes and in a few other cases after 10,000, but for these latter the values had already stabilised. It was necessary to reduce the scale for the second pair of pavements in order to accommodate their very high subgrade resilient strains as failure was approached.

With the exception of pavements 1, the general levels of resilient vertical strain in Fig. 5.8 are higher in the subgrade than in the other two layers and in most cases higher for the pavements including fabric. The overall trends for this parameter show higher strains at the top of the subgrade, reasonably uniform strains in the granular layer and significant differences in the asphalt.

The resilient lateral strains are shown in Fig. 5.9. Some information could not be obtained for pavements 3 and 5 due to coil failure and shortage of coils respectively.

The longitudinal resilient strain results in Fig. 5.10 do not present

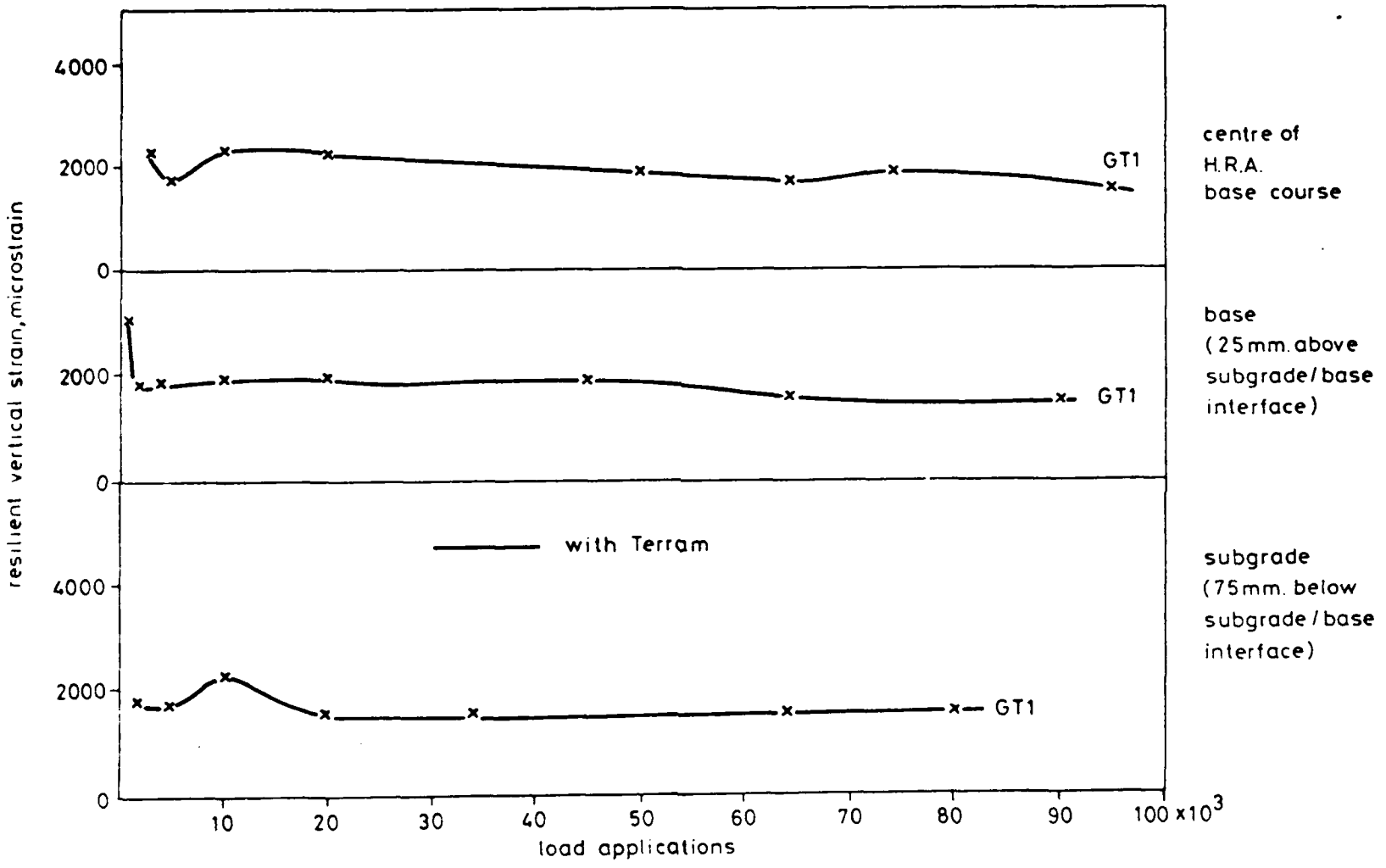


FIG. 5.7 TYPICAL RESILIENT VERTICAL STRAIN VARIATIONS WITH LOAD APPLICATIONS IN EACH LAYER OF GT1

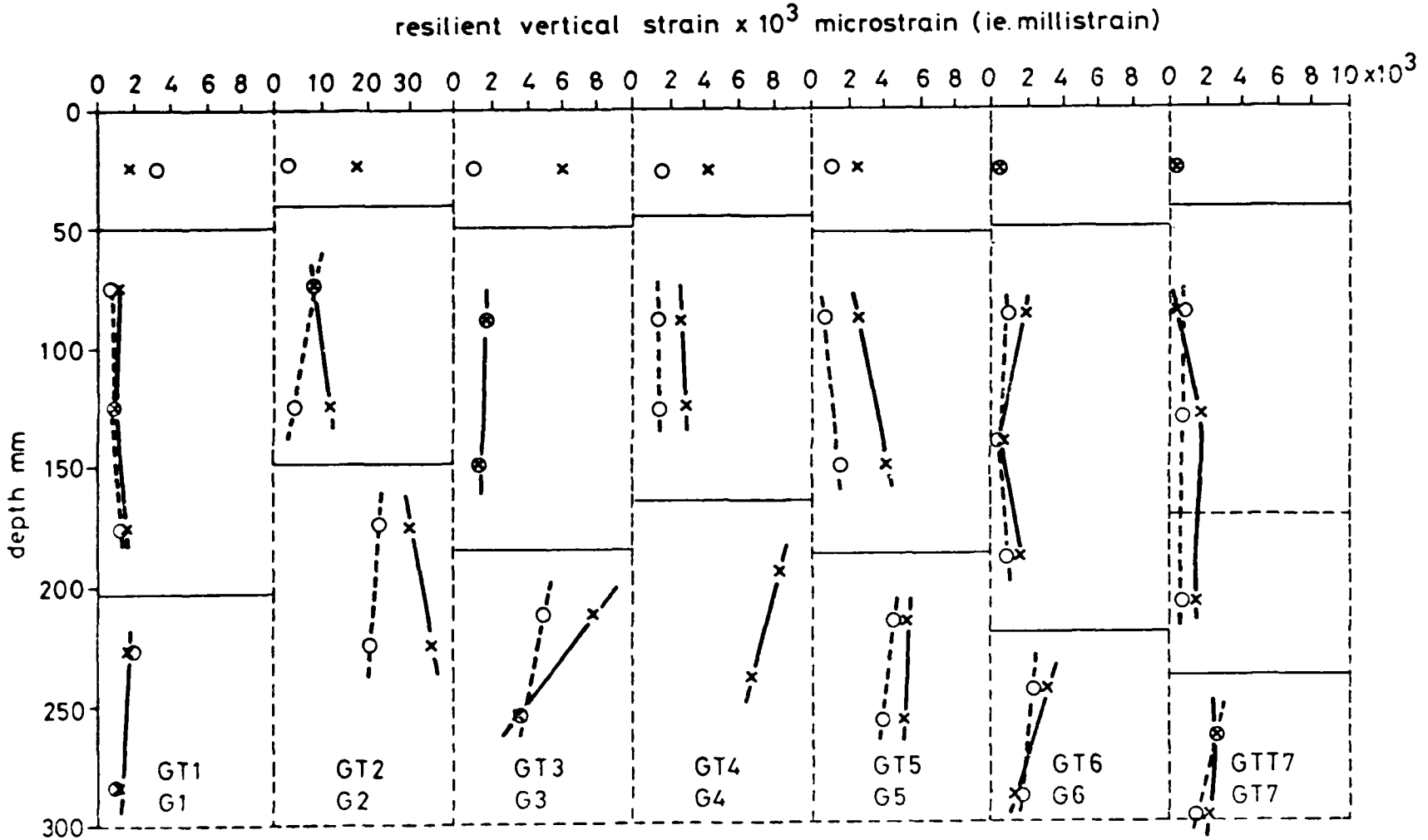


FIG. 5.8 RESILIENT VERTICAL STRAIN AGAINST DEPTH

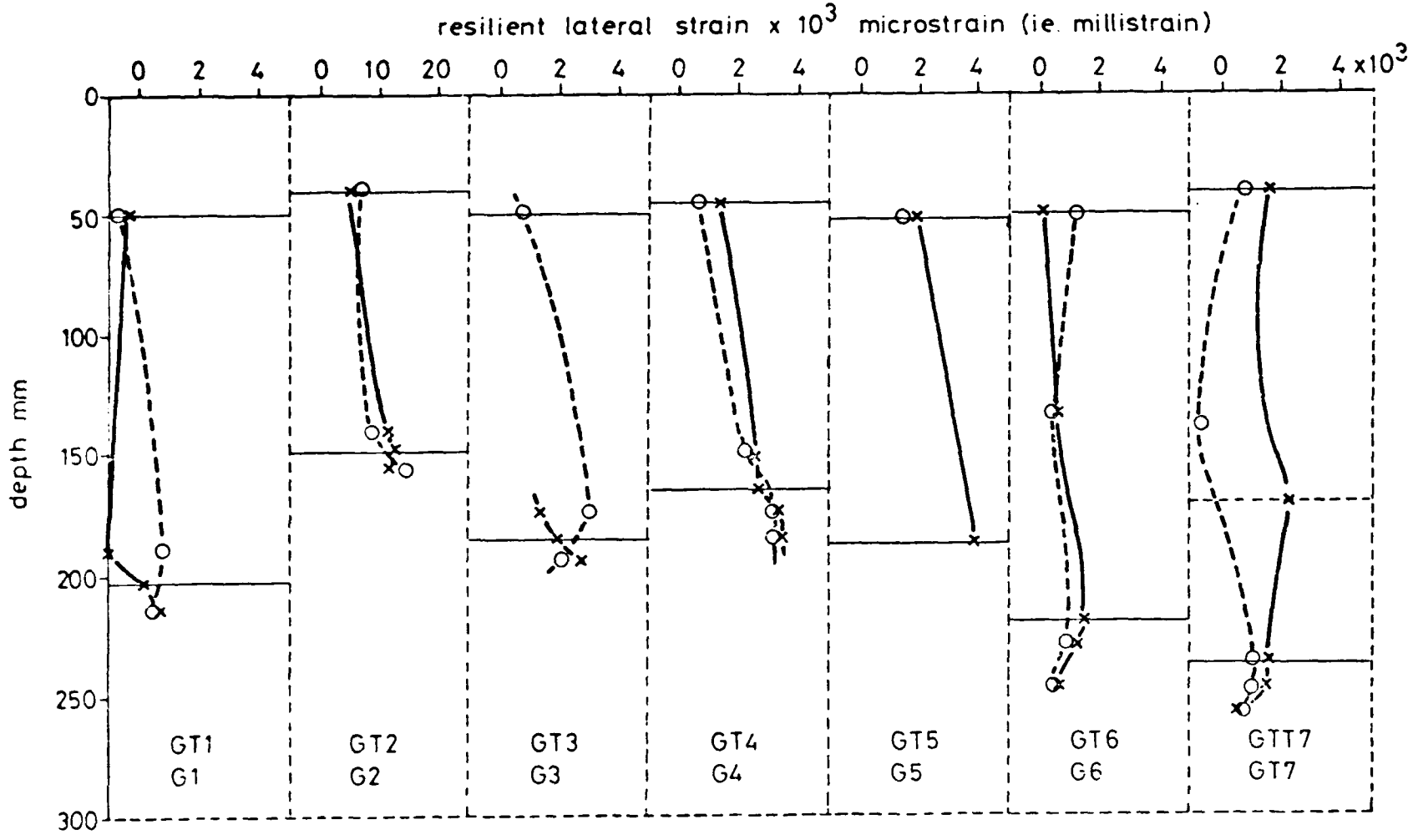


FIG. 5.9 RESILIENT LATERAL STRAIN AGAINST DEPTH

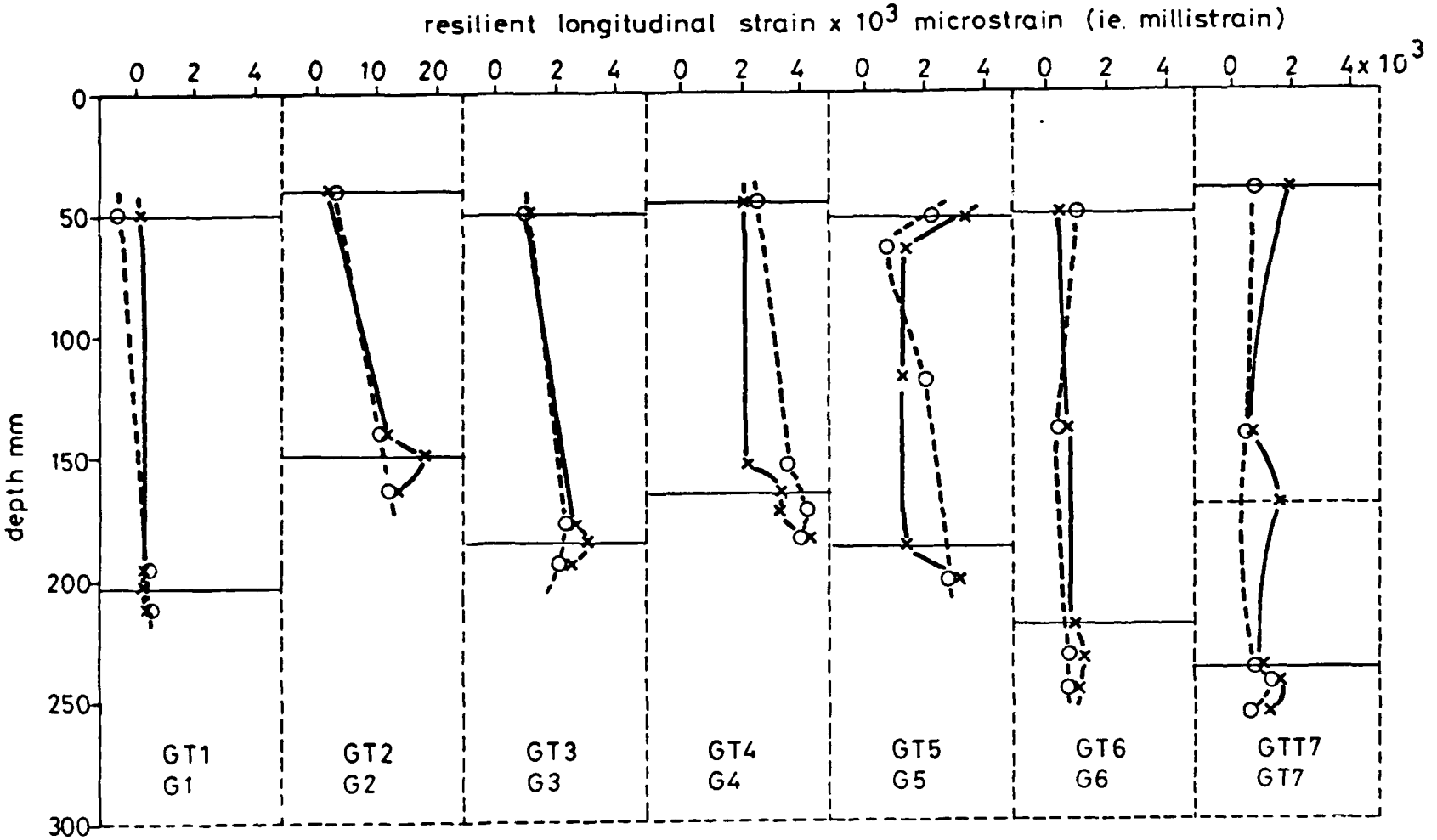


FIG. 5.10 RESILIENT LONGITUDINAL STRAIN AGAINST DEPTH

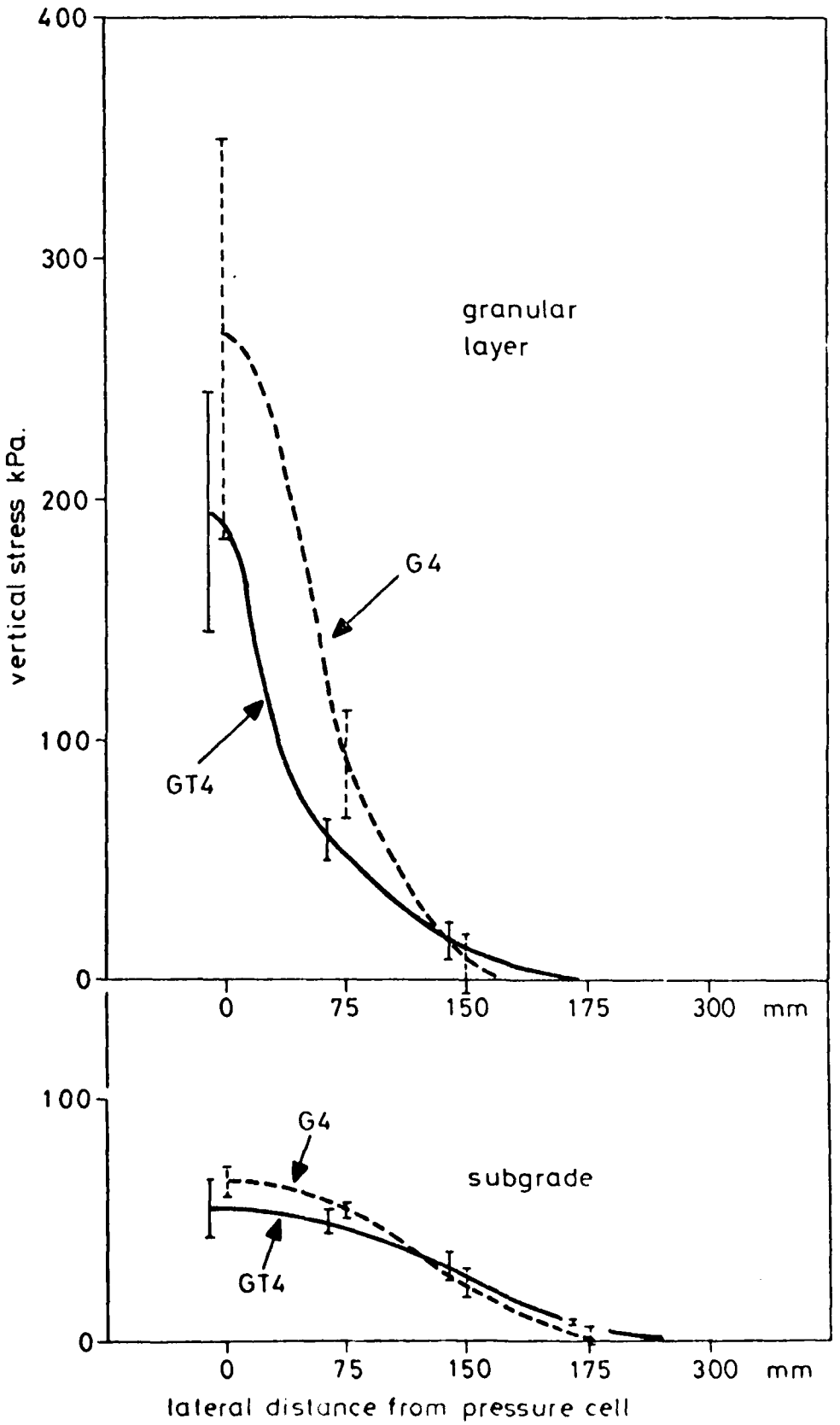


FIG. 5.11 PEAK VERTICAL STRESS AGAINST RADIAL DISTANCE FROM WHEEL LOAD

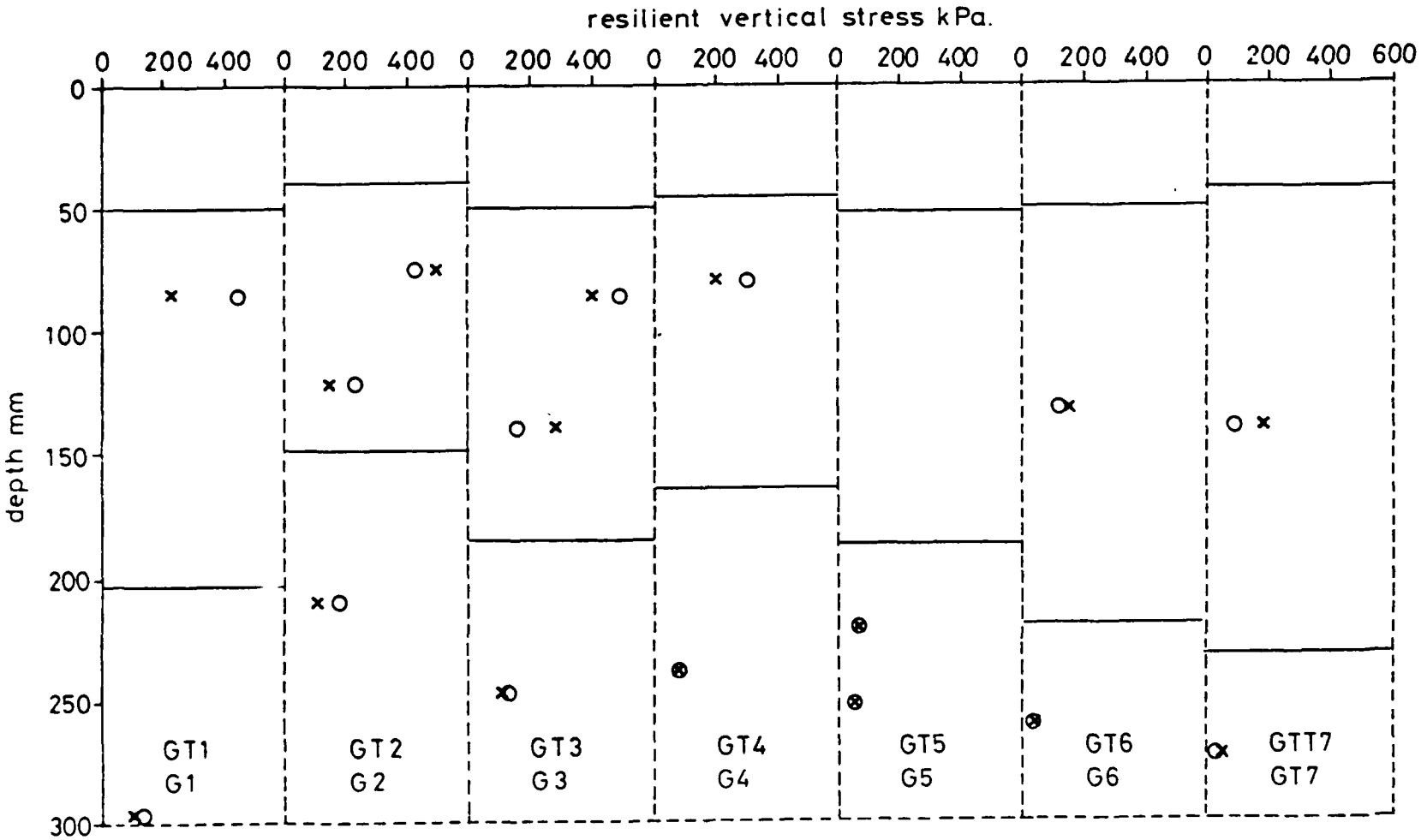


FIG. 5.12 RESILIENT VERTICAL STRESS WITH DEPTH

a consistent picture. In places, higher strains were apparently obtained in the fabric than in the adjacent materials. The recorded pulse usually exhibited a "compression-tension-compression" pattern at the subgrade base interface (see Fig. 6.11 for instance) but it is the tensile output which has been plotted. This tends to be less well defined than for the lateral direction which was purely tensile (see Fig. 6.11) with a definite initial zero.

## 5.5 TRANSIENT STRESSES

Fig. 5.11 shows the variation in vertical stress pulse height with lateral distance from the load for pavements 4. This graph was chosen as it contains results from three pressure cells at the same level in each layer. Duplication to this extent was not possible in the other pavements. The difficulties of using pressure cells in this coarse granular material are well illustrated by the scatter in results which exceeds that in the silty-clay subgrade.

All the transient stress measurements are summarised in Figs 5.12 to 5.14. These are not as comprehensive as the strain measurements because the larger size of the pressure cells resulted in fewer of them being used in order to preserve adequate separation by the minimum of three diameters, which is considered reasonable.

## 5.6 SINGLE TRACK TESTS

The build-up of permanent deformation during unidirectional and bidirectional single track tests is shown in Fig. 5.15. There are separate curves for pavement sections with and without fabric and for the two methods of loading. Unidirectional tests were not carried out for the final pair of pavements.

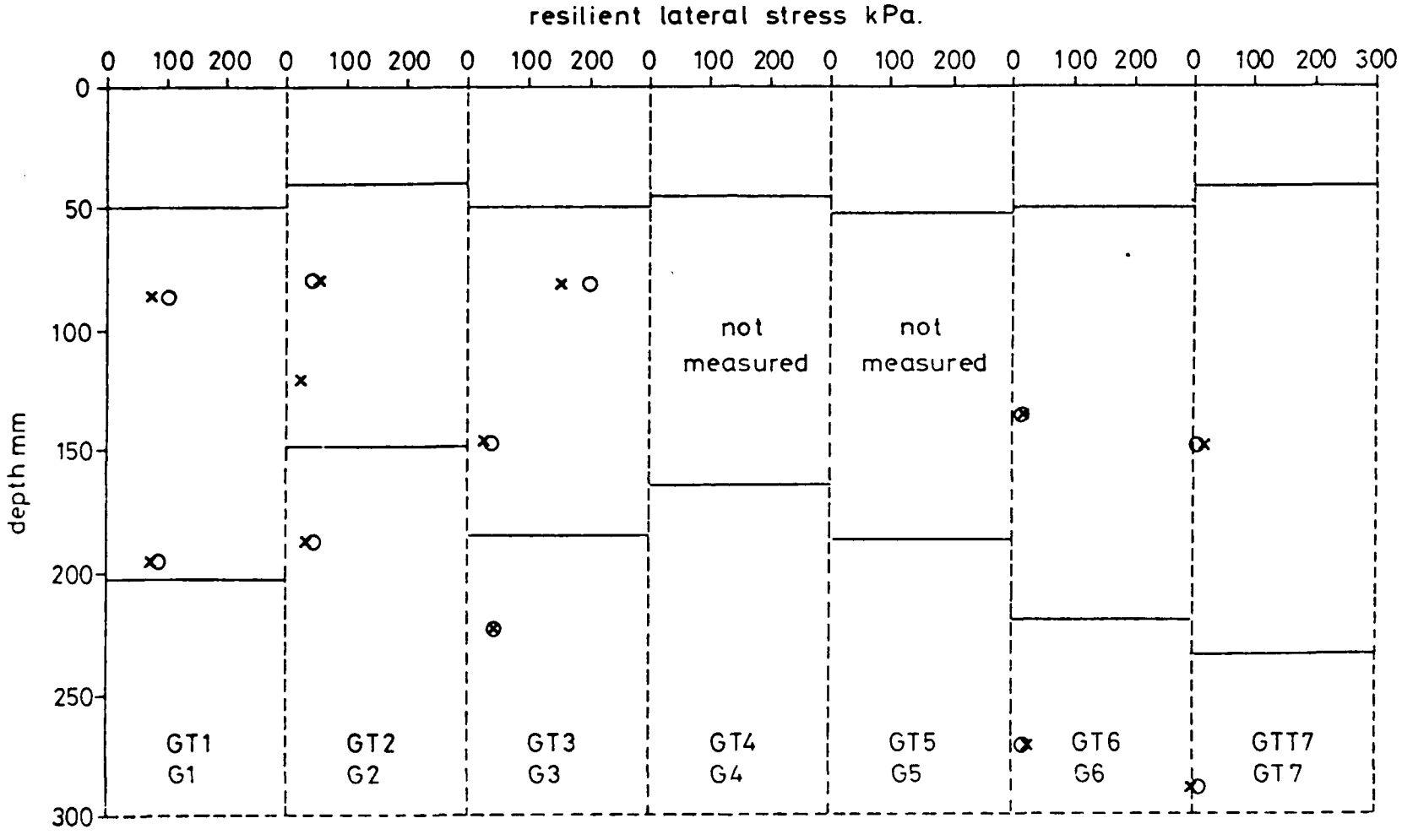


FIG. 5.13 RESILIENT LATERAL STRESS AGAINST DEPTH

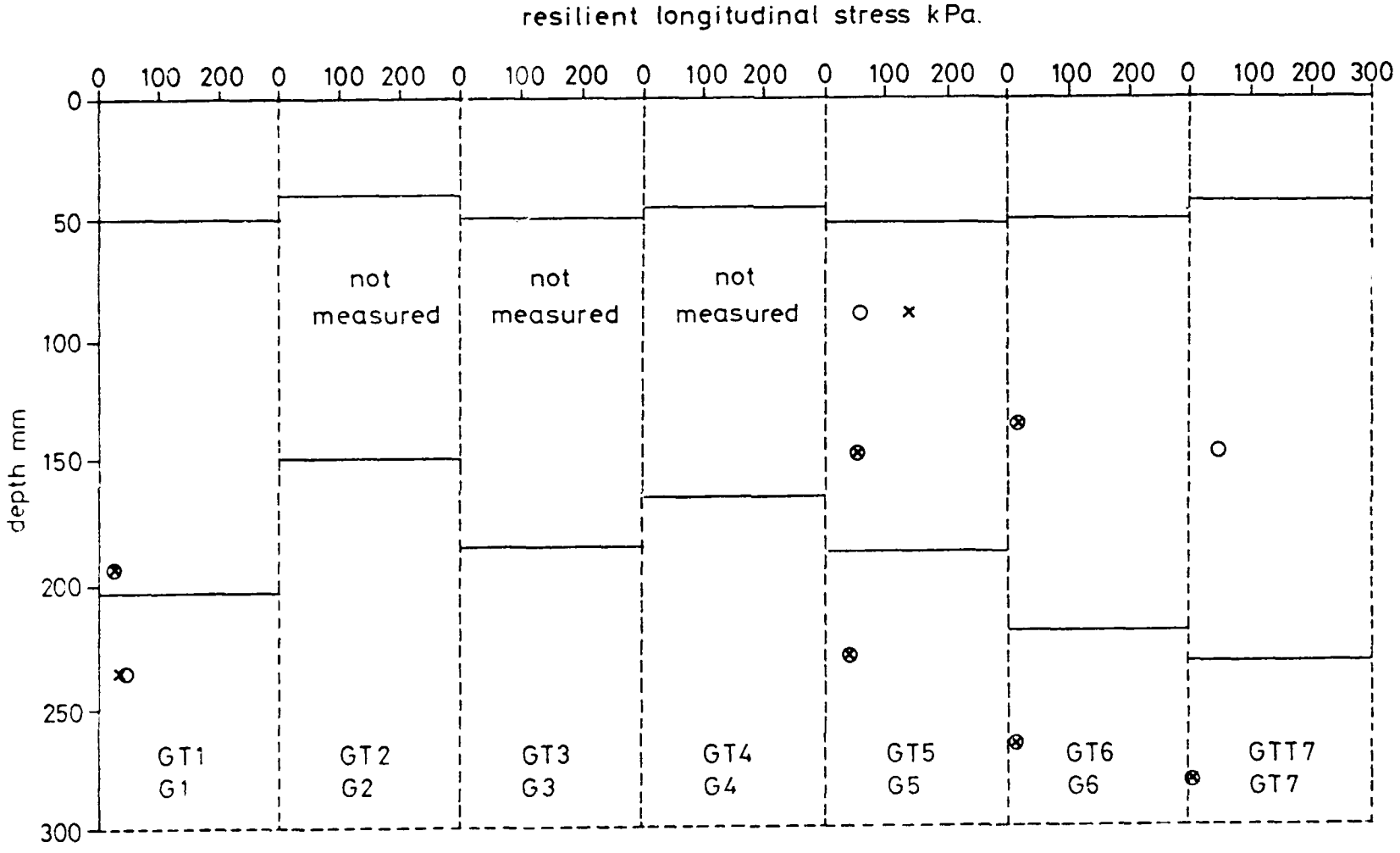


FIG. 5.14 RESILIENT LONGITUDINAL STRESS AGAINST DEPTH

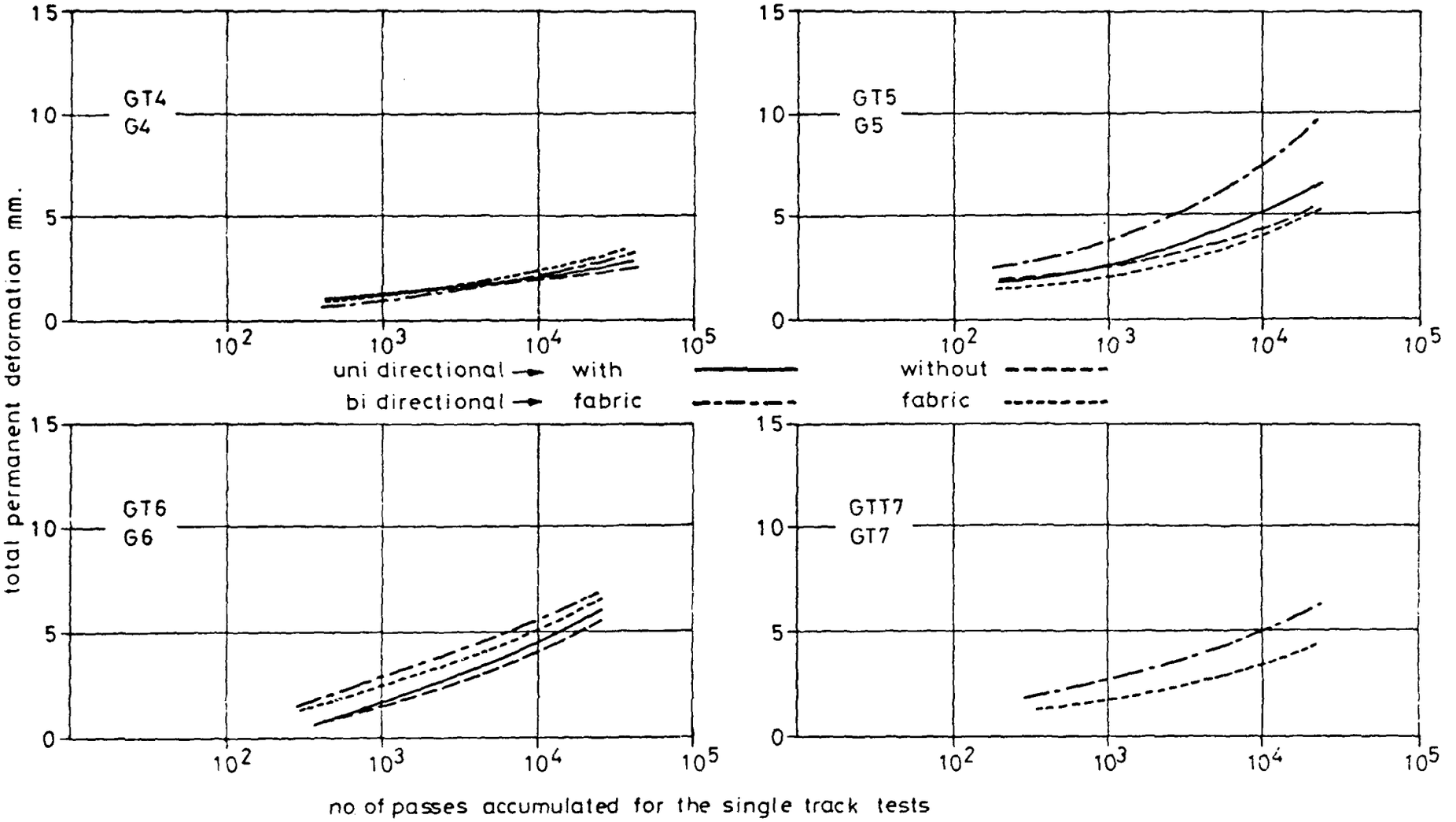


FIG. 5.15 ACCUMULATION OF PERMANENT DEFORMATION AS MEASURED BY THE PROFILOMETER (SINGLE TRACK TESTS)

The lateral rut profiles at the end of these tests are shown in Fig. 5.16. There is some evidence in this figure that the bidirectional tests may have been slightly more damaging than the unidirectional ones.

## 5.7 INFLUENCE OF FABRICS

All the figures presenting measured data from the test pavements (5.1 to 5.16) distinguish between those including fabric and those without.* Fig. 3.6 shows which fabrics were used and where they were located in the structures.

The structural performance of a pavement is assessed by the extent of cracking and rutting whic develops under traffic loading. These experiments were arranged primarily to investigate rutting and this is the major serviceability indicator used in the UK. Cracking was only observed in pavements 2 which were of low strength and could not really be categorised as permanent structures. However, they produced some data which was useful in understanding the mechanisms of fabric behaviour. Hence, the development of permanent deformation and the in situ permanent strains which cause it must be regarded as of most importance.

Figs 5.1 to 5.3 clearly show that the inclusion of fabric did not improve performance. Indeed, in most cases, it resulted in reduced performance. The use of the stronger Terram 7M7 in place of Terram 1000 in pavements GT5 and GT6 did not cause any improvement. Neither did the use of two layers of Terram 1000 in GTT7.

Fig. 5.4 shows that the apparently better performance of GT1 compared with G1 arose from the higher vertical permanent strain in the asphalt layer for the latter. This was a consequence of poor compaction and not related to the presence of the fabric. This result emphasises the danger of drawing conclusions on pavement performance simply on the basis of permanent deformation at the surface.

* Except for pavements 7 where the effects of an additional layer of fabric were investigated.

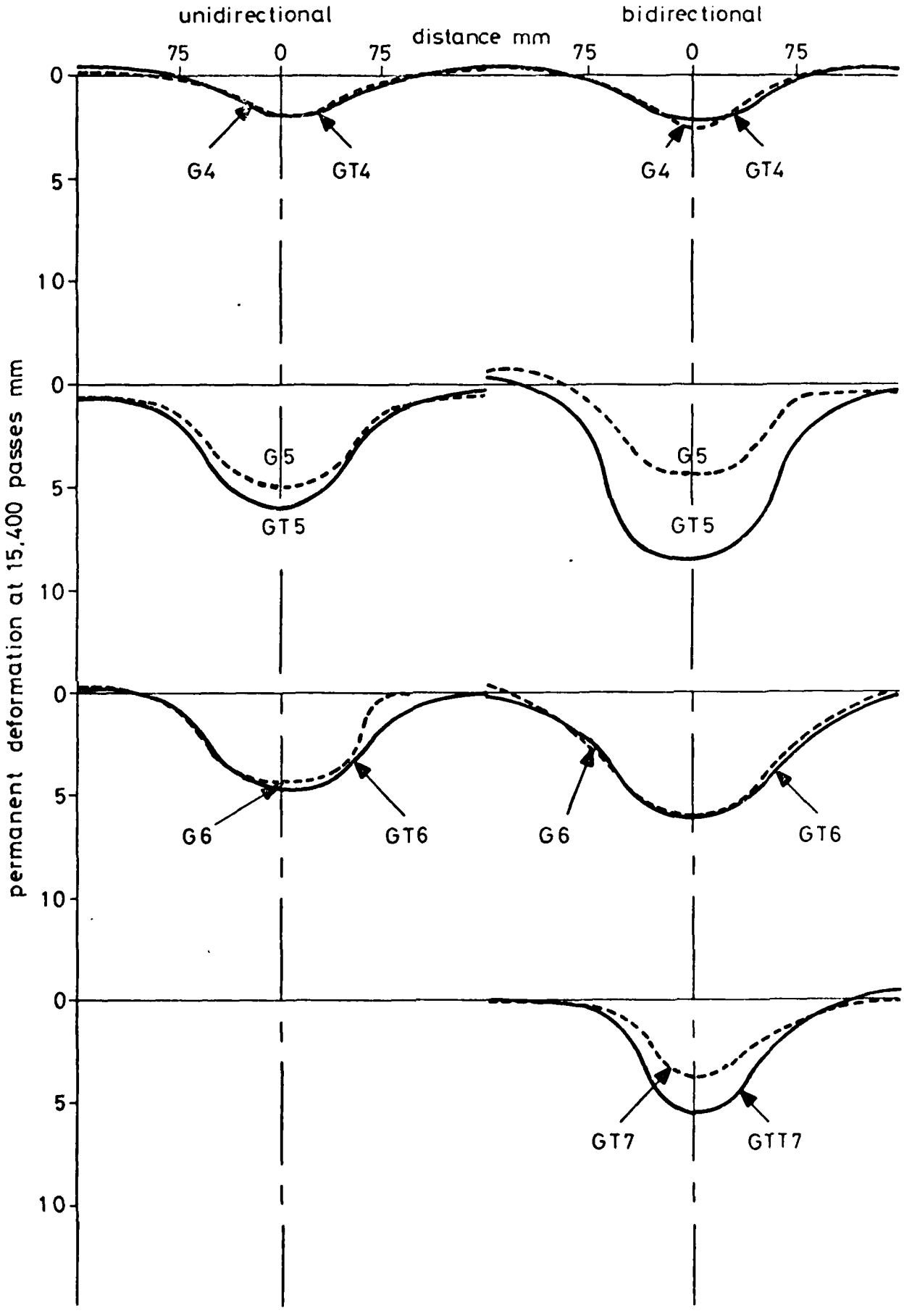


FIG. 5.16 LATERAL SURFACE PROFILES FOR SINGLE TRACK TESTS

The data for pavements 2 in Fig. 5.1 indicates that the difference in performance may have arisen from effects occurring early in the tests. If the permanent deformation developing after 1,000 passes is considered, then pavements 1, 2, 5 and 6 showed no effect of the fabric presence, while the other two pairs indicated poorer performance with fabric.

A study of the lateral permanent strains in Fig. 5.5 indicates that continuity of movement across the fabric was maintained except in pavement GT2 which was very weak and where strains were larger than in other cases. Here, there is a clear discontinuity indicating relative slip between the fabric and the materials on either side.

This pattern of behaviour may be contrasted with that in Fig. 5.9 which shows the lateral resilient strain. There is no evidence of discontinuity even for GT2. It is noticeable, however, that higher resilient strains occurred in pavements 7 when the two layers of fabric were included.

This inspection of strain continuity across the fabric is, at best, approximate because of the way in which the results were obtained. The three data points for lateral strain in the base, on the fabric and in the soil below were obtained at separate locations for practical reasons and then superimposed. All that can be reliably stated is that the potential for slip occurs and should be investigated. This has been done in some detail by Collios et al (21) and in a preliminary way at Nottingham by Leung (22). The results of these shear box and pull-out tests confirm the necessity to match particle size and fabric pore size in order to maximise frictional and interlock forces.

The noted difference between the lateral resilient and permanent strain pattern for GT2 (Figs 5.5 and 5.9) is difficult to explain if it is a genuine effect. It does, however, point to the need for some more fundamental simulative tests of soil-fabric interaction under repeated loading.

FIG. 5.17 SUBGRADE CONDITION BELOW TERRAM 7M7 AFTER TEST ON GT5

FIG. 5.14 SUBGRADE CONDITION BELOW GRANULAR LAYER AFTER TEST ON G5

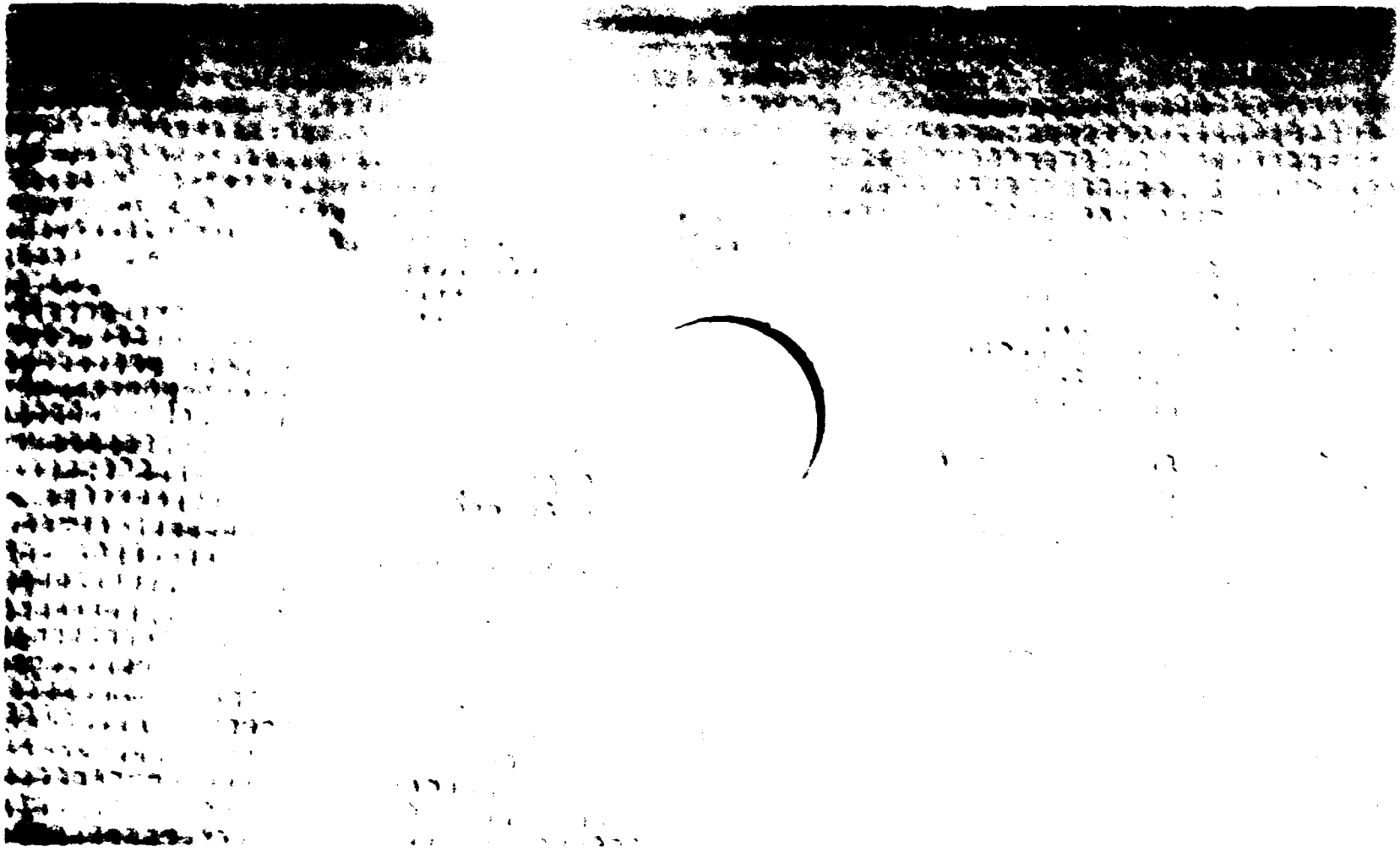

FIG. 5.19 IMPRINT OF TERRAM 7M7 IN SUBGRADE AFTER TEST ON GT5

The summary of vertical stress and resilient strain measurements in Figs 5.8 and 5.12 again confirms that no benefits accrued from the inclusion of fabric. In general, vertical resilient strains both in the granular base and the subgrade, were higher when fabric was used, while no consistent trends emerged for the vertical stresses or indeed for the horizontal stresses (Figs 5.13 and 5.14).

The surface deformation measurements obtained in the single track tests shown in Fig. 5.16 confirm the general conclusion arising from the multi-track tests that fabric inclusion did not improve performance.

The measured data on continuity of strain between fabric and adjacent material was augmented by observations during excavation of each pavement in an attempt to obtain a clearer idea of conditions at this critical location in the structure.

The development of higher early life permanent deformations in some pavements with fabric, notably GT2 and GT5, suggests that compaction of the aggregate may not have been so effective over the fabric as directly on the soil. The density measurements in Table 3.2 do not, however, substantiate this. During excavation, it was apparent that the limestone just above the fabrics, particularly the Terram 7M7, seemed looser than the material in an equivalent position just above the subgrade with no fabric present.

In view of the possibility of slippage between fabric and adjacent materials, careful observations were made during excavation. Figs 5.17 and 5.18 show that the subgrade surface below the 7M7 fabric appears smoother than that immediately below the crushed limestone which keys in to the soil. Closer inspection of the soil below the fabric in Fig. 5.19 shows, however, the well defined pattern of the fabric in the clay indicating good grip. Furthermore, it was found relatively difficult to separate the fabric from the soil, particularly beneath

the wheel track. These observations, together with data from Leung's shear box and pull-out tests (22) suggest that slip is more likely to occur at the upper interface between the crushed limestone and the fabric. This is because the particle sizes are generally much larger than the pore sizes of the fabrics. Therefore, the placing of an extra layer of Terram 1000 within the granular layer in pavement GTT7 would not be expected to improve performance, which was in fact the case.

# CHAPTER SIX

# THEORETICAL ANALYSIS OF PAVEMENT RESPONSE

## 6.1 INTRODUCTION

The analytical work on this project was restricted to its final year. It was able to build on development work done earlier (17) in connection with a project on the repeated load response of granular materials. There was also the experience of the earlier work on full depth asphalt pavements (1) and data on materials testing of various kinds on which to draw. It was, however, found inevitably, that the particular material conditions in the test pavements differed somewhat from those used in earlier materials testing and estimates had to be made of material properties or factors influencing them at various stages of the computations. This section of the report describes the basis for the computations and decisions which were taken with regard to material properties and compares the predicted values of various parameters with those which were measured in the test pavements.

As the pavement structures used in this investigation all had crushed rock bases, the behaviour of this material dictated the type of analysis to be used. It is well known that the resilient behaviour of granular materials is stress dependent and, therefore, the analysis system must be able to cater for this non-linearity. The finite element method is the only system presently available that can handle variations in material properties in both the horizontal and vertical directions simultaneously. Using this type of analysis, therefore, once the appropriate material behaviour characteristics are determined, a complete structural analysis can be performed.

All the pavements described in this report were analysed to determine resilient response and permanent deformations. Comparison between measured

and predicted stresses and strains and rut depths were made. The three full depth dense bitumen macadam pavements reported earlier (1) were also reanalysed.

## 6.2 MATERIAL CHARACTERISATION

The resilient behaviour of pavement materials has been thoroughly investigated at Nottingham in recent years. Most of these experiments have involved the triaxial apparatus with the application of a repeated deviator stress and, in some cases, also a repeated confining stress. These experiments have provided data on two types of material behaviour applicable to the pavement situation. The first of these is the resilient strain response, which is the rebound or "elastic" behaviour of the material under one application of a repeated stress path and the second concerns the permanent strain response, which is the build up of irrecoverable strain after various numbers of applications of any repeated stress path. The first property is clearly required to analyse the resilient or transient response of the pavement system to a single pass of a wheel load, and the second, to analyse the build up in permanent strain, which leads to rut development after many wheel passes. It may be assumed that these two properties are essentially independent for all the materials considered, clear evidence on this having been produced for granular materials (17). This means that the resilient response is virtually unaffected by the number of load applications already applied to a specimen and that no relations can readily be found between the resilient and permanent response of a material to any particular stress path.

The behaviour of the particular materials used in these pavement investigations is discussed in the following sections.

### 6.2.1 Granular Material

The granular, crushed limestone, material used for the pavements was chosen because it had been extensively tested in a repeated load triaxial apparatus (16,17). The results of this testing showed that the resilient behaviour of a granular material under repeated loading was very stress dependent and therefore non-linear. To describe this behaviour, both secant and tangent modulus methods were considered. Fig. 6.1 illustrates the use of both methods for examining a stress path going from stress condition 1 to stress condition 2. In the tangential approach the stress path 1 to 2 is divided into increments and, at each increment, stiffness values are determined and the change in strain (i.e. incremental strain) is calculated. The sum of these incremental strains gives the overall strain change. In the secant method both stress points 1 and 2 are related to the stress origin (point 0, which also gives the strain origin) and the values of strain are determined for each point. The difference between these strains gives the overall strain change. For use in analysis, difficulties in determining computational accuracy are experienced in both methods. In the tangent case, the number of increments required is unknown and, for the secant case, a definition of convergence is problematical.

For linear elastic materials there is no conflict between these two methods and definition of the stiffness relations is the same in both cases. For most geotechnical applications, involving axisymmetric or plane strain configurations, these relations can be written in the form shown in Fig. 6.2. However, for non-linear materials having stress dependent stiffness parameters, the transition from secant to tangent methods is more complex. If equations of the form given in Fig. 6.2 are applicable to the secant method, then it can be readily shown by

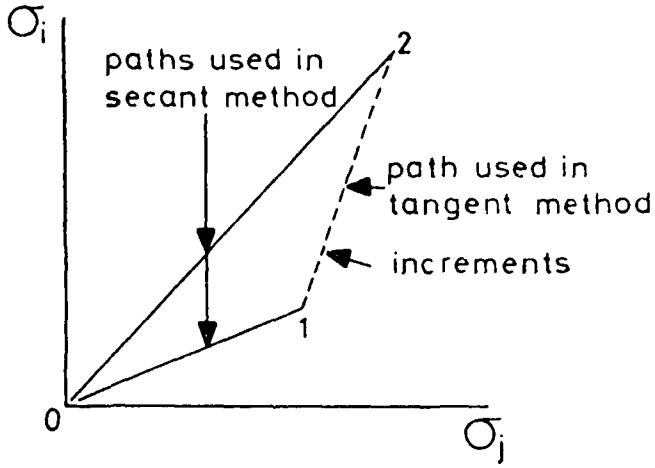


FIG. 6.1 BASIS OF COMPUTATION METHODS BASED ON SECANT AND TANGENT MODULI

$$\begin{bmatrix} \varepsilon_x \\ \varepsilon_y \\ \varepsilon_z \\ \gamma_{xy} \end{bmatrix} = \frac{1}{E} \begin{bmatrix} 1 & -\nu & -\nu & 0 \\ -\nu & 1 & -\nu & 0 \\ -\nu & -\nu & 1 & 0 \\ 0 & 0 & 0 & 2(1+\nu) \end{bmatrix} \times \begin{bmatrix} \sigma_x \\ \sigma_y \\ \sigma_z \\ \tau_{xy} \end{bmatrix}$$

FIG. 6.2 GENERAL STRESS-STRAIN RELATIONSHIP

$$\begin{bmatrix} \varepsilon_x \\ \varepsilon_y \end{bmatrix} = \frac{1}{E_s} \begin{bmatrix} 1 & -\nu_s \\ -\nu_s & 1 \end{bmatrix} \times \begin{bmatrix} \sigma_x \\ \sigma_y \end{bmatrix}$$

(a) SECANT

$$\begin{bmatrix} \varepsilon_x \\ \varepsilon_y \end{bmatrix} = \begin{bmatrix} A & B \\ C & D \end{bmatrix} \times \begin{bmatrix} \sigma_x \\ \sigma_y \end{bmatrix}$$

(b) TANGENT

FIG. 6.3 STRESS-STRAIN RELATIONSHIPS FOR AXIAL SYMMETRY

AD-A087 859 NOTTINGHAM UNIV (ENGLAND) DEPT OF CIVIL ENGINEERING F/G 13/2
PERMANENT DEFORMATION OF FLEXIBLE PAVEMENTS.(U)
JUN 80 S F BROWN, B V BRODERICK, J W PAPPIN DA-ERO-78-G-114
UNCLASSIFIED NL

2 OF 2
AU
AD-A087859

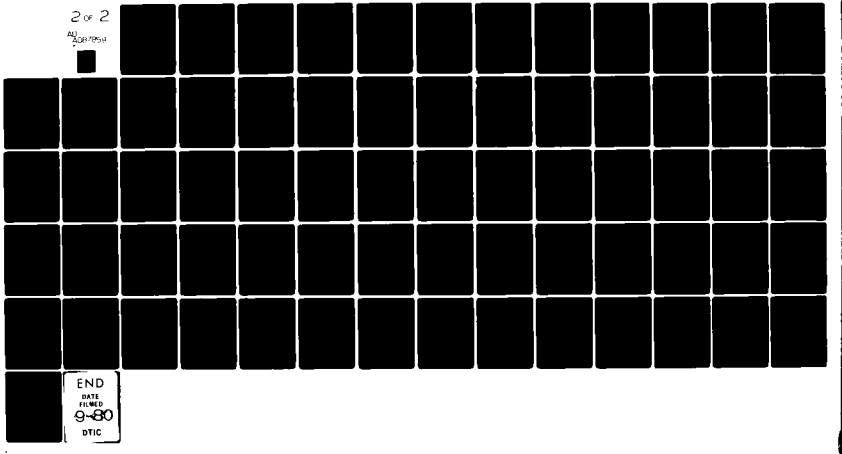

END
DATE FILMED
9-80
DTIC

differentiation that 16 independent stress-dependent terms are required to describe the equivalent set of equations for the tangent method. The deciding factor in choosing a method must, therefore, be related to the ease of application to a particular problem.

The results from the laboratory testing showed that granular materials, when subjected to repeated loading, exhibit dilatancy and stress induced anisotropy (16). It has been shown (23) that the secant method can be readily used to describe the two-dimensional axisymmetric behaviour exhibited by the triaxial test stress system. Fig. 6.3(a) shows the form of the equations linking stress and strain for this situation if the secant method is used. This type of system has been used to successfully describe the comprehensive repeated load triaxial test data (17). From these same results it has been possible to determine the equivalent equations for use in a tangent analysis and these are given in Fig. 6.3(b) where A, B, C and D are independent and all functions of stress. Hence, the secant method is preferable as less variables are examined simultaneously. It can also be seen from Fig. 6.3(b) that the tangent method indicates a non-symmetric matrix which would complicate a solution process considerably. The secant method was therefore chosen.

From the laboratory tests, a secant model was developed (24) for the resilient behaviour of the granular material. The applied stresses were expressed in terms of

$$\text{normal stress:}\quad p = \frac{1}{3}(\sigma_x + \sigma_y + \sigma_z) \tag{6.1}$$

and

$$\text{deviator stress:}\quad q = \frac{1}{\sqrt{2}}\{(\sigma_x-\sigma_y)^2+(\sigma_y-\sigma_z)^2+(\sigma_z-\sigma_x)^2 + 6\tau_{xy}^2+6\tau_{xz}^2+6\tau_{yz}^2\}^{\frac{1}{2}} \tag{6.2}$$

The resulting strains were expressed in terms of:

$$\text{volumetric strain:} \quad v = \varepsilon_x + \varepsilon_y + \varepsilon_z \tag{6.3}$$

and

octahedral shear strain:

$$\varepsilon = \frac{\sqrt{2}}{3}\left[(\varepsilon_x-\varepsilon_y)^2+(\varepsilon_y-\varepsilon_z)^2+(\varepsilon_z-\varepsilon_x)^2 + \frac{3}{2}\gamma_{xy}^2 + \frac{3}{2}\gamma_{yz}^2 + \frac{3}{2}\gamma_{xz}^2\right]^{\frac{1}{2}} \tag{6.4}$$

In the axisymmetric triaxial situation, these equations reduce to:

$$\begin{aligned} p &= \sigma_a + 2\sigma_c \\ q &= \sigma_a + \sigma_c \\ v &= \varepsilon_a + 2\varepsilon_r \\ \varepsilon &= \frac{2}{3}(\varepsilon_a - \varepsilon_r) \end{aligned} \tag{6.5}$$

where $\sigma_a$ and $\varepsilon_a$ are the axial stress and strain, $\sigma_c$ is the confining stress and $\varepsilon_r$ is the radial strain. It was found that the resilient volumetric strain could be expressed as a series of contours in the triaxial compression region of (p,q) stress space. These contours ($v_c$) are shown in Fig. 6.4 and can be expressed as:

$$v_c = 190\ p^{0.33}\{1 - 0.08(q/p)^2\} \text{ microstrain} \tag{6.6}$$

with stress in units of kPa.

The resilient octahedral shear strain was found to be dependent on stress path length but, after this effect was normalised, contours could be established (Fig. 6.5) and are described by:

$$\varepsilon_n = \frac{240q}{p+13} \text{ microstrain} \tag{6.7}$$

This gives rise to a resilient octahedral shear strain of:

$$\varepsilon_r = 240\left[\frac{q_2}{p_2+a} - \frac{q_1}{p_1+a}\right]\left[\frac{2\ell}{p_1+p_2}\right]^{0.4} \text{ microstrain} \tag{6.8}$$

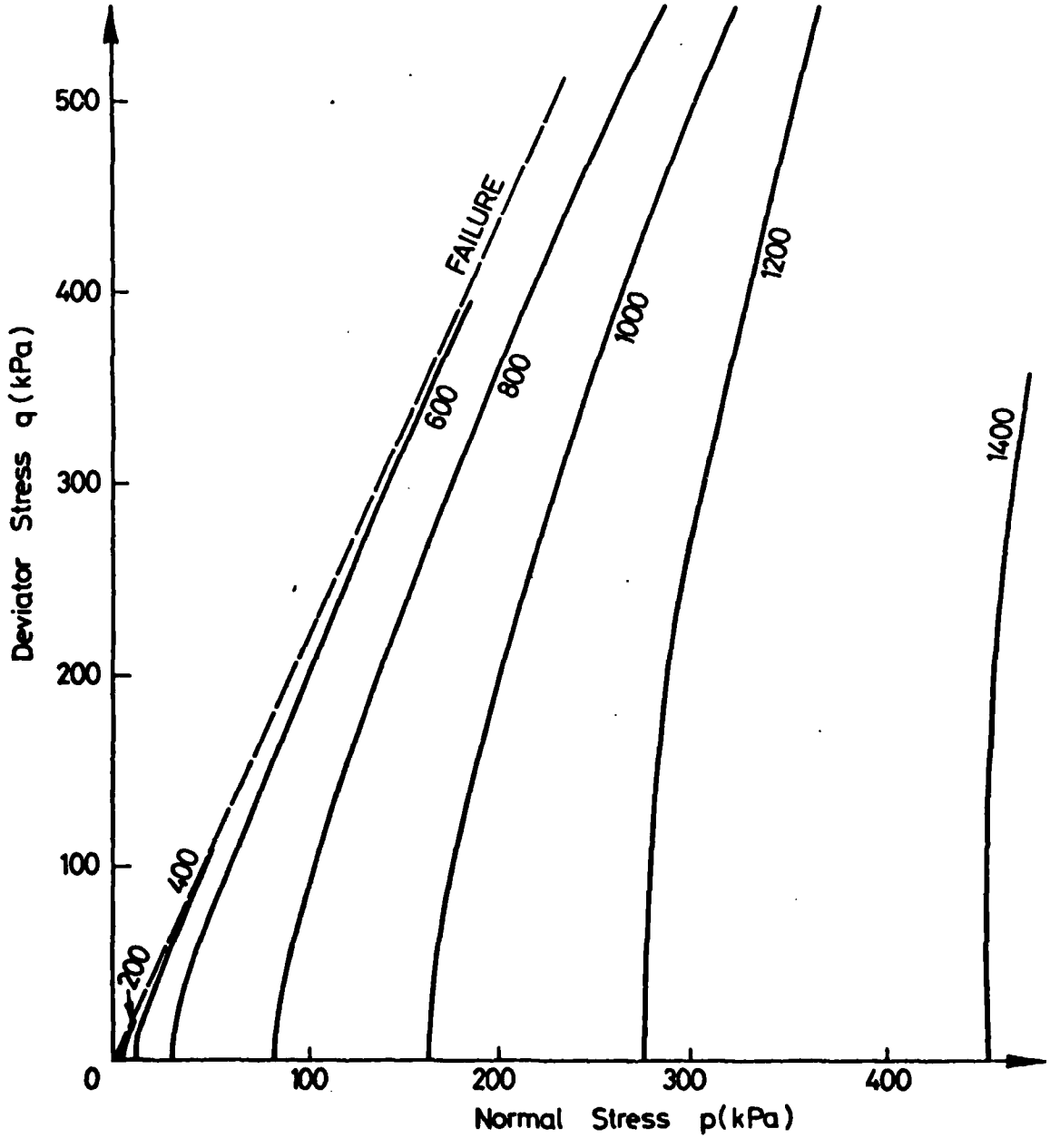


FIG. 6.4 VOLUMETRIC STRAIN CONTOURS FOR A CRUSHED LIMESTONE

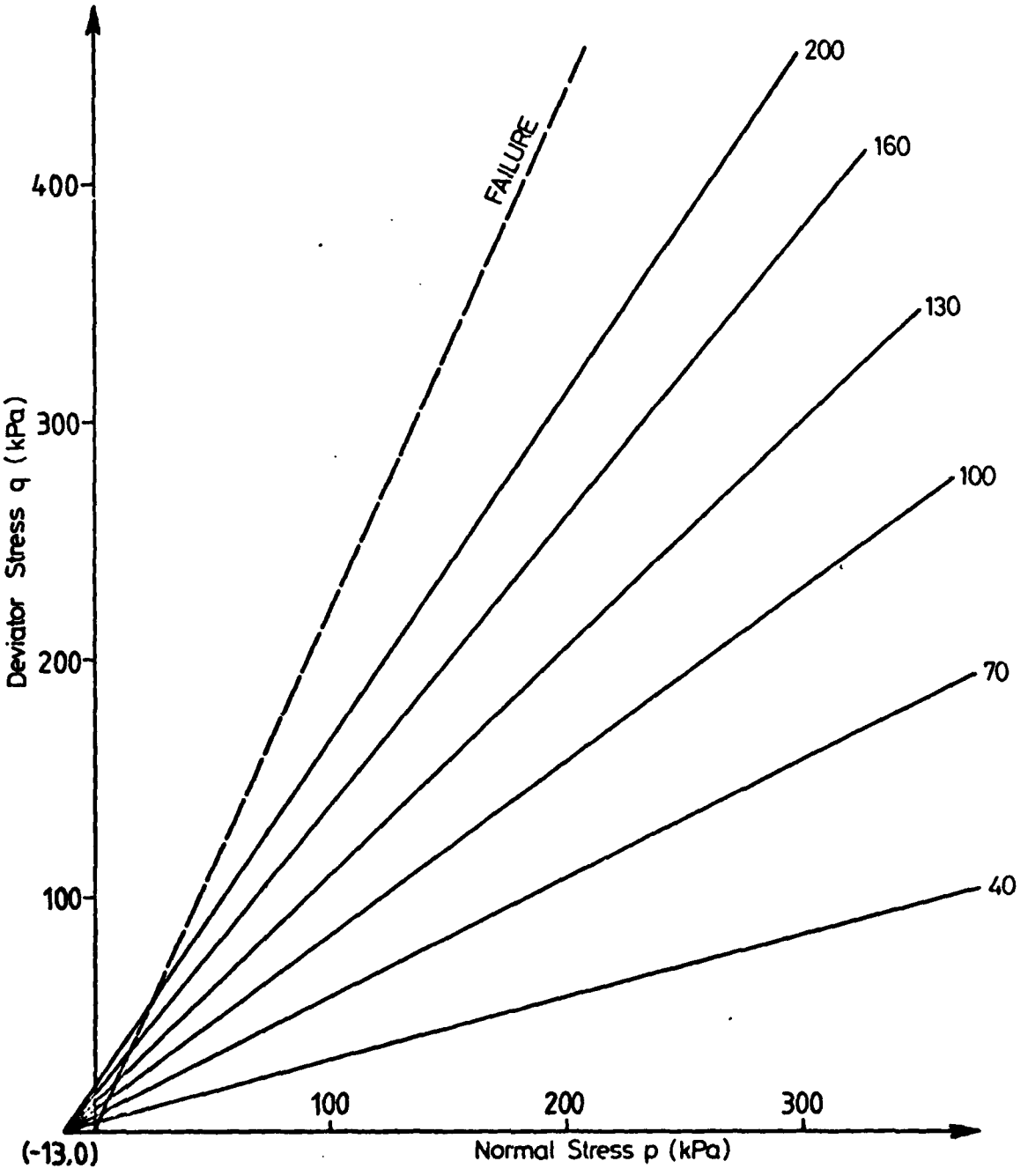


FIG. 6.5 NORMALISED SHEAR STRAIN CONTOURS FOR A CRUSHED LIMESTONE

where a = 13 kPa, $(p_1, q_1)$ and $(p_2, q_2)$ are the stress states at the beginning and end of the stress path respectively, and $\ell$ is the length of the stress path in (p,q) stress space.

From triaxial extension tests, it was found that a good approximation to convert a general three-dimensional stress ($\sigma_x \neq \sigma_y \neq \sigma_z$) to an equivalent point in triaxial compression ($\sigma_z > \sigma_x = \sigma_y$) was achieved by redefining q in Equations 6.6, 6.7 and 6.8 as:

$$q = \left(\frac{3\sigma_1 - 3\sigma_3}{2\sigma_3 + \sigma_1}\right)p \qquad (6.9)$$

This transformation allowed the stress-strain relations developed in the compression region to be more generally applicable.

To determine parameters suitable for a secant non-linear analysis, shear and bulk modulus were determined from the above equations as:

$$\text{bulk modulus:} \quad k = p\,\frac{(k/p)^{0.33}}{\{1 - 0.08(q/p)^2\}} \qquad (6.10)$$

where $k = 1.9 \times 10^{11}$ kPa

and shear modulus at the beginning of the stress path:

$$G_1 = \frac{q_1}{3\varepsilon_1} \qquad (6.11)$$

and shear modulus at the end of the stress path:

$$G_2 = \frac{q_2}{3\varepsilon_2} \qquad \text{where } \varepsilon_2 = \varepsilon_1 + \varepsilon_r \qquad (6.12)$$

Because of the stress path length dependency of the shear modulus, a value is needed for $\varepsilon_1$. This effect also explains the necessity to define a shear modulus at either end of the stress path, while a value for the path is sufficient in the case of bulk modulus.

Investigations have also been performed to examine the effect of moisture on the resilient response of the crushed limestone (17). It was found that if effective stresses were used (i.e. replacing p by p'), the same constituative equations were applicable. In the partially saturated condition, a negative pore pressure exists which may be estimated from the degree of saturation (17).

Unfortunately, in the pavements reported here, the in situ density was about 12% less than that used in the laboratory investigation. It is believed that density has a significant effect on the resilient response of this type of material and it has been indicated (25) that a density reduction of this amount could reduce the stiffness by 75%. Theoretical work by Pappin (17) showed that resilient shear strains were likely to be much more sensitive to density changes than volumetric strains. Hence, the $\varepsilon_r$ value (equation 6.8) was increased by a factor of 4 while the volumetric behaviour was unchanged. Although this seems quite a large and arbitrary adjustment, some subsequent analysis indicated that the in situ effects being predicted were not very sensitive to this parameter.

Other tests in the laboratory programme (17) resulted in the development of an expression for permanent octahedral shear strain:

$$\varepsilon_p = a.fnN.\ell_p.(q/p)^{2.8}_{max} \qquad (6.13)$$

where a is a constant = $3.33 \times 10^{-4}$, fnN is a function of the number of cycles applied (N) and can be expressed as:

$$fnN = 1.05n - .418n^2 + 0.1n^3 - 0.01n^4$$

where $n = \log N - 2$

and $\ell_p$ is the stress path length in $(\bar{p}, \bar{q})$ space divided by the mean $\bar{p}$ value with $\bar{p} = \sqrt{3}p$ and $\bar{q} = \frac{\sqrt{2}}{\sqrt{3}} q$.

This model only works for the range of N between 100 and 100,000 load applications and is seen to give zero strain at N equal to 100. If negative pore pressure is present in the material, it is treated in the same way as for the resilient response, i.e. by using effective stress p' in place of p.

### 6.2.2 Silty Clay Subgrade

As the subgrade material used in these pavements was the same as that used in the previous investigation (1), these earlier results could be used directly.

The resilient behaviour of the material was found to conform to the usual stress softening non-linearity (26) associated with cohesive materials. From triaxial tests with a repeated deviator stress cycling between zero and a peak value, it was found that the resilient modulus was given by:

$$M_r = a\left(\frac{p'_o}{q_{max}}\right)^{0.7} \qquad (6.14)$$

where a is a constant = 50,000 kPa and $p'_o$ is the initial normal effective stress and $\nu = 0.4$.

This tangent modulus had to be converted to a value suitable for secant analysis. The transient vertical strain is given by:

$$\varepsilon_{ar} = \frac{q_r}{M_r} = 20\ q_r \times \left(\frac{q_{max}}{p'_o}\right)^{0.7} \text{ microstrain} \qquad (6.15)$$

where $q_r$ is the repeated deviator stress.

For Poisson's Ration near to 0.5, it can be assumed that the octahedral shear strain is approximately equal to resilient axial strain. Therefore:

$$\varepsilon_2 = \varepsilon_1 + \varepsilon_{ar} \qquad (6.16)$$

and equation 6.12 then gives a value of shear modulus. A bulk modulus can then be determined such that Poisson's Ratio is maintained constant,

$$\text{i.e.} \quad K = \frac{2(1+\nu)}{3(1-2\nu)} G \qquad (6.17)$$

As a $q_r$ value is incorporated in equation 6.15, assumptions have to be made as to the value of $\varepsilon_1$ in the same way as for the granular material.

The model for the permanent octahedral shear strain response of the silty clay was derived from that in the previous report (1). All specimens of the material gave a similar type of response but variation in the moisture content and dry density had a noticeable effect on the magnitude of strain. It was found that this effect could be removed by including $p'_o$ (see equation 6.14) in the relationship as follows:

$$\varepsilon_p = \frac{q_r q}{p'_o a} (\log N_f - \log N_s) \qquad (6.18)$$

where a is a constant equal to 20,000 kPa and $N_s$ and $N_f$ are the number of cycles at the beginning and end of the loading period being investigated.

### 6.2.3 Bituminous Materials

The earlier project (1) involving a continuously graded mix at 30°C showed that the resilient response was non-linear. At a lower temperature, 25°C, however, linear response was found in a more detailed investigation (27).

As stiffness testing on the rolled asphalt used in this project was not possible (see Section 3.1), estimates had to be made of its resilient characteristics. In view of its gap grading, higher binder content and stiffer binder compared with the material tested earlier, it was considered that linear resilient behaviour could be assumed. The established procedures developed by Shell (28,29) for estimating dynamic stiffness were used and Poisson's Ratio was taken as 0.4.

Some recent test results (30) were used to assess permanent strain characteristics for the base course material used in pavements 1. This gave an equation for permanent shear strain of the form:

$$\varepsilon_p = \frac{q}{a}(\log N_f - \log N_s) \qquad (6.19)$$

where a = 80,000 kPa.

As no information was available on the wearing course material used for most of the pavements, a series of creep tests was carried out on some remoulded specimens at 30°C. These were compared with creep results for other materials (28) and an extrapolation made for the permanent strain behaviour. This approximate procedure gave the equation:

$$\varepsilon_p = \frac{q}{a}(N_f^{\frac{1}{2}} - N_s^{\frac{1}{2}}) \qquad (6.20)$$

where $a = 2.5 \times 10^6$ kPa.

## 6.3 RESILIENT STRAIN ANALYSIS

A non-linear axisymmetric finite element analysis was carried out for each pavement using the appropriate material properties described in the previous section. To characterise the subgrade, a value of $p_o'$ had to be estimated from the body force stresses and the soil suction.

A careful investigation of pavements 5 involving analyses, consideration of moisture conditions and some suction tests on soil specimens, showed that a value for $p_o'$ of 5 kPa was appropriate. For the remaining pavements $p_o'$ was derived by comparing the measured CBR values and moisture contents of the pavement with those for pavements 5 and making appropriate adjustments. These values, together with other data used in the analyses, are given in Table 6.1. The asphalt layer thickness was taken as 50 mm for all computations. For pavements 6 and 7, the

Table 6.1 Data used for pavement resilient analyses

| Pavement No. | Load (kN) | Contact pressure (kPa) | Load rad. (mm) | Asphalt stiffness (MPa) | Granular layer | | Subgrade $p'_o$ (kPa) |
|---|---|---|---|---|---|---|---|
| | | | | | Thickness (mm) | Pore pressure (kPa) | |
| G1 | 11 | 550 | 80 | 1930 | 170 | 0 | 5 |
| GT1 | 11 | 550 | 80 | 1340 | 170 | 0 | 5 |
| G3 | 8 | 520 | 70 | 1210 | 130 | 0 | 6 |
| G4 | 5 | 526 | 55 | 560 | 120 | 0 | 4 |
| G5 | 8 | 520 | 70 | 650 | 130 | 0 | 5 |
| G6 | 8 | 520 | 70 | 830 | 170 | -14 | 4 |
| GT7 | 8 | 520 | 70 | 830 | 170 | -14 | 4 |

limestone was partially saturated and the negative pore pressure was estimated as 14 kPa.

### 6.3.1 Non-Linear Solution Method

A flow diagram for the computer program, named SENOL (Secant non-linear), using the secant method of analysis, is shown in Fig. 6.6. This shows that the stresses and strains were calculated (step 3) for body forces before any wheel loading was applied (step 6). Details of the finite element solution method used in steps 3 and 7 are described in the next section. It was a linear elastic solution with the stiffness of each element being individually prescribed (steps 2, 4 and 8).

Initially, the program had to assume elastic properties for each element (step 2). To do this, the vertical stress acting on an element was approximated using the depth of the element and the density of the overlying materials. The horizontal stresses were then estimated using a $K_o$ value of 0.8. For the granular and clay material, an estimate was then made for the initial octahedral shear strain ($\varepsilon_1$). This was easily obtained for the granular material, using the expression for K in equation 6.10. If the pavement is considered to have no horizontal strain when under the action of body forces alone, then

$$\nu = \frac{K_o}{1+K_o} \tag{6.21}$$

and

$$G = \frac{3(1-2\nu)}{2(1+\nu)} K \tag{6.22}$$

For the silty-clay, K was initially assumed to be 100,000 kPa and the process described above was then applied. These values of G and K were inserted in step 2 and step 4 of Fig. 6.6.

Having solved for body force stress and strain (step 3), new element properties were calculated using these stresses (step 4) and a

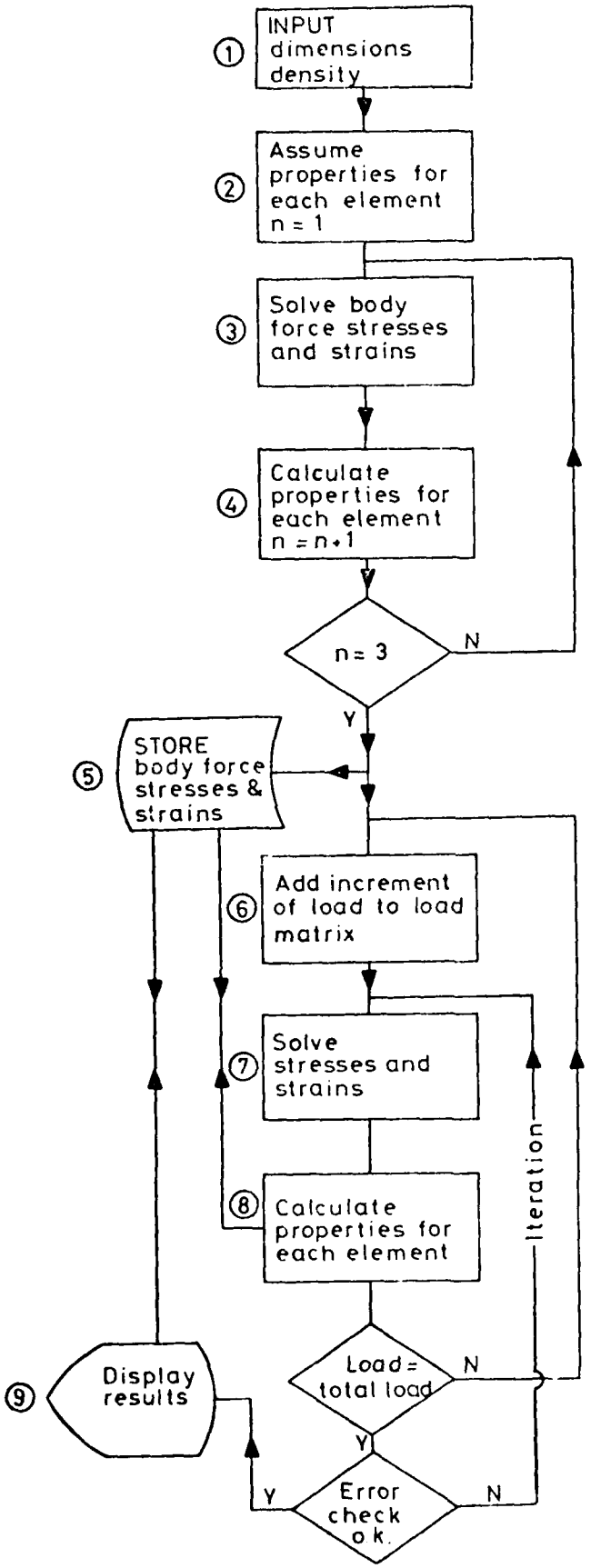


FIG. 6.6 FLOW DIAGRAM OF NON-LINEAR FINITE ELEMENT PROGRAM

final solution for the body force condition was then accurately determined and the results stored for later use (step 5).

The application of wheel loading was an iterative process as the element properties are required to determine the stress state for each element and these stress states are required to determine the element properties. Several attempts were made to produce a method for obtaining convergence. The most reliable one (see Fig. 6.6) involved application of the load in successively larger quantities and then iterating when the full load was applied using a variable damping factor. The load was applied in ten steps (step 6) and, by doing this, the stress state within the pavement was brought reasonably close to the final solution before iteration commenced. To determine if the iteration was being successful, a measure of error was calculated using the equation:

$$\text{Error} = \frac{\Sigma(E_n - E_o)^2}{\Sigma E_n^2} \qquad (6.23)$$

where $E_n$ is the modulus value calculated from the current iteration solution and $E_o$ is the value from the previous iteration. The summation takes place over all non-linear elements.

If the error term increased, then a damping factor (DF) was employed such that the modulus value to be used in the next iteration was determined from:

$$E_u = (DF)E_n + (1-DF)E_o \qquad (6.24)$$

If the error continued to increase, the damping factor was halved successively. Convergence was considered to have been achieved when the error reached a value of less than $2 \times 10^{-3}$.

### 6.3.2 Finite Element Layout

The pavement was considered as an axisymmetric system. Fig. 6.7

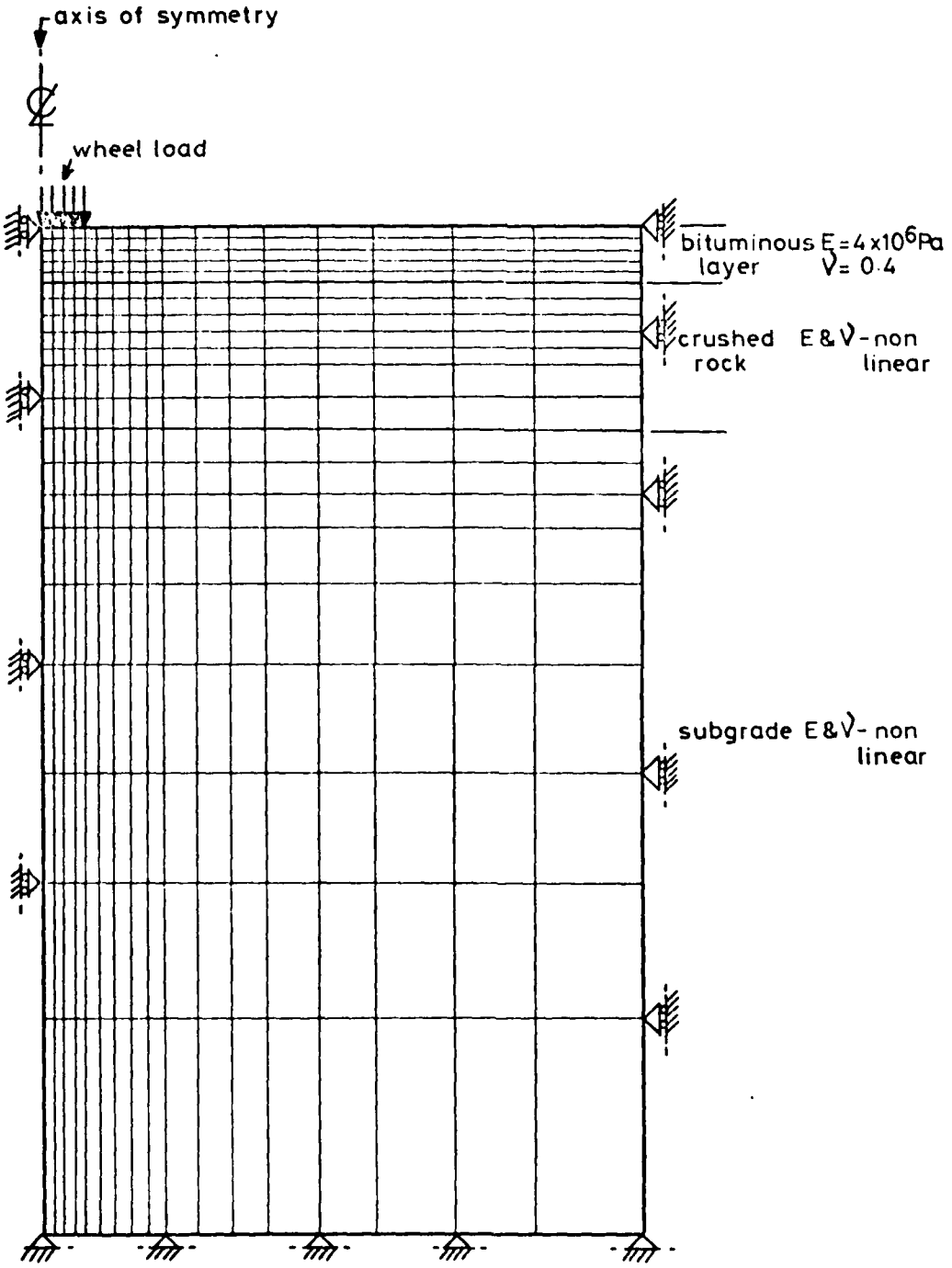


FIG. 6.7 TYPICAL FINITE ELEMENT LAYOUT

shows a typical layout of the elements, material layers, loading condition and boundary supports. The elements, formulated by Barksdale (31), are linear strain rectangles and the displacement functions inside each element are approximated by:

$$u(r,z) = c_1 + c_2 r + c_3 z + c_4 rz$$
$$v(r,z) = c_5 + c_6 r + c_7 z + c_8 rz \qquad (6.25)$$

where u and v are the horizontal and vertical displacements respectively. Using this type of function the $[B]^T[D][B]$ matrix varies continuously within the element. To obtain a value for the total element stiffness,

$$[K] = \int_{vol} [B]^T [D] [B] dV \qquad (6.26)$$

a nine point Gaussian Integration method was used. The $[D]$ matrix is the same as that found by inverting the matrix shown in Fig. 6.2. The values of E and $\nu$ were determined directly from the K and G values found using the equations given in Section 6.1. Solutions for the displacements using the overall system stiffness matrix were obtained by using Choleski triangular matrix decomposition. A summary of the facilities available with the SENOL program is given in Appendix 2.

### 6.3.3 Comparison of Predictions with Measurements

The finite element program SENOL was used to predict transient stress and resilient strain for all elements in the vertical, radial and tangential directions as well as the shear stress and strain. In the base and subgrade, the values of stress ratio q/p were also computed in order to assess whether failure conditions were being encountered. Part of a typical set of results, traced from the graph plotter output, is shown in Fig. 6.8.

Figs 6.9 to 6.15 show the predicted relationships between vertical

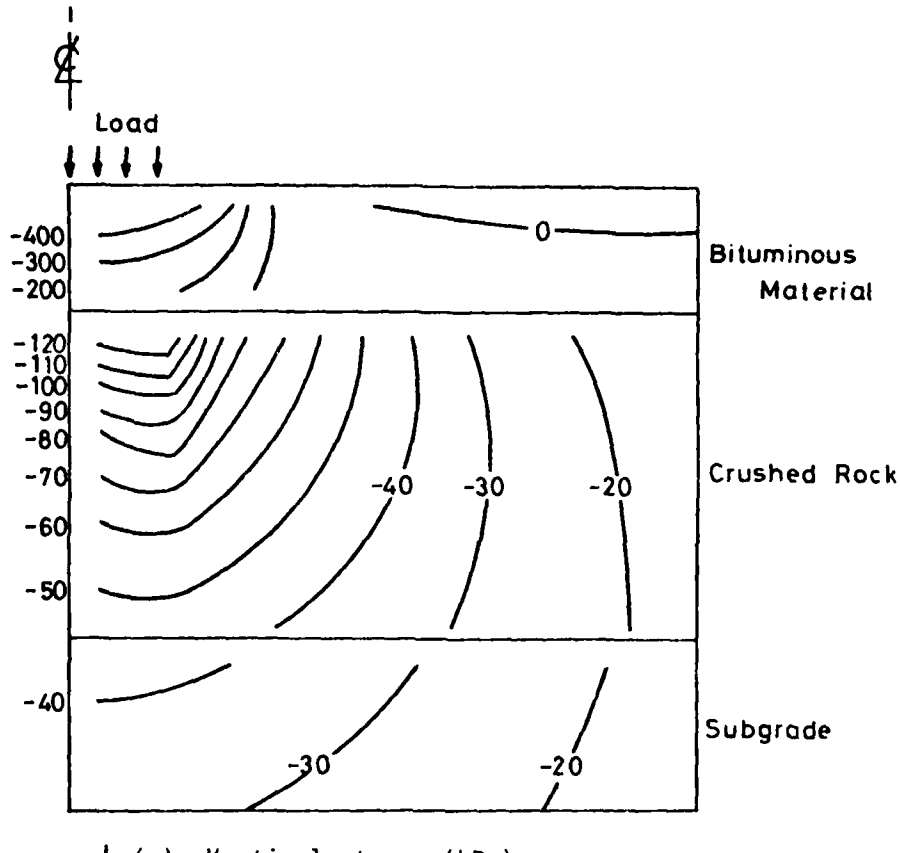


(a) Vertical stress (kPa)

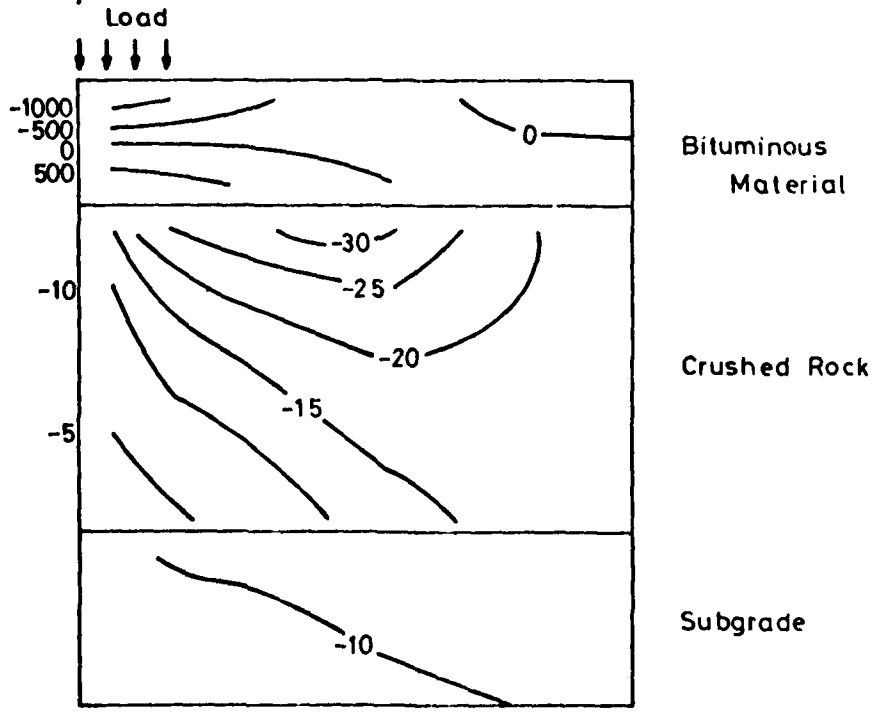


(b) Tangential stress (kPa)

FIG. 6.8 RESULTS OF TYPICAL COMPUTATIONS FOR TRANSIENT STRESSES AND STRAINS (+VE TENSION)

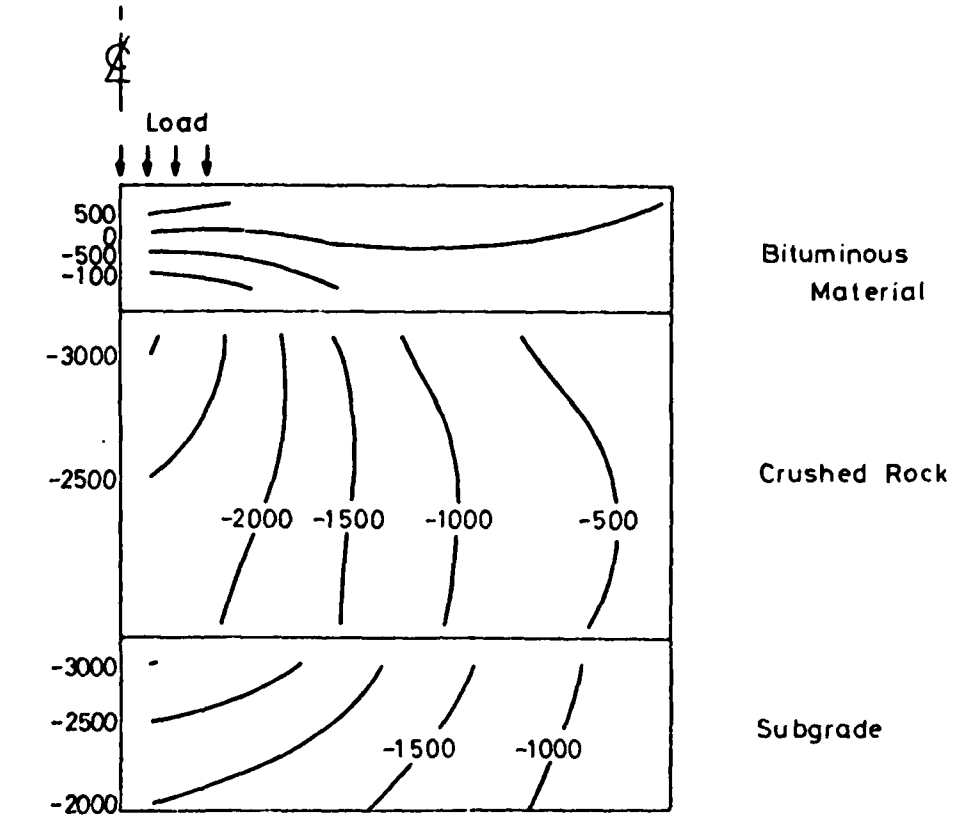


(c) Vertical strain (microstrain)

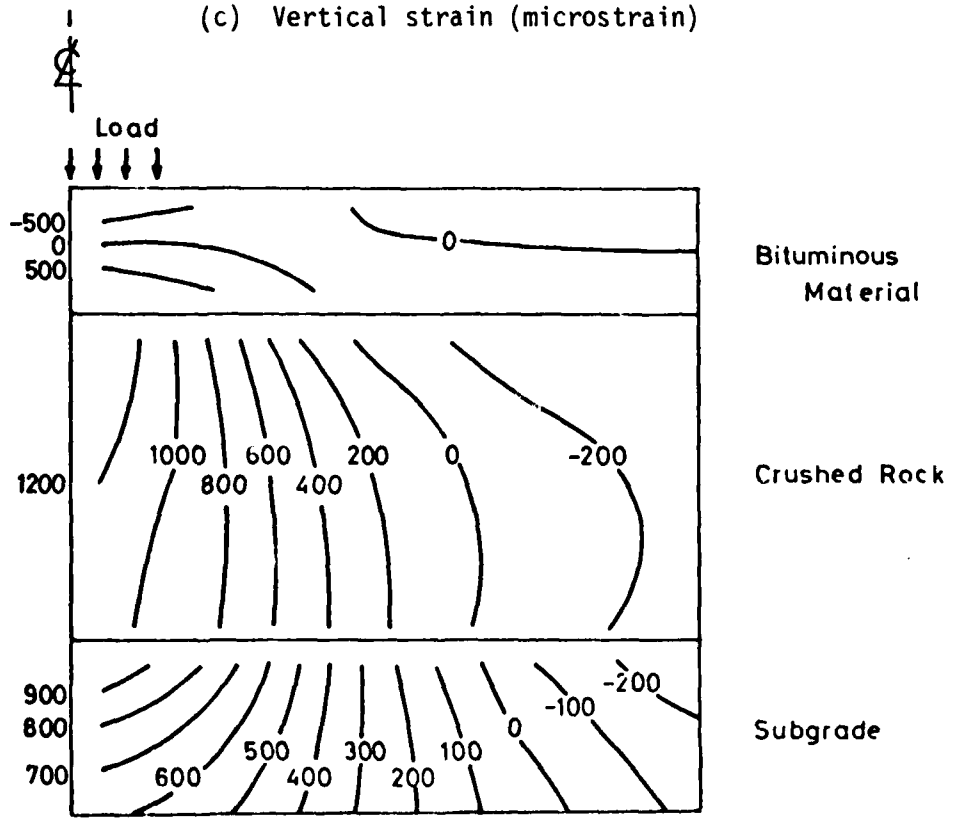


(d) Tangential strain (microstrain)

FIG. 6.8 contd

radial and tangential stress and resilient strain superimposed on the measured pulses taken from the UV recorder output. In all cases, these results are for the situation where the wheel passed directly over the instrument being monitored. Time was converted to radial distance via the wheel speed. Part "a" of each figure shows the stresses while part "b" shows the resilient strains. Each individual plot of a pulse is located with its x-axis at the depth in the pavement where the instrument was placed. Measured pulses marked with a T are from those pavements including Terram fabric. For pavements 4, few experimental results were available so in Fig. 12b the peak values of strains were plotted against depth. No data is shown for pavements 2, since the analysis indicated extensive failure zones and the solution would not converge satisfactorily. In practice, this pair of pavements was observed to fail prematurely so, in general terms, the predicted response was correct. In other pavements, the maximum computed values of q/p for any element in the granular base varied between 1.7 and 2.2 as shown in part "a" of Figs 6.9 to 6.15. The value of q/p at failure for this material, based on laboratory tests, was 2.2 when well compacted. Hence, only an odd element in any of the pavements, other than G2 and GT2, was predicted to be at failure under peak stress conditions. This, again, generally confirms the observed behaviour. If a significant number of elements are at or beyond the failure value of q/p, large permanent strains would be expected to develop.

An overall view of the comparisons between measured and predicted response in Figs 6.9 to 6.15 shows that resilient strains are predicted well but that the accuracy of stress prediction is variable, and in some instances, poor. However, the general pulse shapes for all parameters are well predicted with only a few exceptions. Predictions of vertical stress are low except for the last two pavements. This indicates that

the stiffness used for the asphalt layer may have been too high and points to the need for direct measurement of this parameter which was not possible at the time the experiments were performed (see Section 3.1). The values of vertical stress were found to be relatively insensitive to the method of computation which was used so that linear analysis produced similar values to those from the non-linear technique.

From the point of view of pavement design, the parameters of major interest for permanent deformation are the stress invariants p and q, which are not shown directly on Figs 6.9 to 6.15 since they are not directly measurable parameters. However, they were used for subsequent predictions of permanent deformation as discussed in the next section. The tensile strain at the bottom of the asphalt layer is of interest in assessing the possibility of fatigue cracking. Values in the range 500 to 2000 microstrain were recorded and reasonably well predicted by theory. Strains of this magnitude imply negligible lives based on laboratory fatigue testing (19), but no cracks were apparent except in pavements 2 which are excluded from this discussion as noted above.

Prediction of resilient stresses and transient strains were also carried out for the three full depth bituminous pavements tested in the previous project (1). The resulting predictions were similar to those that were reported and are not, therefore, included here. In general, stress predictions were again low.

In view of the relatively poor predictions of stress and the fact that the accuracy of permanent strain values depends on them, further analytical work is clearly needed. A sensitivity analysis to try and assess which input parameters have most effect on the computed stresses could help to throw light on the problem.

The accuracy of computations has been judged by comparing values with those measured in situ and hence the reliability of the measurements

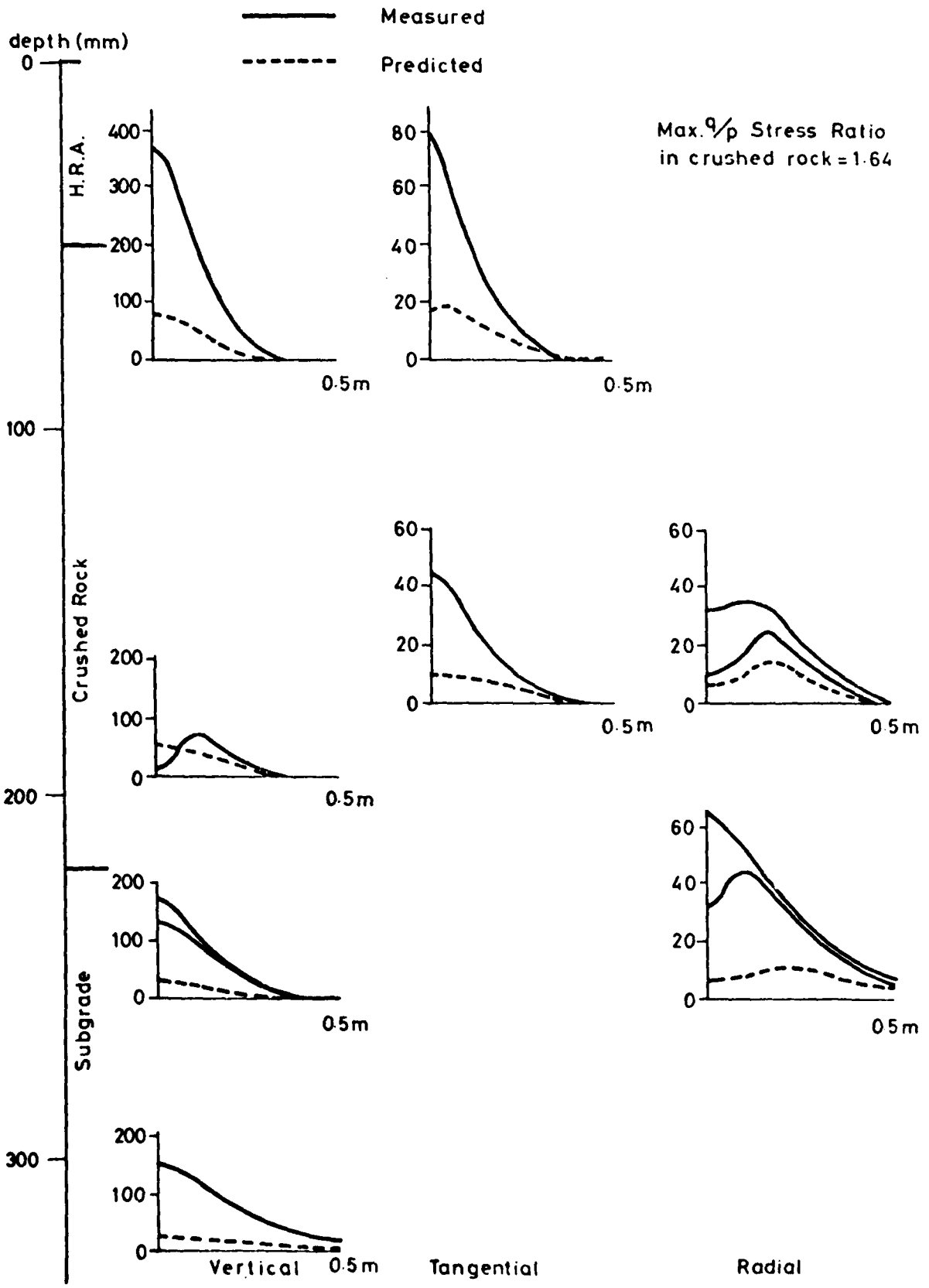


FIG. 6.9(a) MEASURED AND PREDICTED REPEATED STRESSES (kPa) FOR PAVEMENT G1

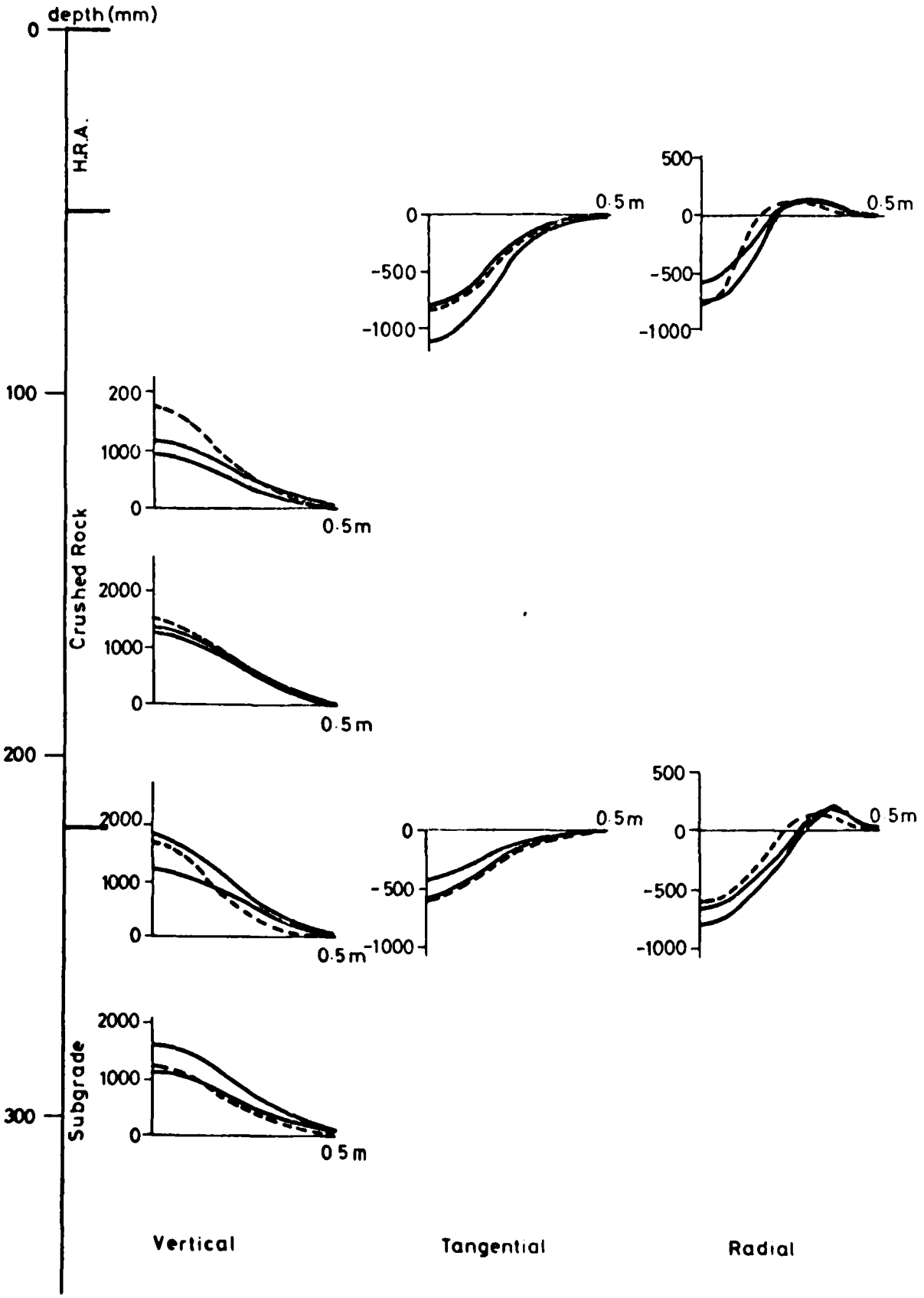


FIG. 6.9(b) MEASURED AND PREDICTED RESILIENT STRAINS ($\mu\varepsilon$) FOR PAVEMENT G1

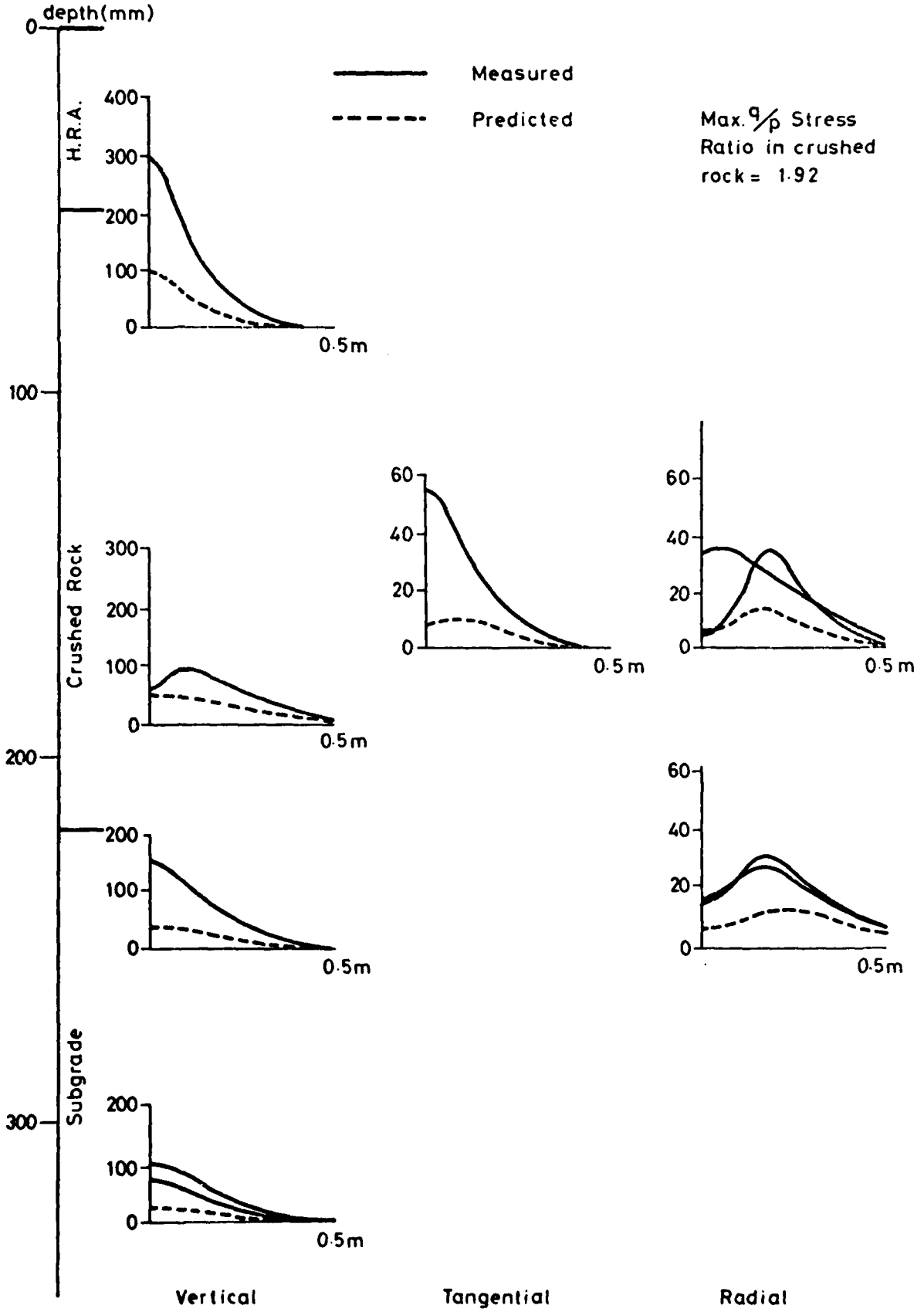


FIG. 6.10(a) MEASURED AND PREDICTED REPEATED STRESSES (kPa) FOR PAVEMENT GT1

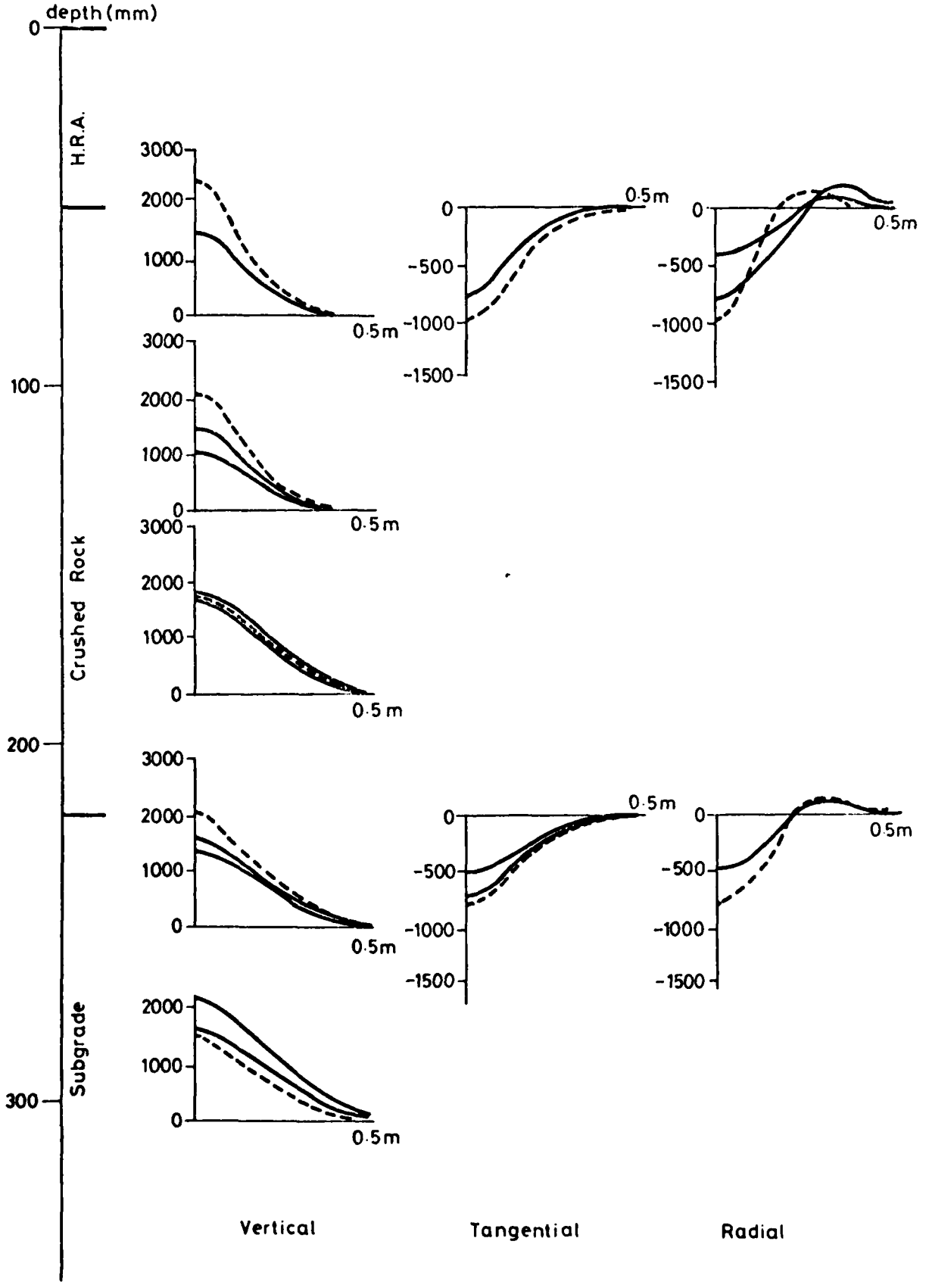


FIG. 6.10(b) MEASURED AND PREDICTED RESILIENT STRAINS ($\mu\varepsilon$) FOR PAVEMENT GT1

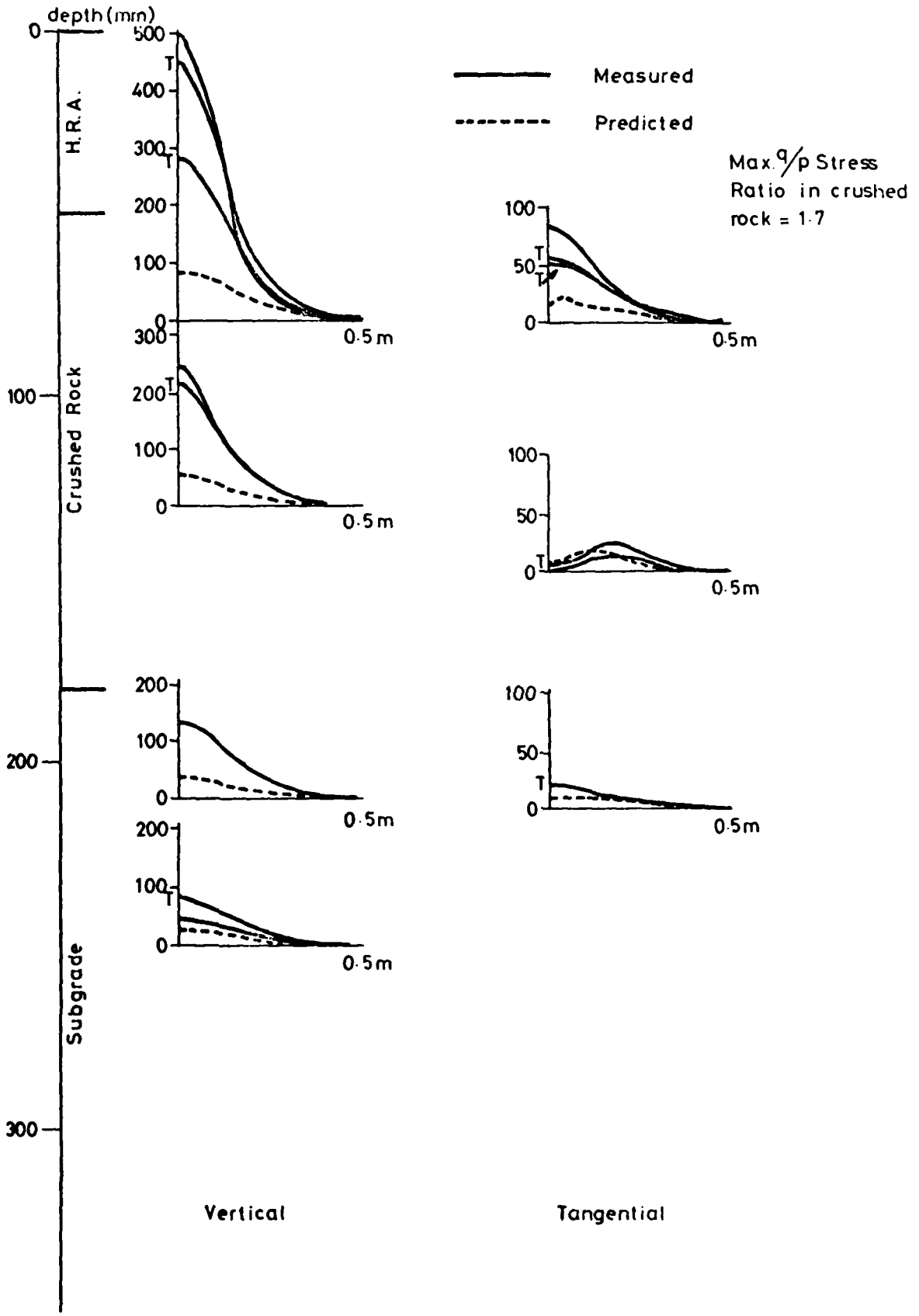


FIG. 6.11(a) MEASURED AND PREDICTED REPEATED STRESSES (kPa) FOR PAVEMENTS G3 AND GT3

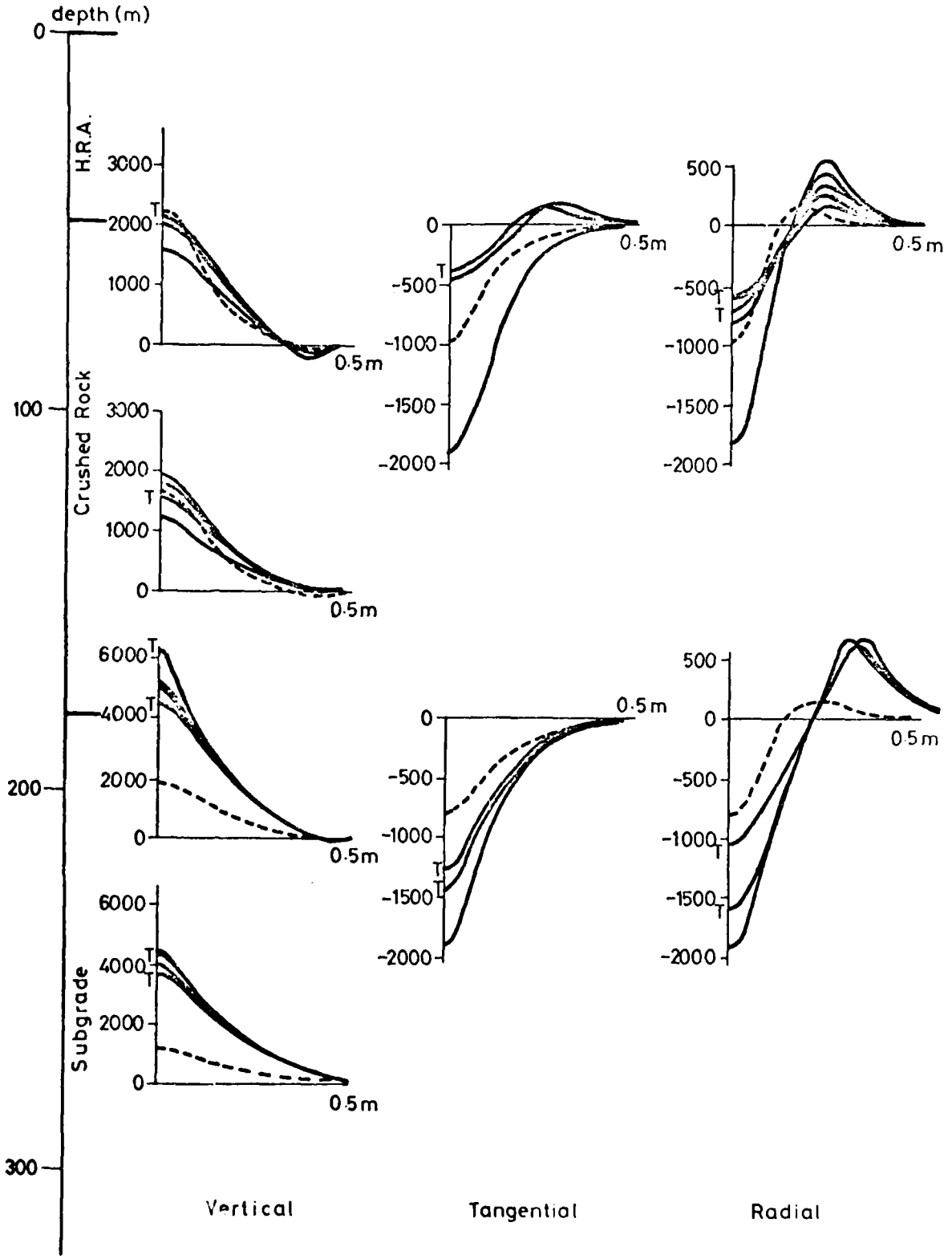


FIG. 6.11(b) MEASURED AND PREDICTED RESILIENT STRAINS ($\mu\varepsilon$) FOR PAVEMENTS G3 AND GT3

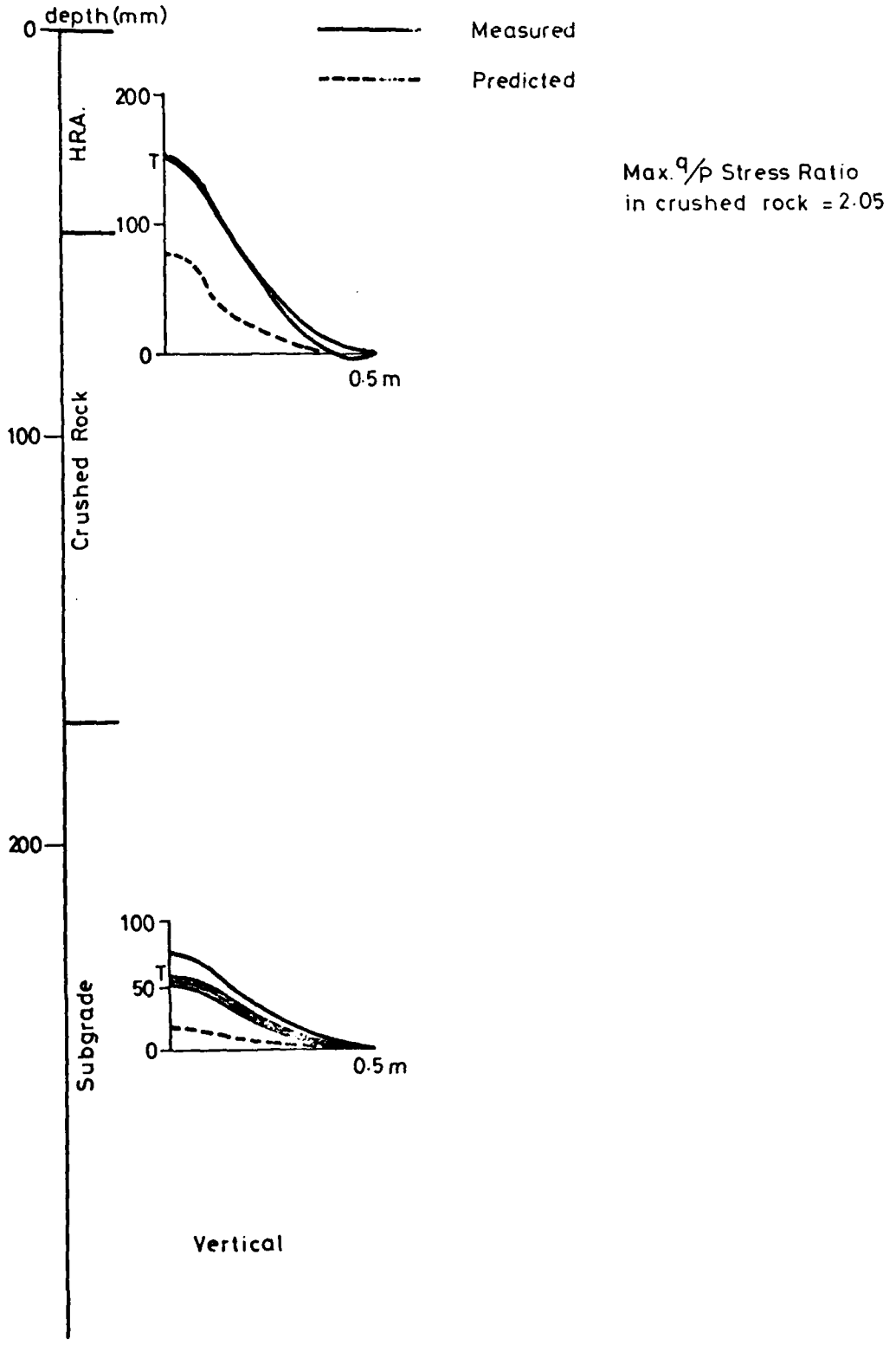


FIG. 6.12(a) MEASURED AND PREDICTED REPEATED STRESSES (kPa) FOR PAVEMENTS G4 AND GT4

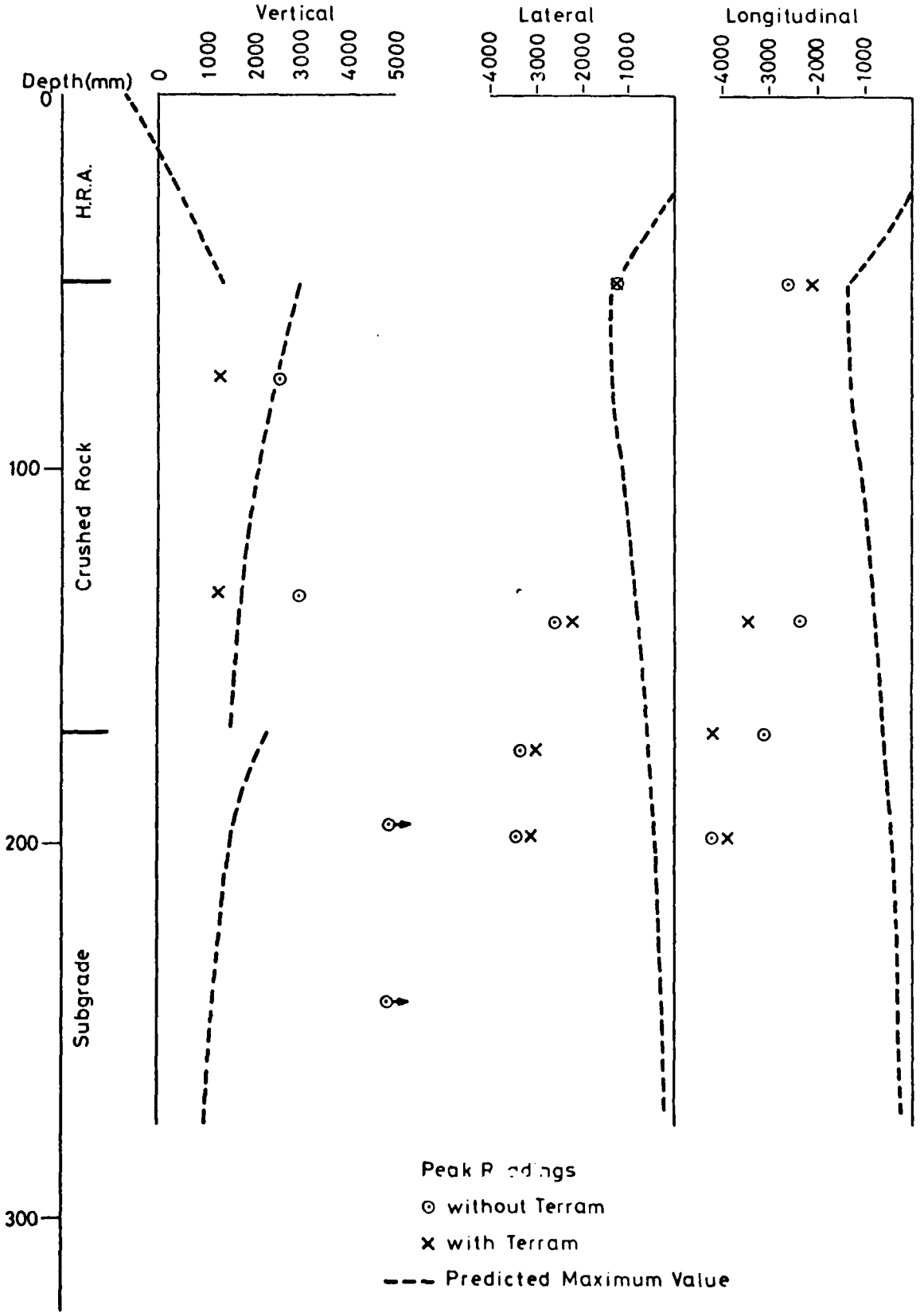


FIG. 6.12(b) MEASURED AND PREDICTED RESILIENT STRAINS ($\mu\varepsilon$) FOR PAVEMENTS G4 AND GT4

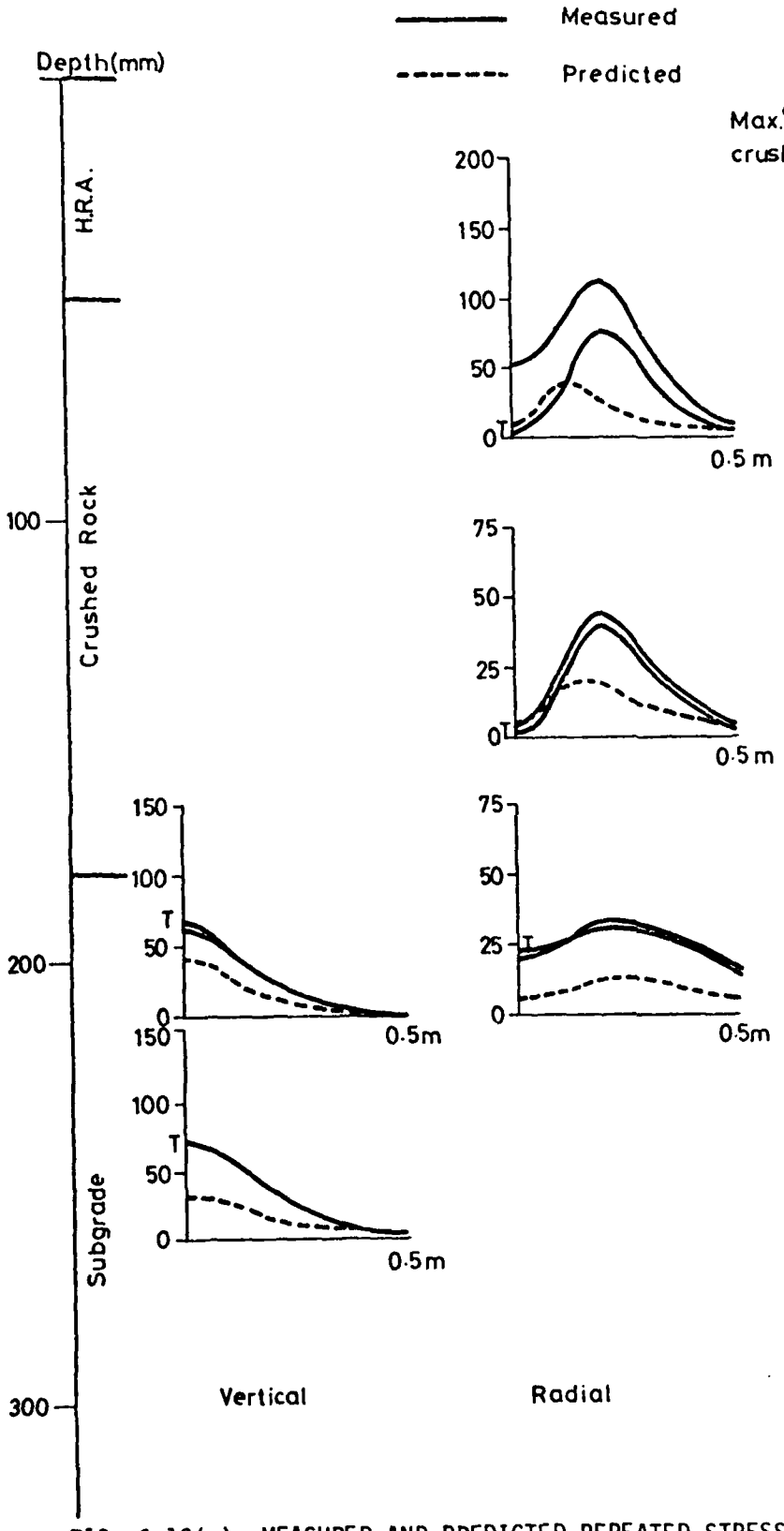


FIG. 6.13(a) MEASURED AND PREDICTED REPEATED STRESSES (kPa) FOR PAVEMENTS G5 AND GT5

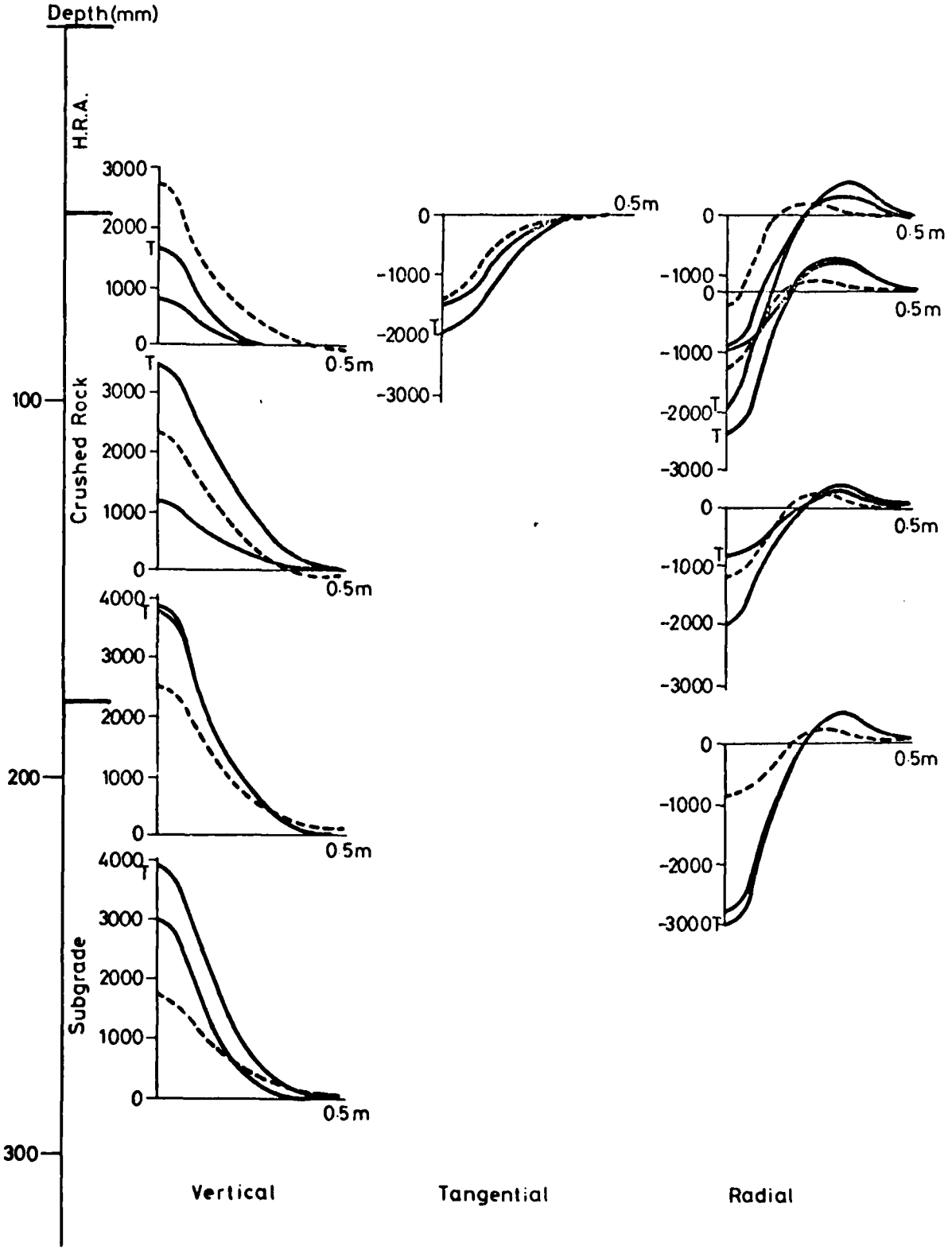


FIG. 6.13(b) MEASURED AND PREDICTED RESILIENT STRAINS ($\mu\epsilon$) FOR PAVEMENTS G5 AND GT5

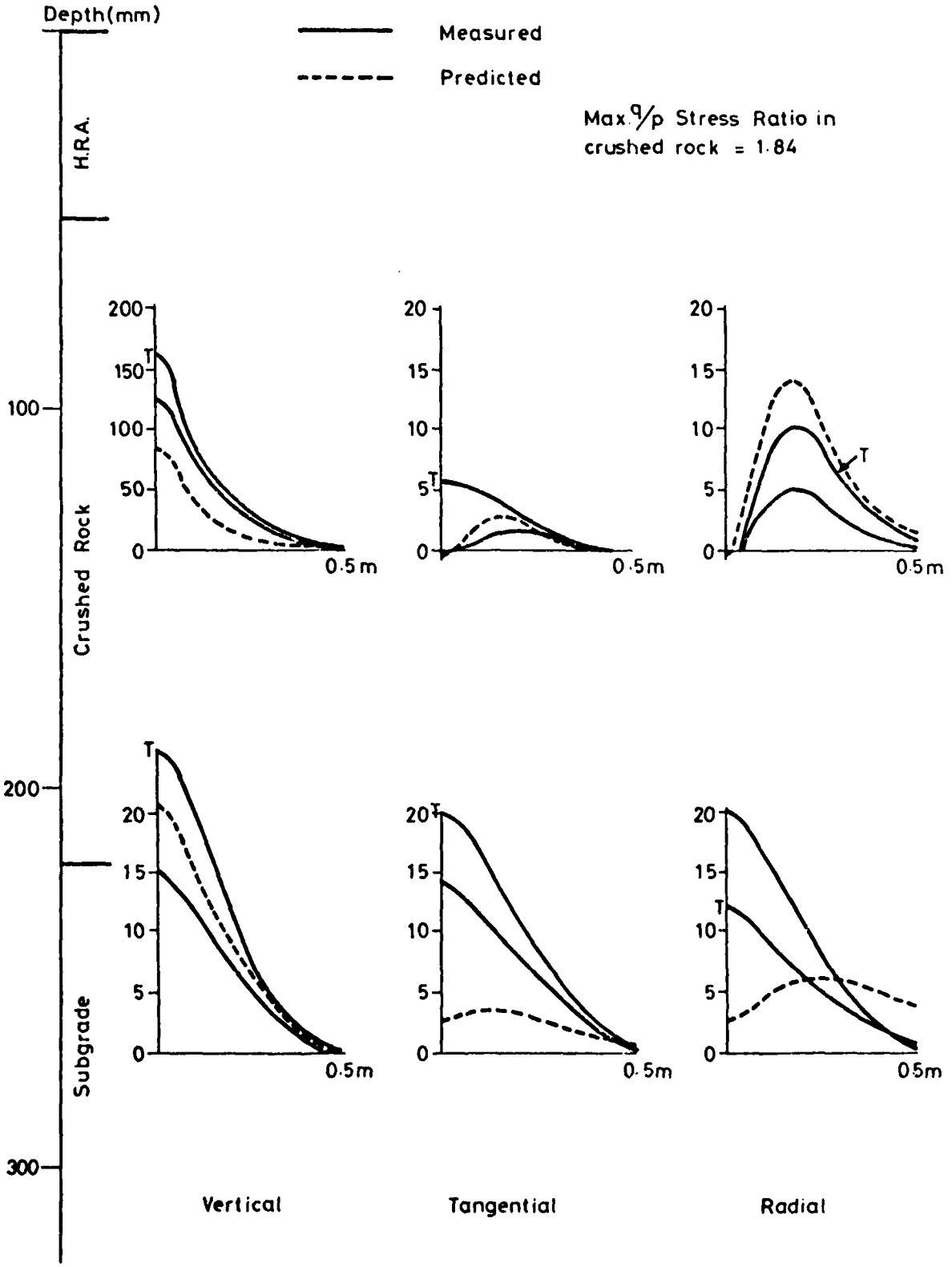


FIG. 6.14(a) MEASURED AND PREDICTED REPEATED STRESSES (kPa) FOR PAVEMENTS G6 AND GT6

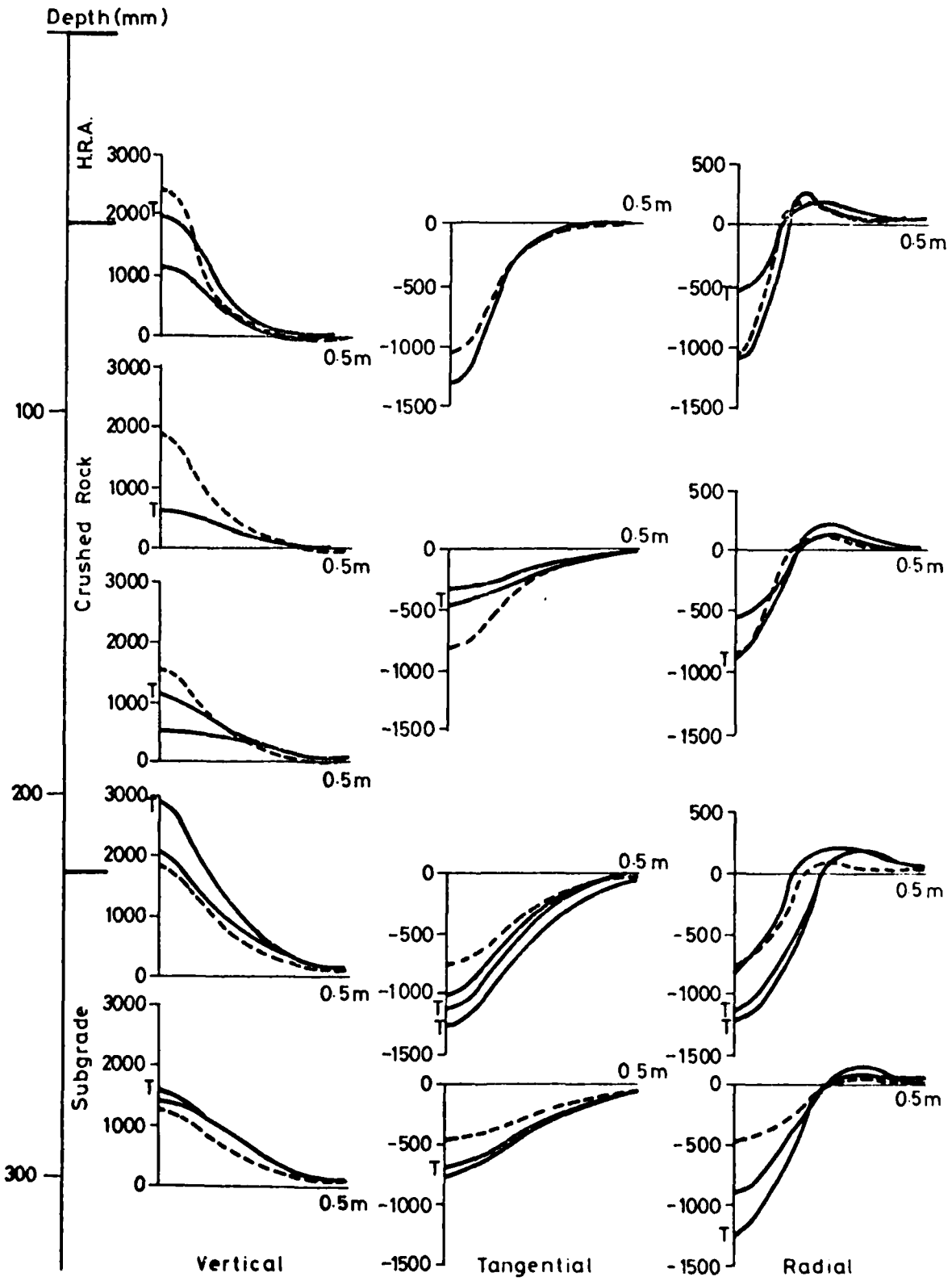


FIG. 6.14(b) MEASURED AND PREDICTED RESILIENT STRAINS ($\mu\varepsilon$) FOR PAVEMENTS G6 AND GT6

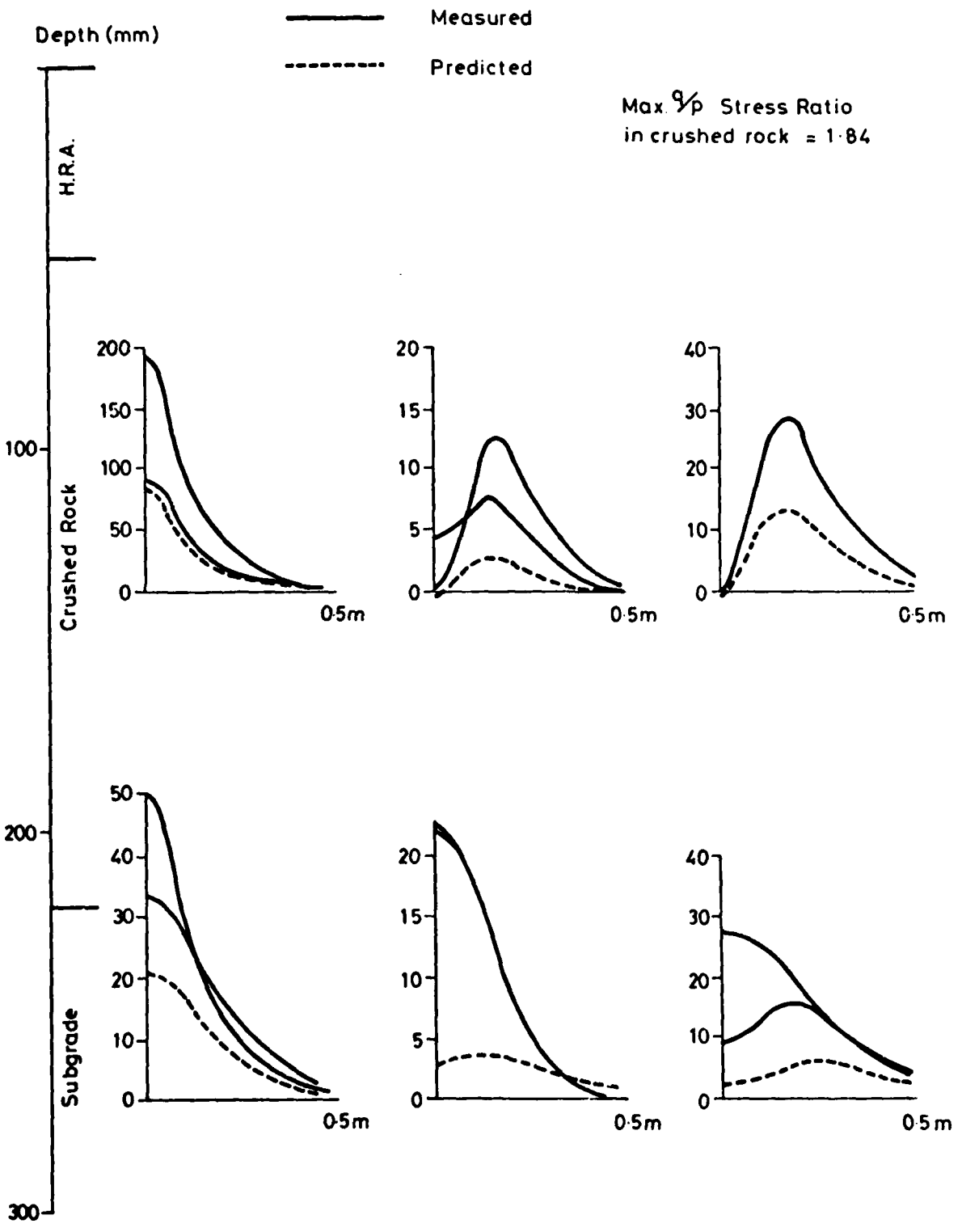


FIG. 6.15(a) MEASURED AND PREDICTED REPEATED STRESSES (kPa) FOR PAVEMENTS G7 AND GT7

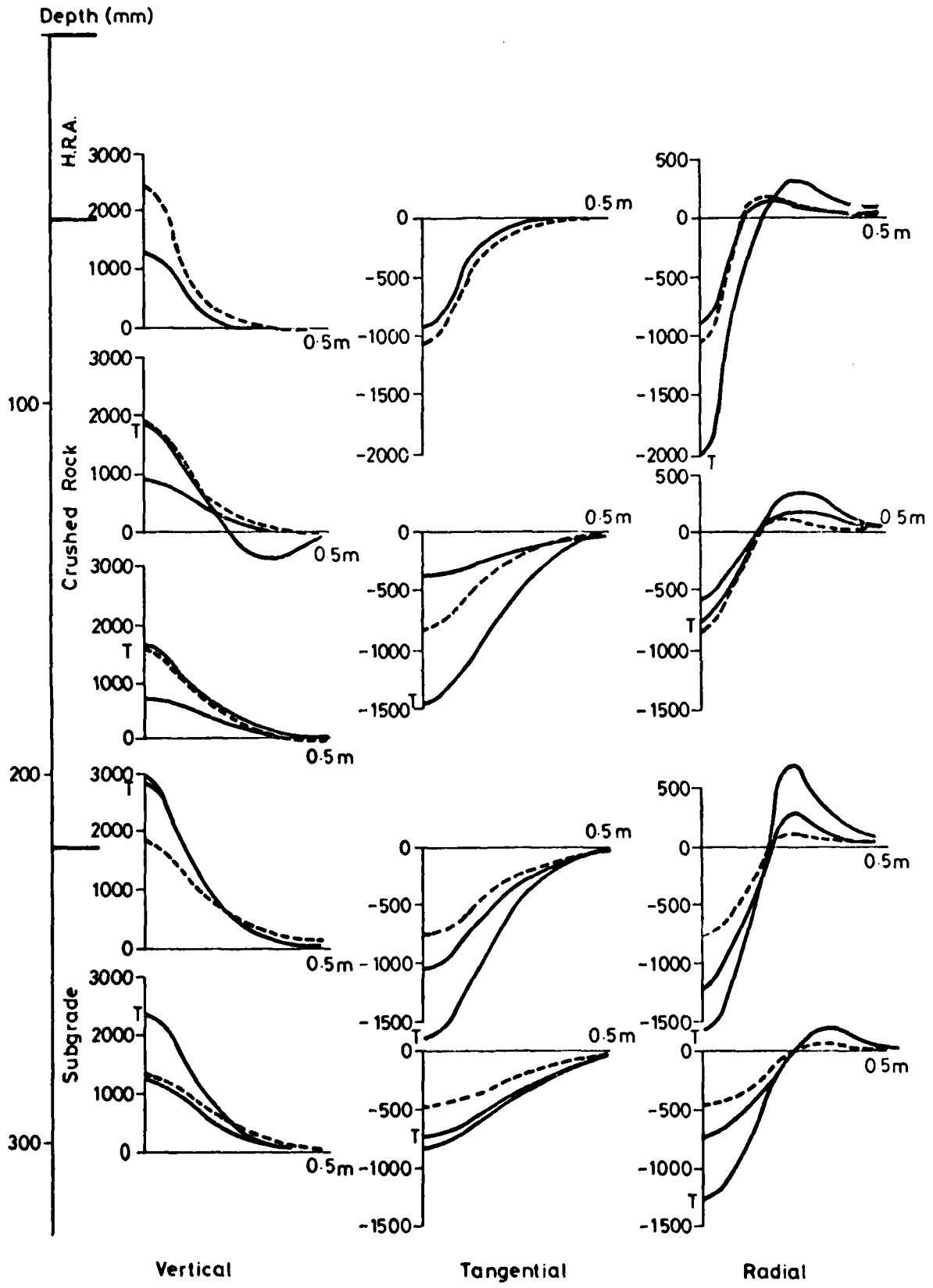


FIG. 6.15(b) MEASURED AND PREDICTED RESILIENT STRAINS ($\mu\varepsilon$) FOR PAVEMENTS G7 AND GT7

must also be questioned. This matter was discussed in the previous report (1) and it is considered that the experimental results are reasonably good considering the inherent difficulties involved with in situ instrumentation. The personnel involved were very experienced and careful calibration procedures were observed. Although more duplicate measurements were desirable, the overall results from 6 pairs of pavements of similar construction indicating similar findings adds confidence to the reliability of the data.

## 6.4 PERMANENT DEFORMATION ANALYSIS

Having predicted the transient stresses throughout the pavement using the resilient analysis, it was then possible to undertake prediction of permanent strains and rut depths. Using the material models described in Section 6.1, estimates of the permanent octahedral shear strain developed after a particular number of wheel passes were made for each element. It was assumed that zero strain occurred at 100 passes as for the granular material model reported in Section 6.2.1, and subsequently developed strain was calculated at 3,000, 6,000, 12,000 and 22,000 passes.

The surface permanent deformation is a summation of vertical permanent strains with depth. In the previous report (1) and related papers (2,3) the problem of calculating vertical strain for off-axis elements from given shear and volumetric strains was shown to require some assumptions. The procedure used in this earlier work was to assume that the major principal strain equalled the vertical strain. In the present work, a new technique was adopted.

The same finite element layout as that used in the resilient analysis was considered and a displacement field for the nodes computed such that each element had the correct octahedral shear strain. This

type of analysis resulted in the element strains being compatible with their neighbours, both horizontally and vertically. To perform this operation, it was decided that the elements should have no strain in the longitudinal direction and the problem therefore became one of plane strain, i.e. all permanent strains were assumed to occur in a transverse plane. To solve for the displacements, it was assumed that all elements had a Poisson's Ratio of 0.33 and were arranged and bounded in the same way as that shown in Fig. 6.7. A unit pressure load was then applied to the top layer of elements and self-weight forces were neglected. Using equation 6.21, an initial estimate of $K_o$ and, hence, the horizontal stress was made, a value of deviator stress (q) determined and a value for shear modulus (G) calculated using equation 6.11 and the previously evaluated permanent shear strain for that element. A solution was then obtained, new stresses predicted, and new values of q and then G calculated. This iteration process was continued until the accumulated error (equation 6.23) was below 2%, whereupon the strains in the elements and displacements of the nodes were printed out.

### 6.4.1 Comparisons of Predictions with Measurements

In the Pavement Test Facility, two methods of investigating permanent deformation were used. These were the single track tests which only involved surface deformation measurements, and the multitrack tests which also included permanent strain measurement at various locations within the pavement. The single track situation is much simpler to analyse than the multitrack case because predictions of rut development can be obtained directly from the finite element results. By contrast, in the multitrack case, the net effects of wheel passes in various lateral positions have to be computed.

Comparisons between predicted and measured rut depths for the single

track tests are shown in Figs 6.16 to 6.19. The upper part of each figure shows the variation of permanent deformation with distance from the centre line of the wheel path, while the lower part shows the development of the rut with the number of wheel passes. To avoid problems of initial "settling in", only the development of the rut after 440 load applications was considered. This starting point, which was convenient from a practical point of view, is analogous to that used in the development of the material model and the associated computations, which was taken as 100 applications. Generally, the measured and predicted rut depths agree quite well, but the shapes of the deformation profiles show some discrepancies. The predictions seem to peak at the centre and to have a wider spread than those measured. The central peak can be explained by the severe transient stress situation that is predicted to occur directly under the centre of the wheel load (Fig. 6.8) in the bituminous material. Contrary to the figures, the slope of the prediction line must be zero as it crosses the axis of symmetry.

To predict the final strains and deformations for the multitrack tests, it was necessary to obtain displacement components resulting from the wheel travelling in each of the nine tracks (see Chapter 5). This was achieved by adopting the cumulative loading procedure used previously and described in the earlier report (1). The concept of "mean number of equivalent wheel passes" was again used. This involved the computation of the number of wheel load applications required in the central track in order to produce the same permanent deformation as the real transverse load distribution at the surface and at each interface. The same computation then had to to be performed for several transverse positions, radii of 75, 150, 225, 300 and 375 mm being taken. It was found that at the two interfaces, the equivalent number of wheel passes was only slightly greater than the number of passes actually applied

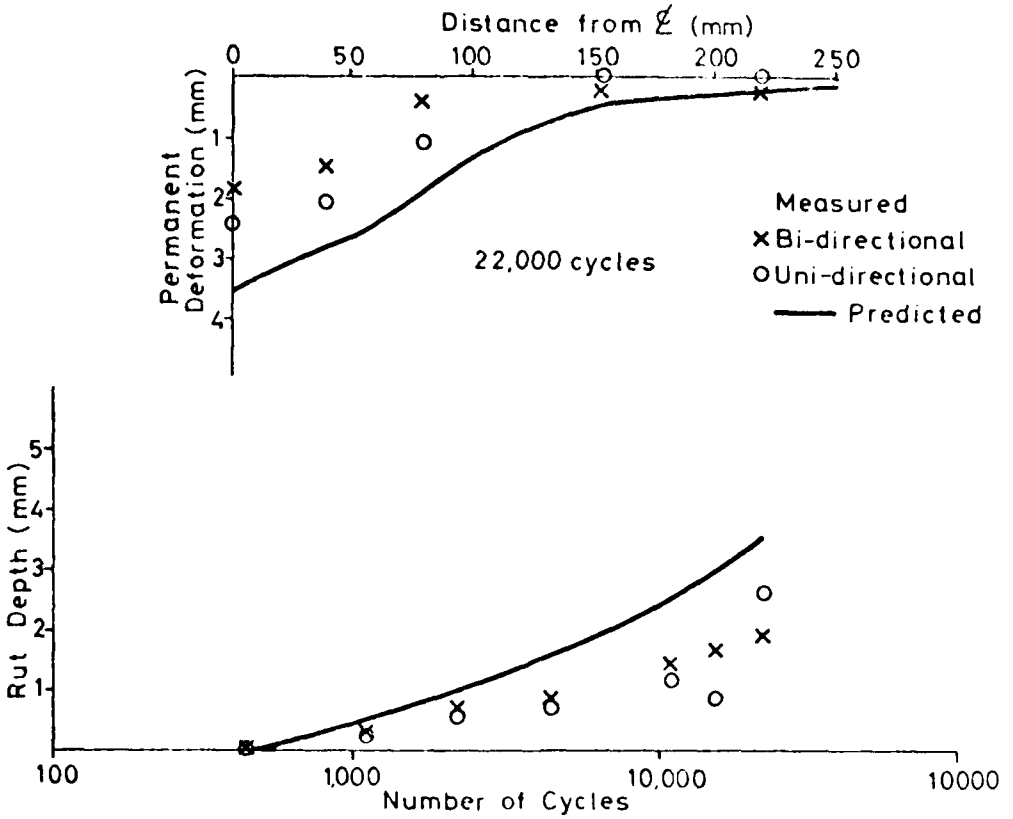


FIG. 6.16 MEASURED & PREDICTED DEFORMATIONS FOR SINGLE RUT TESTS - PAVEMENTS G4 AND GT4

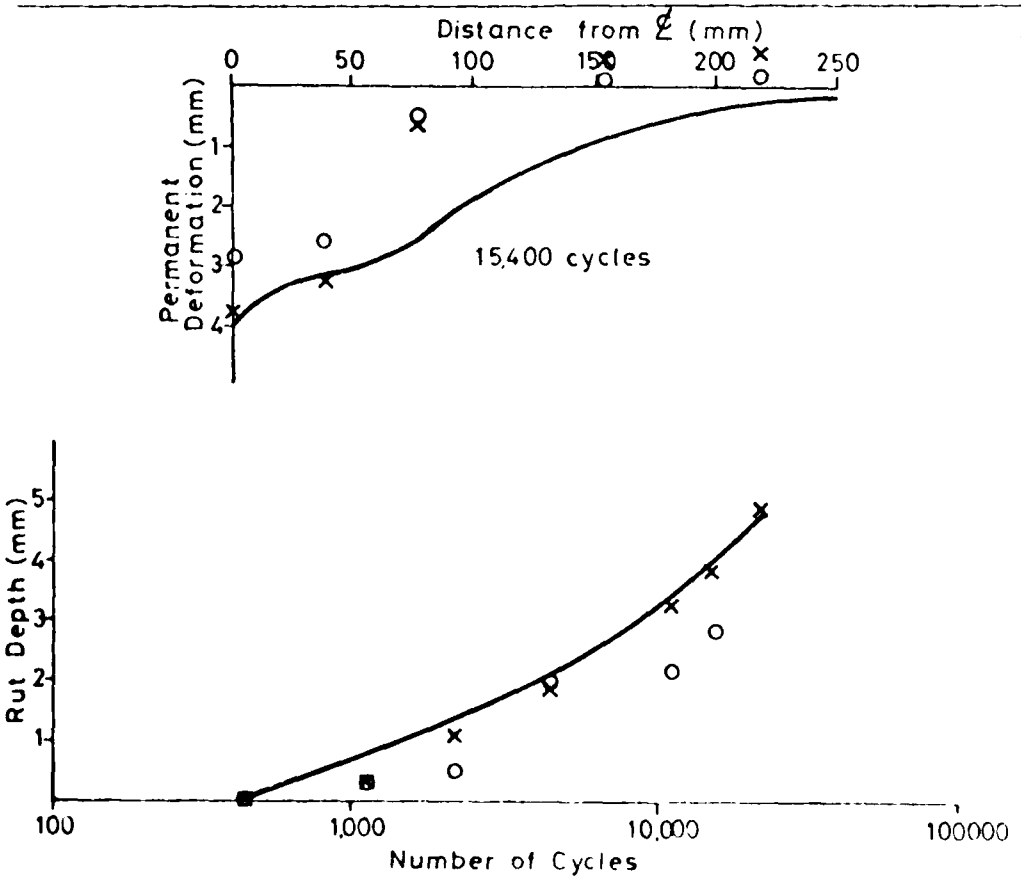


FIG. 6.17 MEASURED AND PREDICTED DEFORMATIONS FOR SINGLE RUT TESTS - PAVEMENTS G5 AND GT5

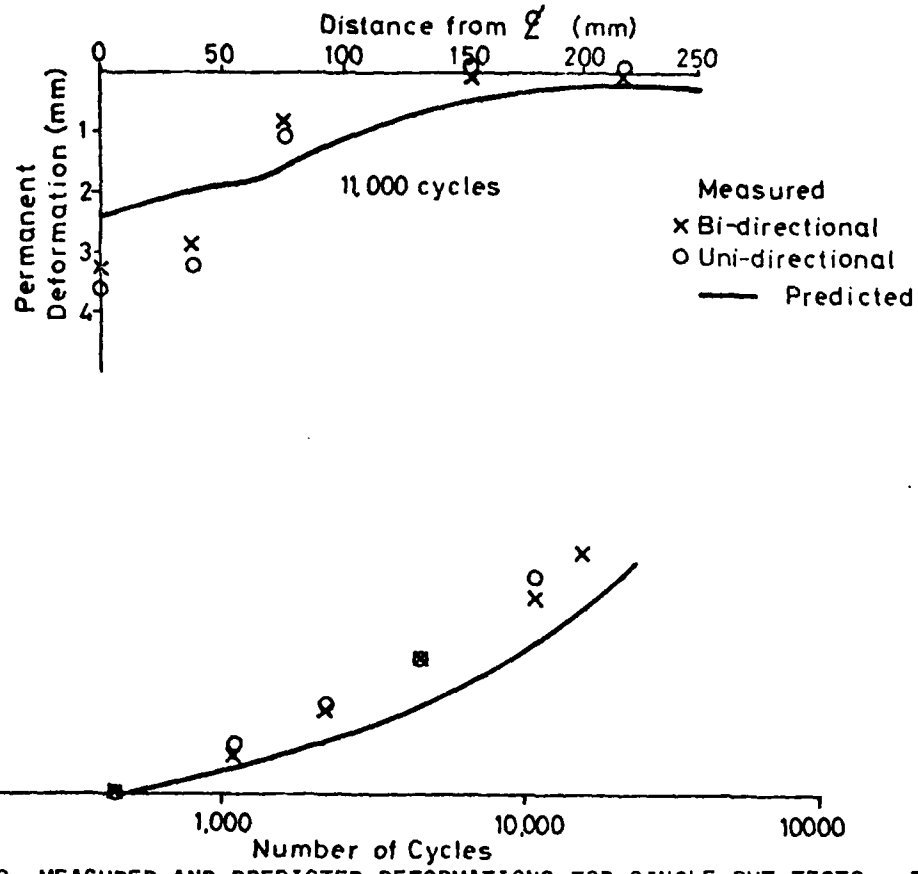


FIG. 6.18 MEASURED AND PREDICTED DEFORMATIONS FOR SINGLE RUT TESTS - PAVEMENTS G6 AND GT6

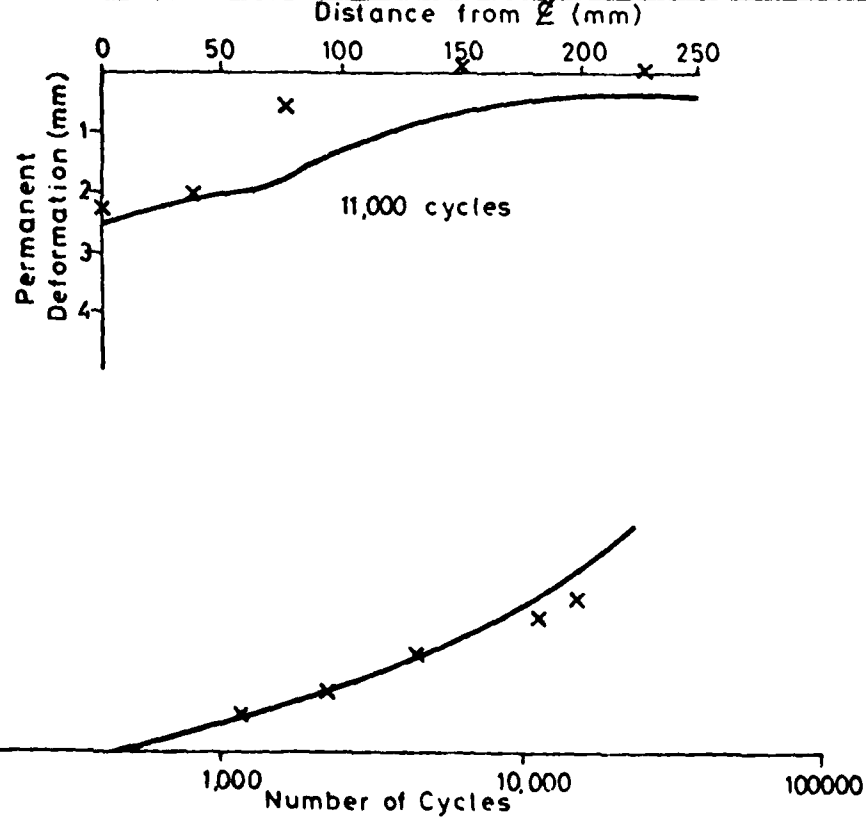


FIG. 6.19 MEASURED AND PREDICTED DEFORMATIONS FOR SINGLE RUT TESTS - PAVEMENTS G7 AND GT 7

directly over that point. The mean number of equivalent wheel passes for all pavements are shown in Table 6.2. To be consistent with the measurements actually made on the pavements, predictions were made for the increase in displacement after 1000 load applications. The equivalent number of wheel passes to determine the initial strain was taken as the same ratio of the final equivalent number of wheel passes as that found for the ratio of 1000 actual wheel passes to the total number.

Table 6.2 Mean equivalent wheel passes for 70,000 actual wheel passes

| Pavement No. | Distance from central wheel position (mm) | | | | | |
|---|---|---|---|---|---|---|
| | 0 | 75 | 150 | 225 | 300 | 375 |
| G1 | 20000 | 17000 | 11800 | 7000 | 3900 | 1100 |
| GT1 | 19400 | 16600 | 11500 | 6700 | 3800 | 960 |
| GT3, G3 | 42000 | 31500 | 11700 | 2700 | 600 | 280 |
| GT4, G4 | 20500 | 17500 | 12000 | 6800 | 3300 | 780 |
| GT5, G5 | 22400 | 19000 | 13500 | 7500 | 3800 | 1000 |
| G6, GT6,GT7, GTT7 | 26000 | 23000 | 16000 | 9000 | 45000 | 1200 |

Predictions were then made for the final surface deformation profile and the vertical permanent strains directly under the central wheel path. Comparisons of these predictions with the measured values are given in Figs 6.20 to 6.26. The upper part of each figure gives the profile of the surface deformation and the lower part the permanent vertical strain directly below the central wheel path.

A summary of the measured and predicted rut depths is presented

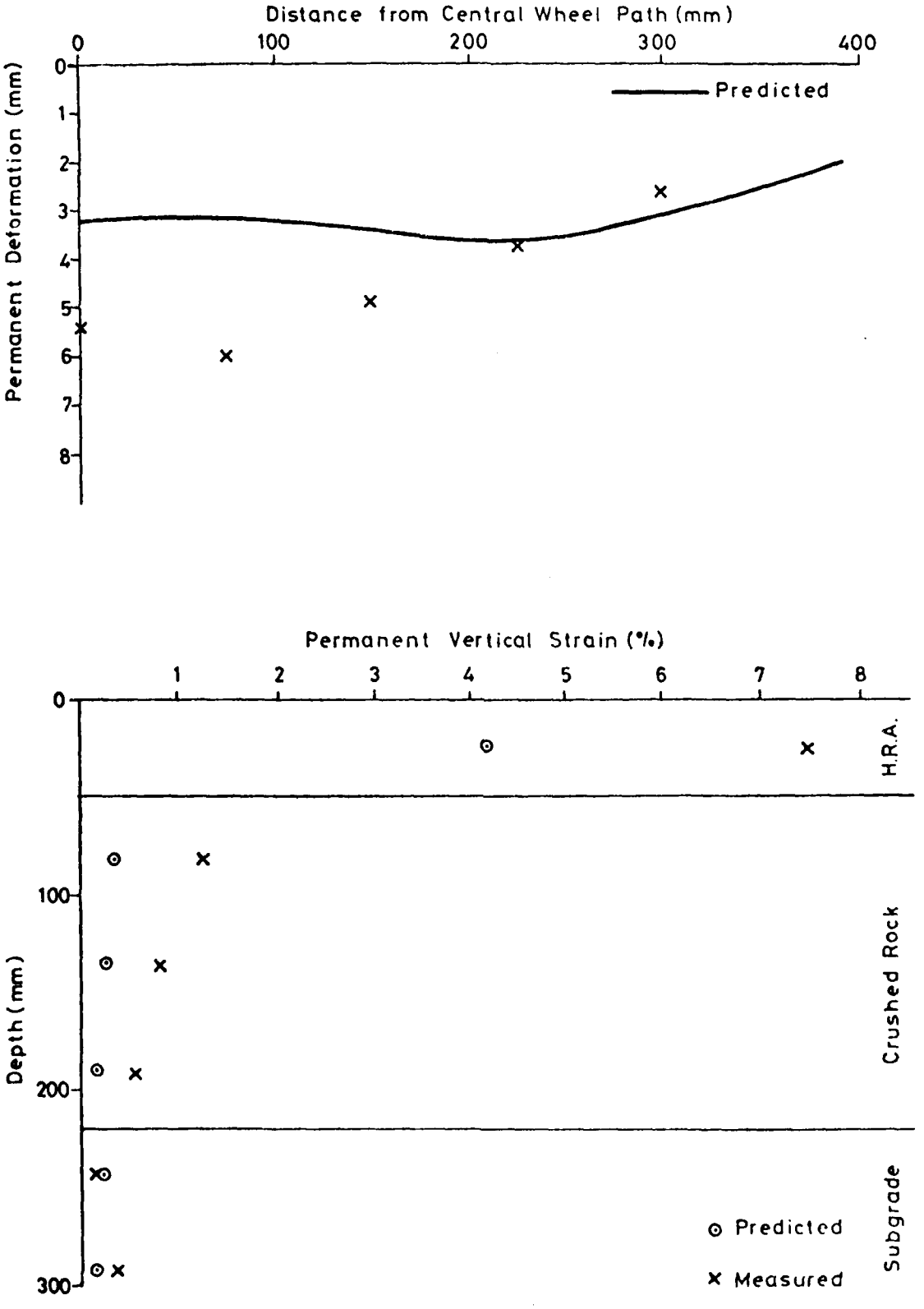


FIG. 6.20 MEASURED AND PREDICTED DEFORMATIONS AND PERMANENT VERTICAL STRAINS FOR PAVEMENT G1

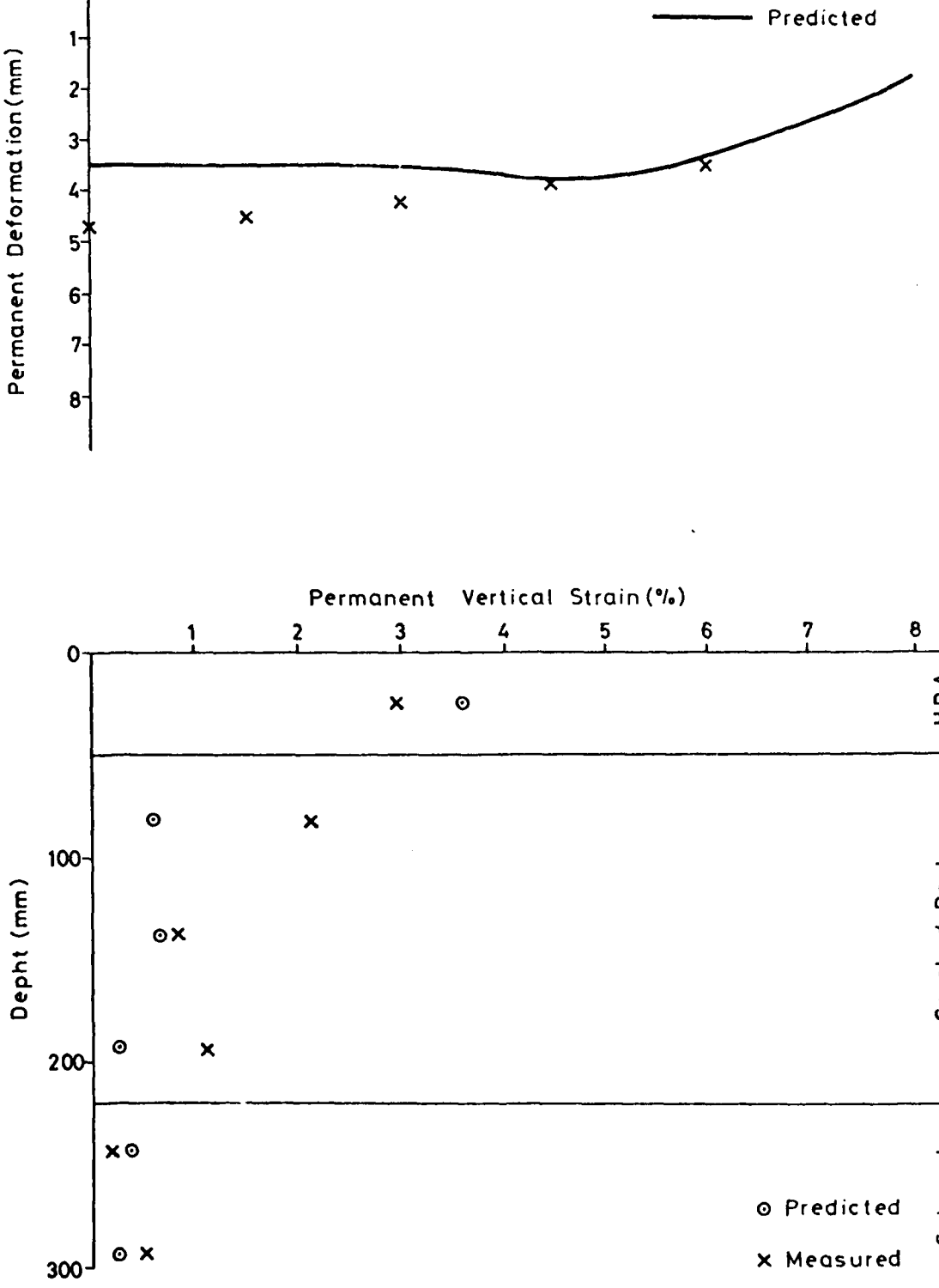


FIG. 6.21 MEASURED AND PREDICTED DEFORMATIONS AND PERMANENT VERTICAL STRAINS FOR PAVEMENT GT1

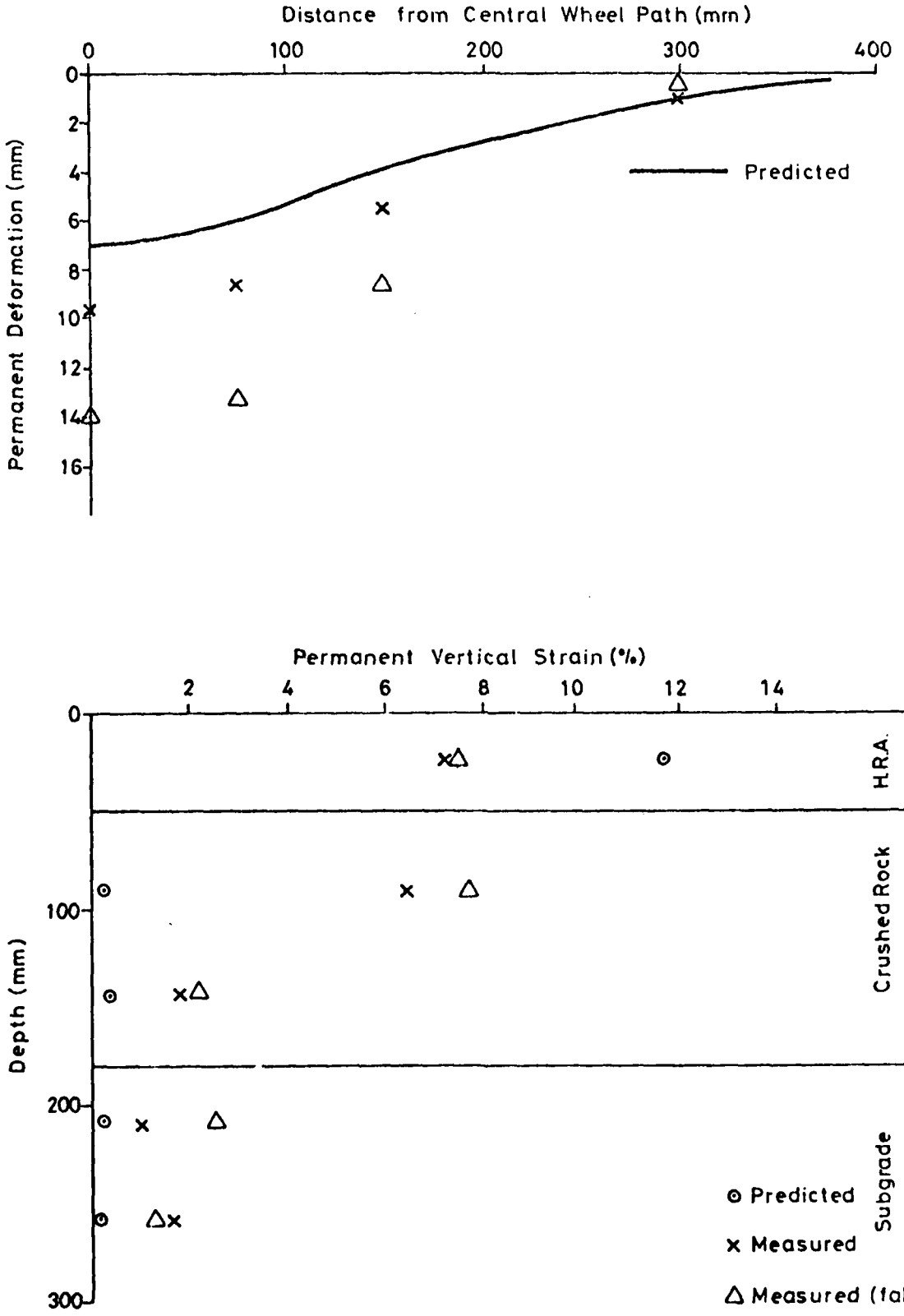


FIG. 6.22 MEASURED AND PREDICTED DEFORMATIONS AND PERMANENT VERTICAL STRAINS FOR PAVEMENTS G3 AND GT3

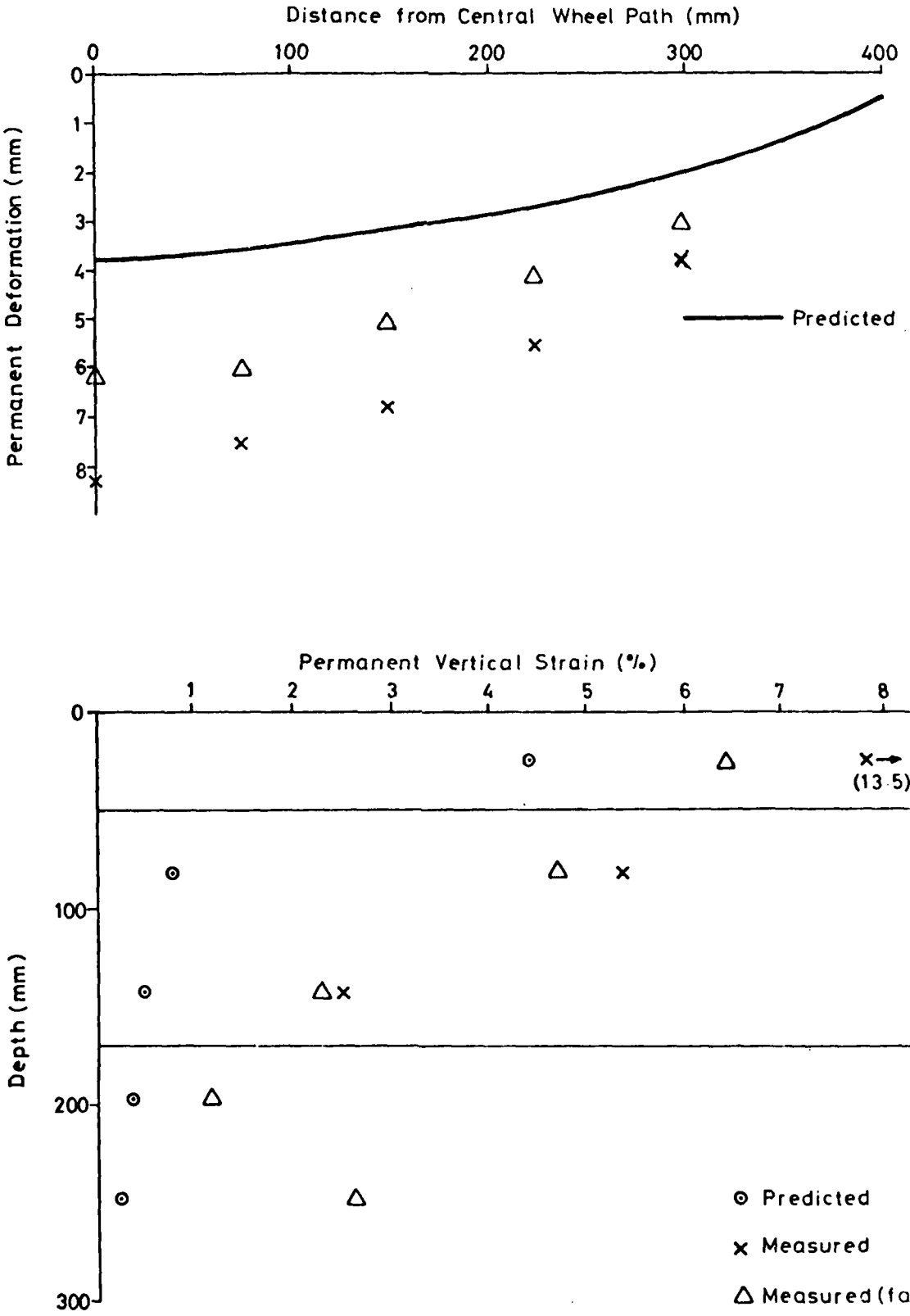


FIG. 6.23 MEASURED AND PREDICTED DEFORMATIONS AND PERMANENT VERTICAL STRAINS FOR PAVEMENT G4 AND GT4

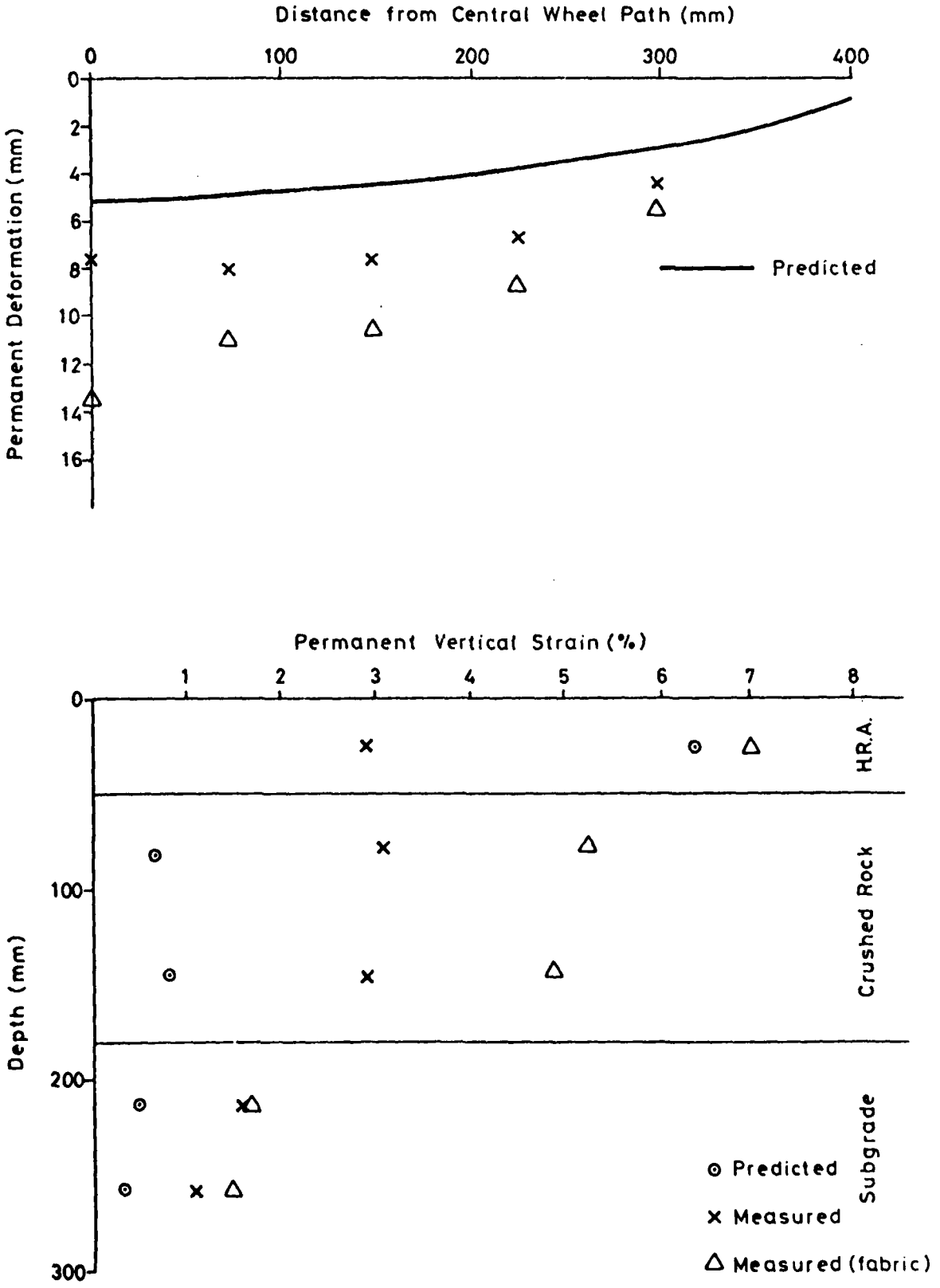


FIG. 6.24 MEASURED AND PREDICTED DEFORMATIONS AND PERMANENT VERTICAL STRAINS FOR G5 AND GT5

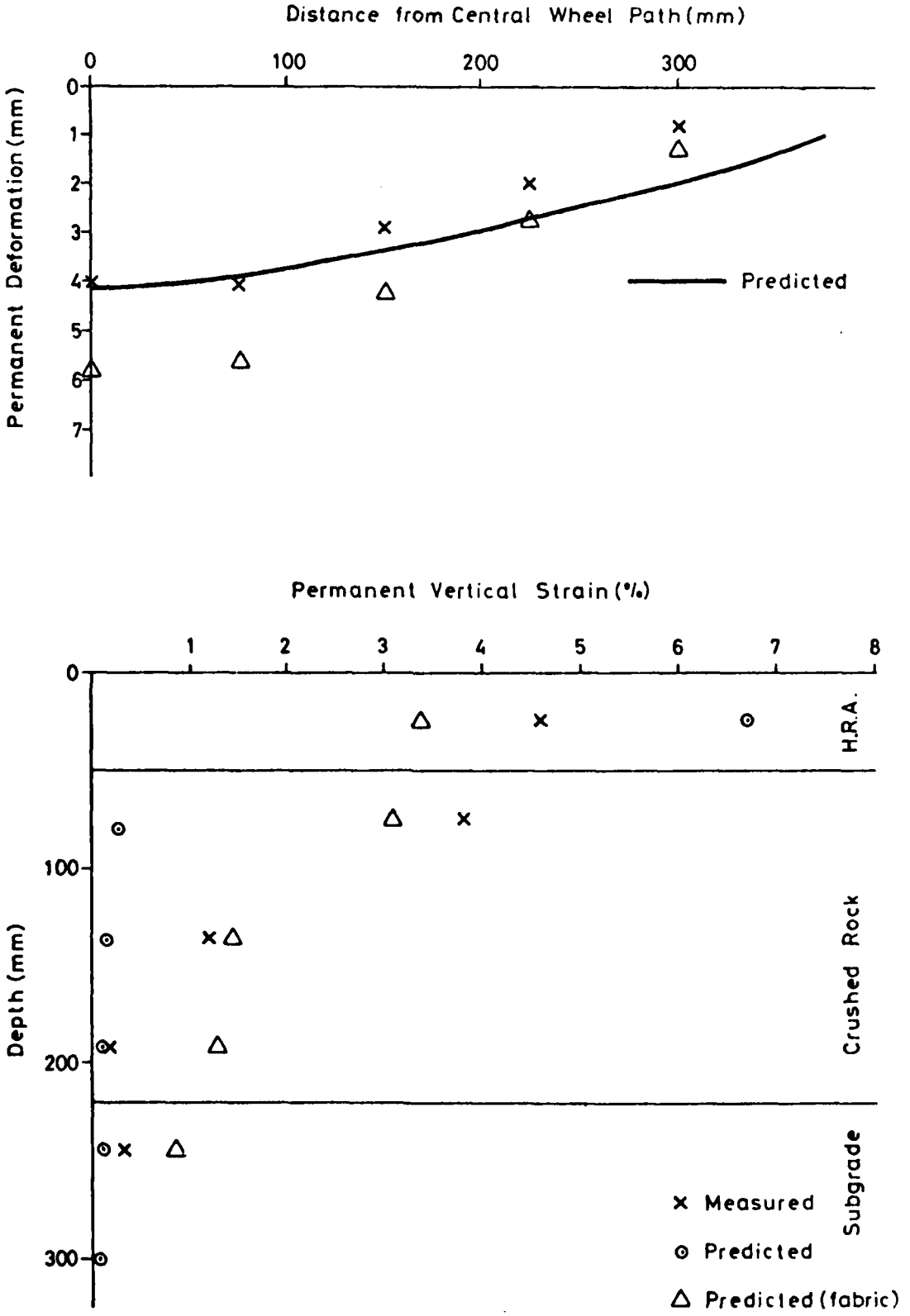


FIG. 6.25 MEASURED AND PREDICTED DEFORMATIONS AND PERMANENT VERTICAL STRAINS FOR PAVEMENTS G6 AND GT6

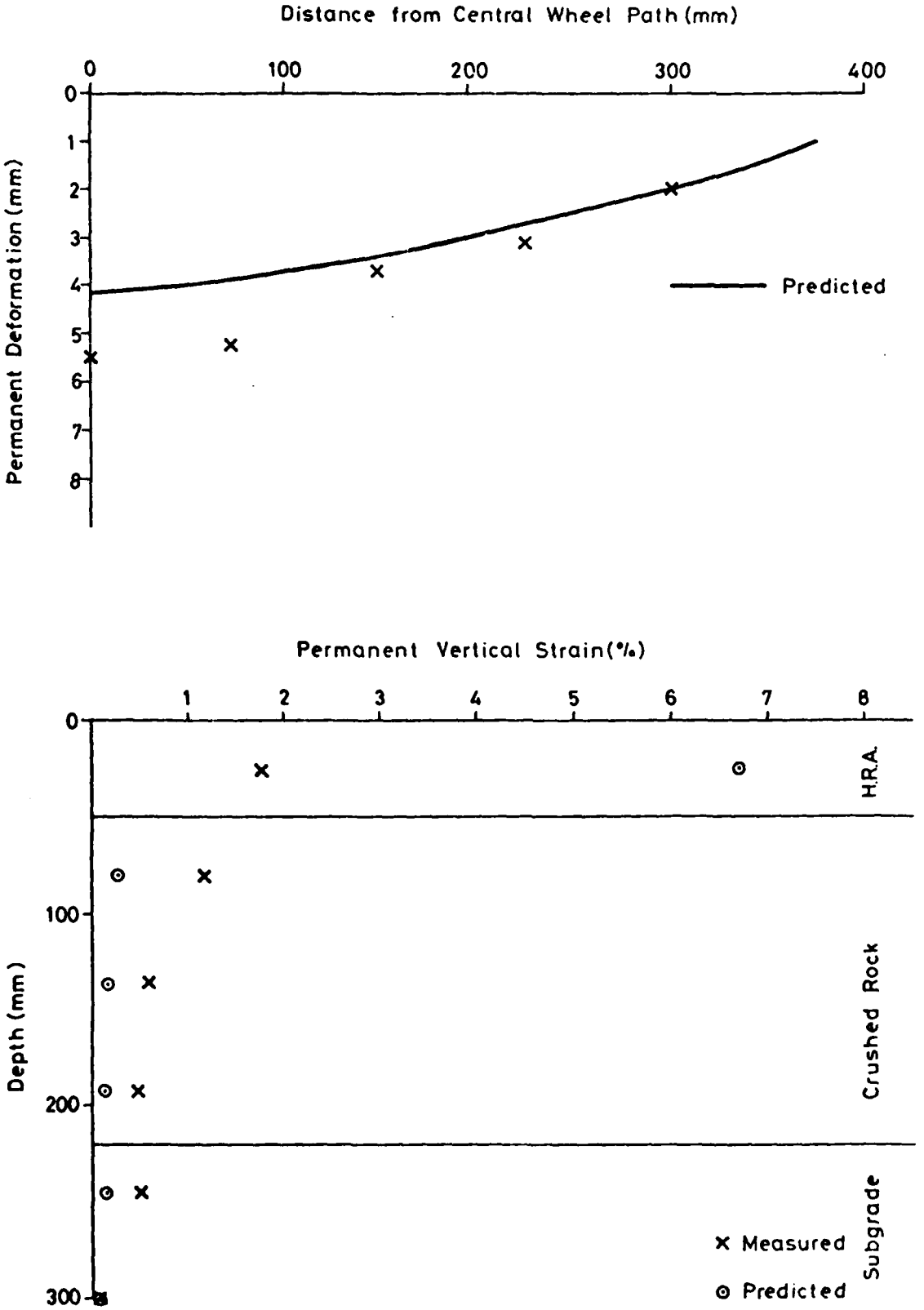


FIG. 6.26 MEASURED AND PREDICTED DEFORMATIONS AND PERMANENT VERTICAL STRAINS FOR PAVEMENTS G7 AND GT7

Table 6.3 Comparison of measured and predicted rut depths

| Pavement No. | Multitrack | | | Single Track | | |
|---|---|---|---|---|---|---|
| | Rut depth (mm) | | $\frac{M}{P}$ | Rut depth (mm) | | $\frac{M}{P}$ |
| | Measured (M) | Predicted (P) | | M | P | |
| G1 | 5.4 | 3.2 | 0.59 | - | - | - |
| G3 | 9.8 | 7.0 | 0.71 | - | - | - |
| G4 | 8.2 | 3.8 | 0.46 | 2.4 | 3.6 | 1.50 |
| G5 | 7.7 | 5.0 | 0.65 | 2.8 | 4.0 | 1.42 |
| G6 | 4.0 | 4.2 | 1.05 | 3.6 | 2.4 | 0.67 |
| | | Mean $\frac{M}{P}$ = 0.69 | | Mean $\frac{M}{P}$ = 1.20 | | |

in Table 6.3 from which it will be noted that the predicted values vary between 46 and 105% of the measured ones with an average of 69%. Only measurements in the pavements with no fabric were considered. The figures for the unidirectional single track tests, also shown in Table 6.3, indicate a tendency to overpredict by 20%. The single track predictions are likely to be more accurate and are in fact closer. The concept of mean equivalent wheel passes used in the multitrack predictions is complex and, at best, approximate. It could, therefore, lead to errors. The permanent strain distributions within the pavements clearly indicate that the predictions are too high in the bituminous layer and too low in the underlying materials. The reasons for this discrepancy can be explained by examining the predicted transient stresses on which these permanent deformation predictions were based. In the subgrade and base layers, the predicted stresses were usually lower than the measured values. This implies that

in the resilient analysis the bituminous material was assumed to have too high a stiffness, and, therefore, the predicted stresses in this layer were also too large. Allowances were also made for the reduced density of the granular material in the pavement when compared with that used in the triaxial tests. No account of this change in density was made in the permanent strain analysis as no information on its effect was available. However, it is probable that deformations will increase as density reduces. All these effects will add to the discrepancies noted above. More comprehensive laboratory materials testing is therefore needed to improve the accuracy of the permanent strain predictions.

# CHAPTER SEVEN

# CONCLUSIONS

This, largely experimental, project involved the testing, under controlled conditions, of seven pairs of pavements with granular bases. One pavement in each pair contained a fabric inclusion. Only one of the three years spent on this work was devoted to theoretical computations to predict pavement performance and the content of this report reflects this relative effort.

The Pavement Test Facility has continued to be improved during the course of this work and has proved to be a valuable means of investigating the response of pavements to wheel loading under controlled conditions. The instrumentation used to make in situ measurements was largely the same as that developed in earlier projects, although improvements to installation techniques and the introduction of data acquisition equipment has improved the efficiency of testing. The major improvements to the Pavement Test Facilty may be summarised as follows:

1. New servo-hydraulic system for the loading carriage allowing better control and the introduction of one-way loading when required.
2. New amplification system for the pressure cells and read-out system for all the in situ instrumentation.
3. Development of a lineariser unit for the strain coils to ease data acquisition.
4. Introduction of transducers for measuring vertical and resilient deflection and permanent deformation at fixed points in a pavement.
5. Development of techniques for measuring in situ strain on fabric inclusions using post-yield strain gauges and strain coils.
6. More extensive use of the nuclear density meter on all layers of the pavement structure.

One of the aims of this research was to investigate the effects of fabric inclusions in permanent pavement construction, i.e. low deformation applications. The following conclusions were drawn on this aspect of the work:

1. No improvement in pavement performance, as measured by surface permanent deformation, was obtained by inclusion of either Terram 1000 non-woven or Terram 7M7 stitched fabrics.
2. No consistent reduction in in situ stresses, resilient strains or permanent strains was observed as a result of the fabric inclusions.
3. No consistent improvement in in situ densities was achieved by the inclusion of fabrics.
4. Some evidence of slip between fabric and adjacent material was evident from tests on the weakest pavements which involved the largest deformations.
5. Observations during excavation and associated soil-fabric friction testing indicated that slip was likely to occur between the fabric and the crushed limestone base rather than between the fabric and the underlying silty-clay subgrade.

The major aim of this research was to continue to investigate computational methods for the prediction of permanent deformation in flexible pavements. A previous contract had studied full depth asphalt construction, so the emphasis in this present work was on pavements with granular bases and relatively thin surfacings. The following conclusions were drawn concerning these theoretical developments and the comparison of their predictions with measurements from the test pavements.

1. A finite element program, SENOL, using a secant modulus, incremental-iterative type of analysis has been successfully developed to model problems involving materials with non-linear resilient stress-strain characteristics.
2. A two-stage computational approach was used to calculate permanent deformations. The first stage was an axisymmetric resilient analysis, the stress conditions in which defined the permanent shear strain distribution on the basis of laboratory test data. The second stage was a plane strain analysis to determine the permanent deformations needed to produce this shear strain pattern.
3. Transient stresses in the base and subgrade were not well predicted in the test pavements; measured values generally being higher than the computed values. It would appear that the stiffness of the asphalt layer was assumed to be too high.
4. Resilient strains were well predicted in all layers.
5. Rut depths were overpredicted by 20% for the single track tests and underpredicted by 31% for the multitrack tests. The computation procedures for dealing with multitrack tests need further development.
6. The vertical permanent strain predictions were too high in the asphalt layer and too low in the materials below, perhaps as a consequence of the predicted stress distribution.

It may be concluded in general, that further work of the type described in this report is required in order to develop a satisfactory theoretical model to describe the response of pavements with non-linear materials to repeated wheel loading. In particular, a sensitivity analysis should be carried out using the SENOL program in order to establish the relative importance of the many factors which could influence

stresses and, hence, permanent strains in structures of this type. The continued laboratory testing of all constituent materials under relevant repeated load conditions is required so that knowledge of stress-strain relationships can be gradually improved. The Pavement Test Facility should continue to be used as a means of validating theoretical ideas for ultimate use in practical design.

## ACKNOWLEDGEMENTS

This research was jointly sponsored by the European Research Office of the US Army and ICI Fibres Ltd. The Authors are grateful for this support and the interest shown in the work by Dr H Lemons and Mr W Grabau of ERO and Messrs B Myles and H Murray of ICI. Additional help has been rendered by Tarmac Roadstone Ltd in supplying and laying the asphalt, by ARC Ltd in supplying the crushed limestone, and by the Butterley Brick Company in supplying the silty-clay. The assistance of TRRL in loaning a nuclear density meter at various times is also gratefully acknowledged.

## REFERENCES


1. Brown, S.F., Bell, C.A. and Brodrick, B.V., "Permanent deformation of flexible pavements", Final Technical Report to US Army, Grant No. DA-ERO-75-G-023, March 1977.

2. Brown, S.F. and Bell, C.A., "The validity of design procedures for the permanent deformation of asphalt pavements", Proc. 4th Int. Conf. on the Struct. Design of Asphalt Pavements, Vol. 1, Ann Arbor, Michigan, 1977, pp 467-482.

3. Brown, S.F. and Bell, C.A., "The prediction of permanent deformation in asphalt pavements", Proc. AAPT, Vol. 48, 1979, pp 438-474.

4. Claessen, A.I.M., Edwards, J.M., Sommer, P. and Ugé, P., "Asphalt pavement design - the Shell method", Proc. 4th Int. Conf. on the Struct. Design of Asphalt Pavements, Vol. 1, Ann Arbor, Michigan, 1977, pp 39-74.

5. Ibid Brown, S.F., Pell, P.S. and Stock, A.F., "The application of simplified, fundamental design procedures for flexible pavements", pp 327-341.

6. Ibid Santucci, L.E., "Thickness design procedure for asphalt and emulsified asphalt mixes", pp 424-456.

7. Ibid Barker, W.R., Brabston, W.N. and Chou, Y.T., "A general system for the structural design of flexible pavements", pp 209-248.

8. Ibid Barksdale, R.D. and Hicks, R.G., Moderators' Review, Vol. 2.

9. Barksdale, R.D., "Laboratory evaluation of rutting in base course materials", Proc. 3rd Int. Conf. on the Struct. Design of Asphalt Pavements", Vol. 1, London, 1972, pp 161-174.

10. Ibid Romain, J.E., "Rut depth prediction in asphalt pavements", pp 705-710.

11. Barenberg, E.J., Dowland, J.H. and Hales, J.H., "Evaluation of soil-aggregate systems with Mirafi fabric", Res. Rep. University

of Illinois, 1975.

12. Brown, S.F. and Brodrick, B.V., "The performance of stress and strain transducers for use in pavement research", Research Report to SRC, 1973.

13. Brodrick, B.V. and Brown, S.F., "Performance of flexible pavements incorporating fabric", Report submitted to ICI Fibres Ltd, January 1979.

14. British Standards Institution, "Methods of testing soils for civil engineering purposes", BS 1377, 1967.

15. Department of Transport, "Specification for road and bridge works", London, HMSO, 1976.

16. Boyce, J.R., "The behaviour of a granular material under repeated loading", Ph.D. thesis, University of Nottingham, 1976.

17. Pappin, J.W., "Characteristics of a granular material for pavement analysis", Ph.D. thesis, University of Nottingham, 1979.

18. British Standards Institution, "Specification for rolled asphalt (hot process) for roads and other paved areas", BS 594, 1973.

19. Cooper, K.E. and Pell, P.S., "The effect of mix variables on the fatigue strength of bituminous materials", TRRL Report, LR 533, 1974.

20. "Development fabric information", ICI Fibres Ltd, Harrogate, England, 1979.

21. Collios, A., Delnos, P., Gourc, J.-P. and Giroud, J.-P., "Experiments on soil reinforcement with geotextiles", ASCE Convention, Portland, Oregon, 1980.

22. Leung, R.T.H., "Frictional characteristics of soil-fabric systems", B.Sc. thesis, University of Nottingham, 1980.

23. Thrower, E.N., Discussion on paper by Boyce, Brown and Pell, Aust. Road Research, 1977.

24. Pappin, J.W. and Brown, S.F., "Resilient stress-strain behaviour of a crushed rock", Proc. Int. Symp. on Soils under Cyclic and Transient Loading, Swansea, Vol. 1, 1980, pp 169-177.

25. Black, W., Private communication, 1979.

26. Brown, S.F., Lashine, A.K.F. and Hyde, A.F.L., "Repeated load triaxial testing of a silty clay", Geotechnique, 25, No. 1, 1975, pp 95-114.

27. Brown, S.F. and Cooper, K.E., "A fundamental study of the stress-strain characteristics of a bituminous material", Proc. AAPT, 1980.

28. Van der Poel, C., "A general system describing the visco-elastic properties of bitumens and its relation to routine test data", Journ. App. Chem., 4, 1954, pp 221-236.

29. Heukelom, W. and Klomp, A.J.G., "Road design and dynamic loading", Proc. AAPT, Vol. 33, 1964, pp 92-123.

30. Cooper, K.E., Brown, S.F. and Pell, P.S., "Development of improved procedures for asphalt mix design", Research Report to Mobil Oil Ltd, February 1980.

31. Barksdale, R.D., "Analysis of layered pavement systems", Res. Rep. Georgia Institute of Technology, 1969.

# APPENDIX 1

## THE STRAIN COIL LINEARISER

Fig. A1.1 shows the non-linear relationship between amplitude dial reading and the strain equivalent of a 2 volt output from the Bison instrument (calibration signal). For linearisation, the relationship between sensitivity, i.e. volt output for 1% strain, and amplitude dial reading is more useful. This is shown in Fig. A1.2 as a solid line with the broken horizontal line illustrating the required output which is independent of amplitude dial reading. To achieve this constant output, the Bison Instrument curve is conditioned with a variable gain amplifier.

Figs A1.1 and A1.2 show that the amplitude dial readings increase from 0-1000 in increments of 100. The sensitivity curve on Fig. A1.2 is adjusted to the 1 v for 1% strain level using the gain on the lineariser which is controlled by two binary numbers. The larger of these is an eight digit number which sets the gain of each amplitude dial reading of 100 by the scaling factor of 'x' divided by 'y' (see Fig. A1.2). A smaller five digit number sets the gain in a straight line approximation between the hundreds and has a slope of 'a' divided by 'b' (see Fig. A1.2), b being equal to 100. This slope is proportional to the scaling factor and will increase as sensitivity decreases. The sensitivity relationship with amplitude dial reading is a slight curve and the increasing gain requirement is reflected in the steepening curve shown in Fig. A1.1. It is recommended that the coils should be spaced at amplitude dial readings below 900 as the higher gains above this level magnify errors in the straight line approximation, and in variations between pairs of coils.

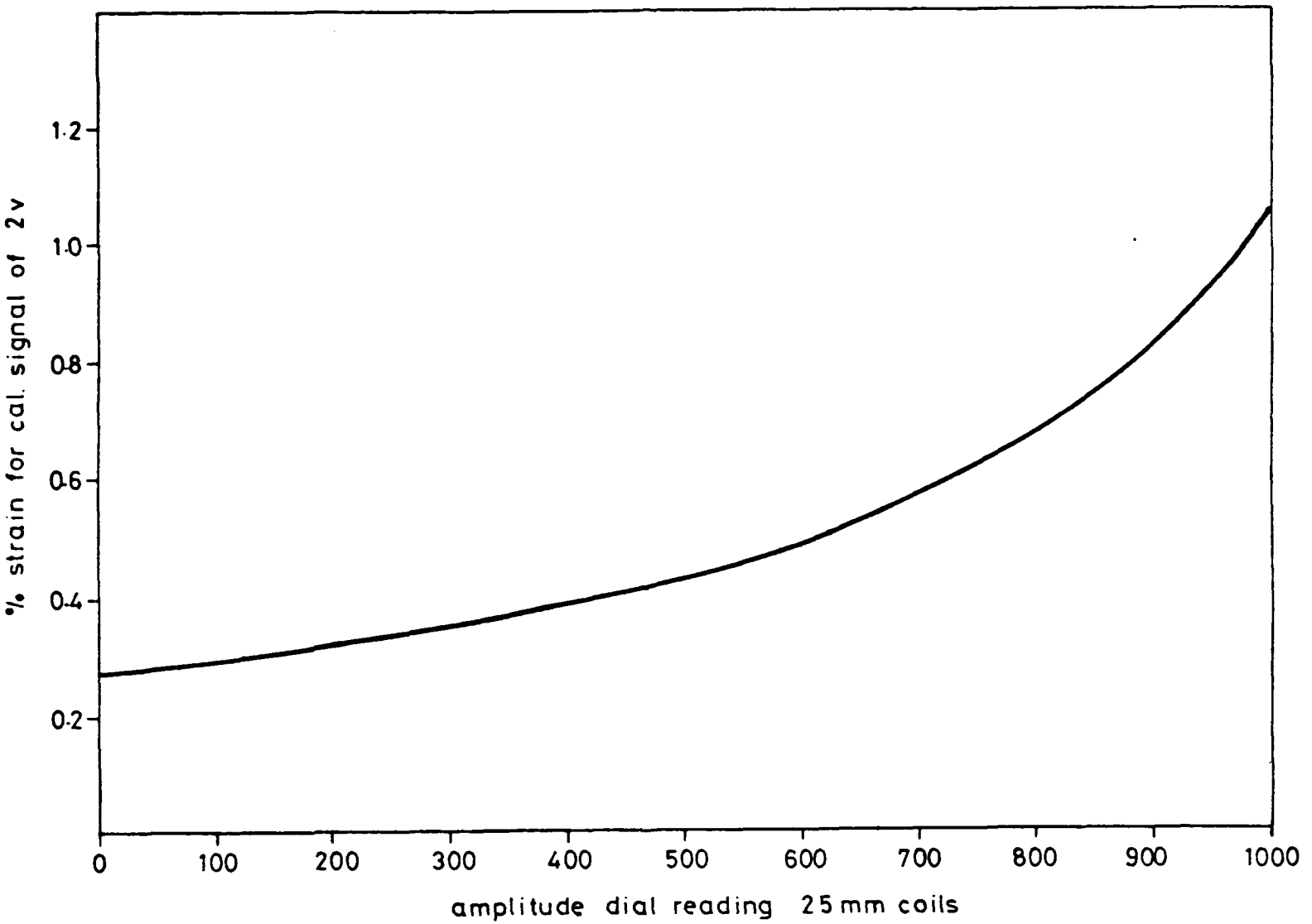


FIG. A1.1 RELATIONSHIP BETWEEN AMPLITUDE DIAL READING AND STRAIN FOR A 2 VOLT CALIBRATION SIGNAL

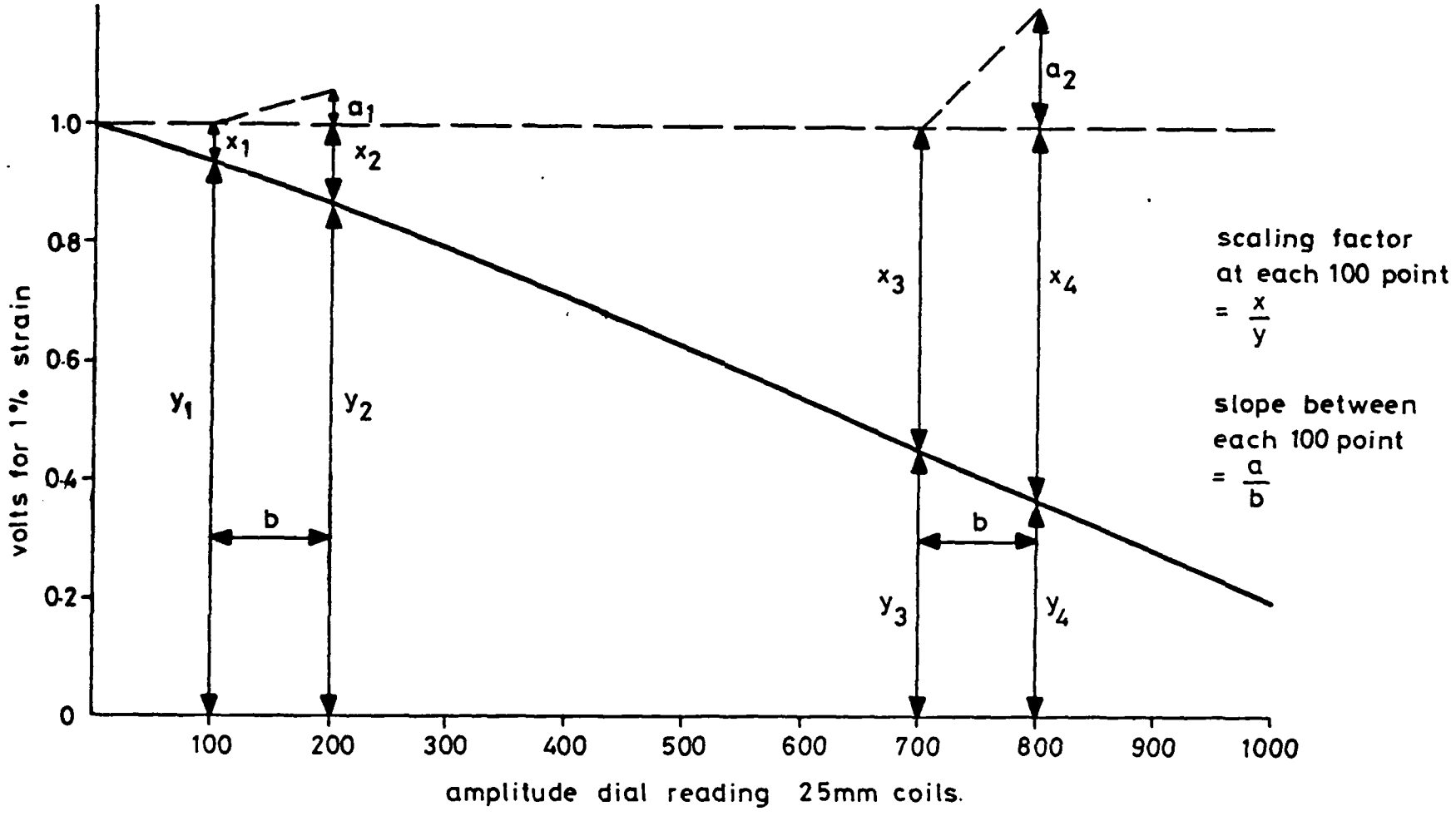


FIG. A1.2 RELATIONSHIP BETWEEN AMPLITUDE DIAL READING AND VOLTAGE OUTPUT FOR 1% STRAIN

Diode programmable cards are used to fix the values of the binary numbers. This is accomplished by a manual diode selection facility consisting of indicators for each digit of the two binary numbers. The diodes representing the larger number are switched in during calibration, Fig. 2.7, to produce an output of, for example, 1.0 volt for 1% strain at all the "100" positions on the amplitude dial. The diodes representing the smaller number are used to set the gain between each consecutive hundred point and this can be carried out at the same time. For example, the change in scaling factor (gain slope) between 200 and 300 is set at 300, and will cover the change in gain between 200 and 300. In practice, this is controlled by a potentiometer with a linear calibrated dial from 1 to 99. A note is made of each combination of indicators required for 1% strain as the calibration proceeds, and diodes are then soldered into the cards to reproduce the gain settings on the amplifier in the linearisor. These settings can then be called up by dialling in the amplitude dial readings, for a pair of coils at balance, using discreet switches for the hundreds and the potentiometer for the intermediate positions. Under these circumstances, the manual facility is cancelled, but the diode position indicators still operate and the gain programme can be checked.

It is necessary to have cards for each of the three ranges of coil separation specified by Bison Instruments in their manual and for each mode of coil orientation (coaxial and coplanar). A galvanometer matching facility is built in to the linearisor and is used to set the strain output of 1% over the full width of the recording paper. Ranges of 1.0 to 0.1% strain over a 150 mm width can be switched in with a sensitivity control and this should give a satisfactory resolution. It is important to select coils with very similar relationships between amplitude dial reading and strain. Reprogramming or extra cards would be necessary if

the Bison Instrument is changed. The bench calibrator in Fig. 2.8 needs to be precisely manufactured as very small movements are involved during calibration.

## APPENDIX 2

## THE FINITE ELEMENT COMPUTER PROGRAM

This program performs a finite element analysis of an axisymmetric or plane strain two-dimensional solid and consists of two versions:

(1) SENOL - Linear or non-linear analysis

(2) SELIN - Linear analysis only

The linear version is significantly more efficient than the non-linear version and is, therefore, recommended for linear analysis.

### Element Type

The program uses linear strain rectangles which are described in full by Barksdale (31). The displacement function within the elements is described by:

$$u = a_0 + a_1 r + a_2 z + a_3 rz$$
$$v = b_0 + b_1 r + b_2 z + b_3 rz \qquad \text{(A2.1)}$$

where u, v are the horizontal and vertical displacement,

and r, z are the horizontal and vertical co-ordinates.

This equation implies that the horizontal strain varies linearly with vertical distance, the vertical strain varies linearly with horizontal distance and the shear strain ($\gamma_{rz}$) varies linearly in both directions.

### Element Layout

An automatic node and element generation routine is incorporated into the program. A typical layout of the nodes, elements, boundaries

and central loadings is shown in Fig. A2.1. The nodes and elements are always numbered from the top left hand corner which normally has the co-ordinates (0,0). For all loads and displacements and nodal co-ordinates, directions downwards vertically and horizontally to the right are positive. The only input required to develop this mesh is the number (NUMR) and ordinates of the horizontal node positions and the number (NUMZ) and ordinates of the vertical node positions. To reduce the bandwidth required by the program, the nodes and elements are numbered horizontally to the right if NUMZ > NUMR and numbered vertically downwards if NUMR > NUMZ.

The program will automatically include layers of materials with material number 1 at the surface and the maximum number (NUMMAT) material will continue to the base of the structure. Extra materials can be inserted into any number of elements (Number of elements affected = NUMSE). If only one material layer is to be used and then inclusions of other materials incorporated, the main material must be material number 1. Different boundary conditions of the nodes can also be effected and this includes imposed displacements and/or point loading. The automatically arranged boundaries can also be altered by this method. The central load is automatically placed on NUMPC elements starting at the top left hand node. If NUMPC is equal to zero, no loading is applied at this point. Additional normal and tangential pressure loadings can be applied to any element (Number of elements loaded = NLD).

Method of Load Application

In both versions of the program, the structure is initially solved for body forces only and then the external loads are applied.

In the linear version this can be overwritten and a single solution

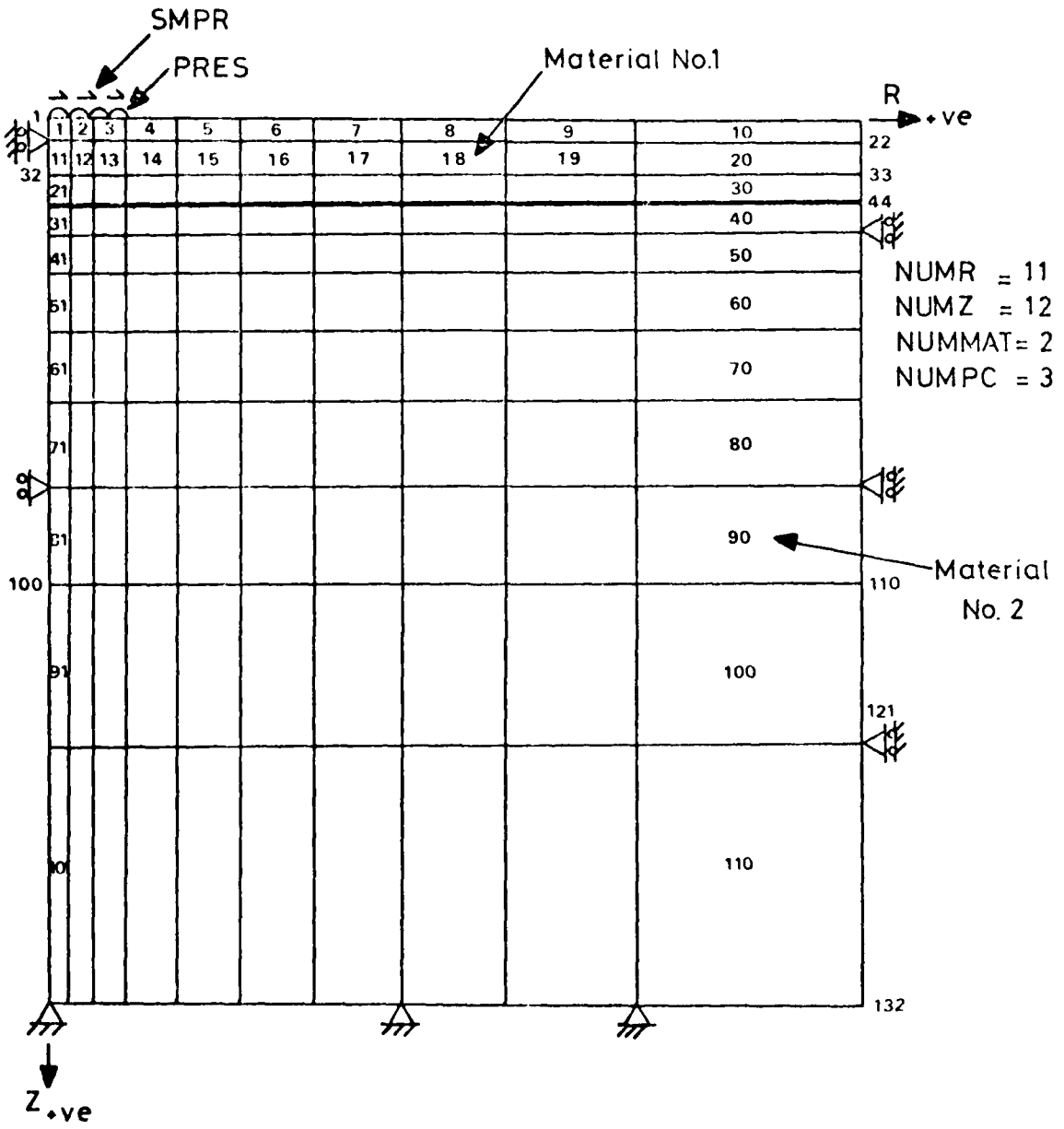


FIG. A2.1 TYPICAL EXAMPLE OF AUTOMATIC ELEMENT GENERATION

(If NUMR > NUMZ elements and nodes are numbered downwards)

for body forces and external applied load produced by putting the number of load increments (NINC) equal to zero. If NINC is greater than zero, the first solution is for body forces and the second (i.e. final) solution for body forces and applied load.

In the non-linear version, only body forces are solved initially and then the external load applied in gradually increasing values until the total value is reached. The number of steps for this process (NINC) is typically equal to 10.

Maximum Sizes and Cost of Running

The maximum number of nodes is 15 by 25, i.e. in one direction the maximum is up to 15, and in the other, 25. It is arbitrary which direction is the maximum. The program is written to be able to cater for 24 different materials. The total number of pressure loads (NUMPC + NLD) is 50. The number of boundary conditions is unlimited.

Using the maximum number of nodes the program uses 107K and 96K central core memory for the non-linear and linear version respectively.

Material Properties Required

For all analyses, the densities of the materials are required if body forces are needed. For linear analysis the additional information required is Young's Modulus and Poisson's Ratio. In the non-linear program any material can be specified as being non-linear. For each non-linear material the behaviour model must be written into the main program at the point indicated.

In the non-linear solution process, initially, the body force situation only is solved (see Fig. A2.2, steps 2, 3, 4). This is done by iteration in two ways. Firstly, if only layered materials are considered, an accurate solution is reached with the second iteration.

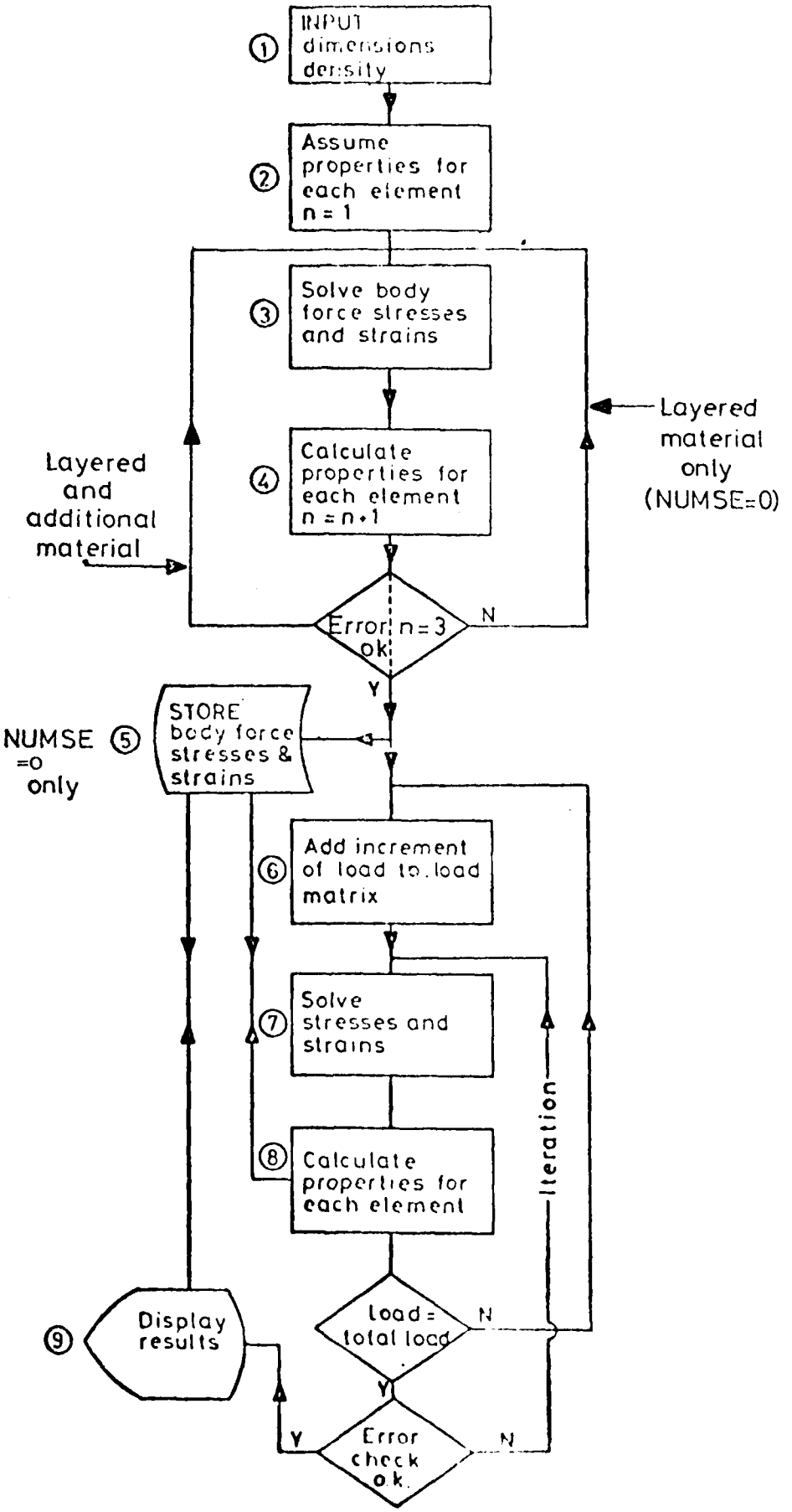


FIG. A2.2 FLOW CHART

If, however, there are inclusions of different materials, the number of iterations required will increase to solve the body forces accurately. At each iteration, an error check is performed by comparing the newly calculated modulus with the old modulus for all non-linear elements as follows:

$$\text{Error} = \frac{\Sigma(E_n - E_o)^2}{\Sigma E_n^2}$$

When this is below a specified value, the iteration process is terminated. If the error begins to increase, a variable damping factor (DF) is introduced. If, after 5 (or more) iterations have been performed, the error is still 10 (or more) times the required value, then the program will stop. The applied load is then inserted in successively larger quantities and no iterations are used (see Fig. A2.2, steps 6, 7, 8). When the full load is reached the iteration process is again carried out.

The non-linear model for the material must produce a secant bulk modulus (K) and shear modulus (G). In this case, secant implies relationships such that the strain at any stress state can be determined by using the appropriate linear K and G values. In other words, for any q and p the shear strain ($\varepsilon$) and volumetric strain (v) must be known to give:

$$K = \frac{P}{v} \quad \text{and} \quad G = \frac{q}{3\varepsilon} \qquad \text{(A2.2)}$$

The actual positioning of these models is clearly indicated in the main program, the first command in the non-linear portion of which directs the program to the correct model (Fig. A2.3).

It is possible to predict permanent strain with the program once the stresses have been determined. This is done in subroutine PERMSH (Fig. A2.3) using material models which are built in to the program as

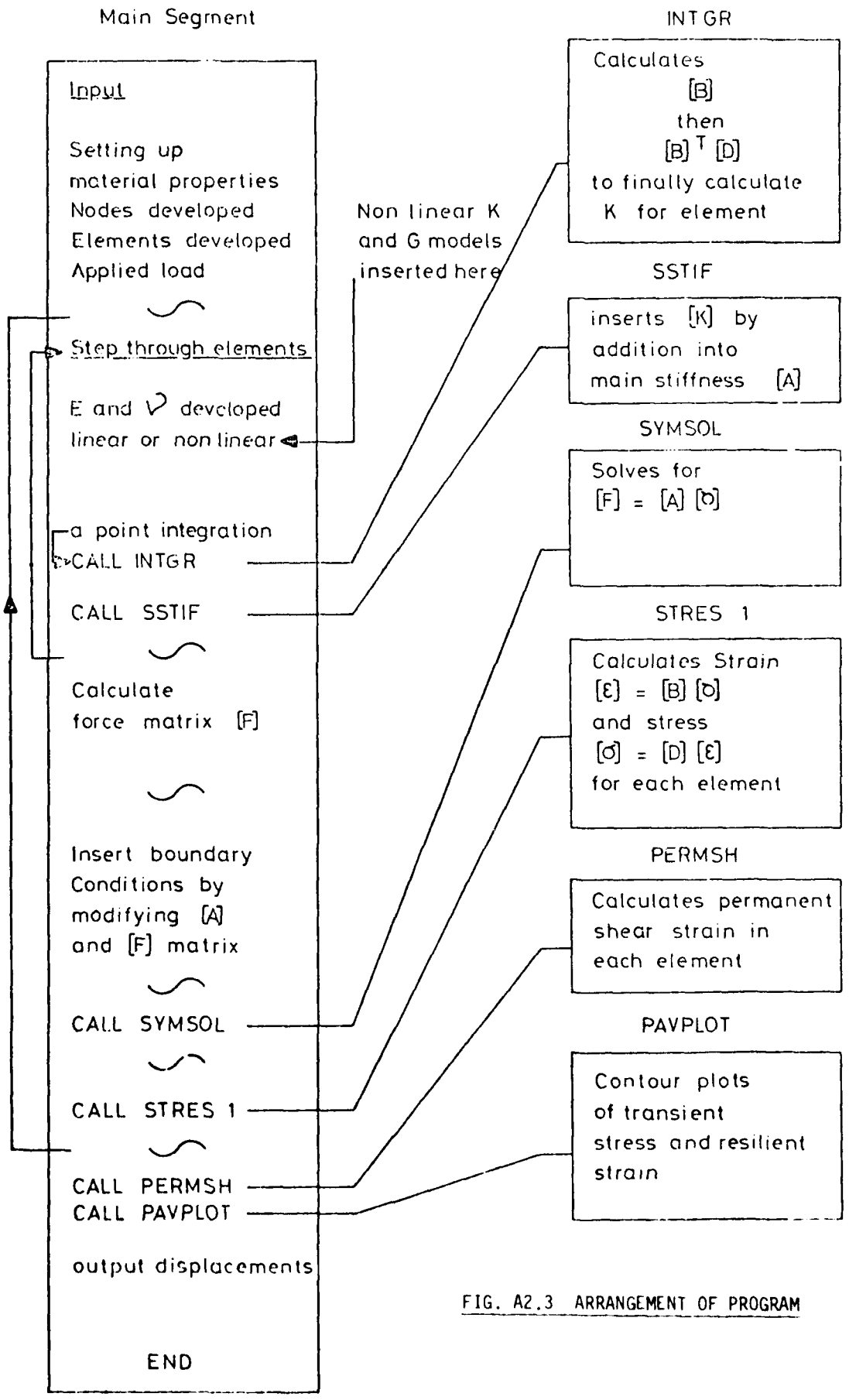


FIG. A2.3 ARRANGEMENT OF PROGRAM

indicated in Section 6.2, but could be changed in the same way as those for the resilient characteristics.

Included in the subroutine is a read statement where it is possible to include the initial and total number of load applications to be examined. Intermediate states can also be accommodated.

Arrangement of Program

The basic finite element formulation in this program is:

$$[F] = [A][\delta]$$

where $[F]$ is the applied load (or reaction) matrix of the form:

$$\begin{bmatrix} F_{h1} \\ F_{z1} \\ F_{h2} \\ \vdots \\ F_{hi} \\ F_{zi} \\ \end{bmatrix} \quad \begin{array}{l} \leftarrow \text{horizontal force at node 1} \\ \leftarrow \text{vertical force at node 1} \\ \leftarrow \text{horizontal force at node 2} \\ \\ \leftarrow \text{horizontal force at node i} \\ \leftarrow \text{vertical force at node i} \\ \text{etc.} \end{array}$$

$[\delta]$ is the node displacement vector arranged in the same way as $[F]$, and $[A]$ is the overall stiffness matrix (stored in the program in the upper triangular banded form) as it is symmetric and is signficantly banded. This matrix is developed by adding components from each element. These element components $[k]$ of stiffness are calculated as:

$$[k] = \int_0^{vol} [B]^T [D][B]\,dv$$

where $[B]$ is the shape function relating strain and displacement, i.e.

$$[\epsilon] = [B][\delta]$$

within each element and is derived direction from equation (A2.1), while [D] relates stress to strain using E and $\nu$ (stored in the program as U1(L), U2(L) and (3(L)), such that:

$$U1(L) = \frac{\nu}{1-\nu}, \quad U2(L) = \frac{1-2\nu}{2(1-\nu)}, \quad \text{and} \quad U3(L) = \frac{E(1-\nu)}{(1+\nu)(1-2\nu)}$$

The stress/strain relationship is as follows:

$$\begin{bmatrix} \sigma_z \\ \sigma_r \\ \sigma_\theta \\ \tau_{rz} \end{bmatrix} = \frac{E(1-\nu)}{(1+\nu)(1-2\nu)} \begin{bmatrix} 1 & \frac{\nu}{1-\nu} & \frac{\nu}{1-\nu} & 0 \\ & 1 & \frac{\nu}{1-\nu} & 0 \\ & & 1 & 0 \\ & \text{Symmetrical} & & \frac{1-2\nu}{2(1-\nu)} \end{bmatrix} \begin{bmatrix} \varepsilon_z \\ \varepsilon_r \\ \varepsilon_\theta \\ \gamma_{rz} \end{bmatrix}$$

The program is organised to perform these calculations as shown in Fig. A2.3.